Modelling of the Forging Process for a Magnesium Alloy Automotive Control Arm

by

Talal Paracha

A thesis
presented to the University of Waterloo
in fulfillment of the
thesis requirement for the degree of
Master of Applied Science
in
Mechanical and Mechatronics Engineering

Waterloo, Ontario, Canada, 2018

Author's Declaration

I hereby declare that I am the sole author of this thesis. This is a true copy of the thesis, including any required final revisions, as accepted by my examiners.

I understand that my thesis may be made electronically available to the public.

Abstract

The automotive industry has placed significant emphasis on weight reduction to achieve better fuel economy while maintaining safety and quality standards. One way this can be achieved is by using forged magnesium alloys due to their high stiffness- and strength-to-weight ratios. In order to assess the feasibility of forging magnesium alloys into a complex automotive component, numerical simulation using the commercial Finite Element (FE) package DEFORM 3D was performed and verified. For this study, two magnesium alloys AZ80 & ZK60 in extruded forms were considered.

Key material parameters required for input into DEFORM 3D included material flow stress data as a function of temperature, strain rate and strain. This data was extracted from flow curves which were developed by others in this research group using uniaxial hot compression tests of the as-cast and extruded starting material. Since magnesium has a Hexagonal Close Packed (HCP) crystal structure with limited slip systems which are activated under different deformation conditions, it was determined that anisotropy which is induced through the processes such as rolling, extrusion and forging plays an important role during deformation. As a result, Hill's anisotropic material model available in DEFORM 3D was used. Hill's anisotropic material model requires a strain rate sensitive flow curve for each temperature in addition to 6 anisotropic coefficients. Anisotropic coefficients were generated using measured compression and shear yield strength in the extruded starting material. Shear hat tests were performed at strain rates of 0.1/s and 1/s at multiple temperatures for AZ80 & ZK60 alloys.

After the simulation was complete and verified, multiple parametric and sensitivity studies were performed to determine the effect of factors such as flash land, friction, temperature and ram speed on the predicted forging load and material flow. It was determined that increasing the flash width will increase the press load while decreasing it too much will result in under-fill in the die cavity. It was determined that a flash width of 5 mm created a good balance to achieve a complete die fill while minimizing the forging load for this application. Friction plays a similar role as flash land: increasing it increases the load while reducing it too much results in under-fill. A friction factor of 0.2 was used based on testing with the friction modifier used in subsequent testing.

Multiple preform shapes were examined to ensure the final geometry for the control arm could be achieved in one forging step using the CanmetMATERIALS 1500 tonne press. The preform shapes studied included a multi-section cylindrical, flat plate and bend cylindrical billet. The bent cylindrical billet was selected as it met all the project requirements.

Acknowledgements

Firstly, I would like to offer my sincere gratitude to my supervisors Prof. Mary Wells and Prof. Steve Lambert for their outstanding support, expertise and understanding. They provided me not only with the technical guidance and support but also the moral support and motivation. Without them my thesis would not have been possible. I would also like to thank Tharindu Kodippili for his support and help during my research work.

I would like to also offer my special thanks to Bruce Williams and Jonathan McKinley of CanmetMATERIALS laboratory in Hamilton, Ontario for the valuable suggestion and detailed discussions.

I am also grateful for the guidance, support and insight provided by Alex Duquette, Jim Prsa, Tom Sparrow and Andy Georgiou of Multimatic Inc. The detailed discussions raised many critical question and hopefully I answered most of them in this thesis.

I am very thankful for the help and support provided by the research group at University of Waterloo. I would like to specially thank Andrew Gryguc, Paresh Prakash, Massimo DiCiano, Rick Wong, Amir Hadadzadeh, and last but not least Behzad Behravesh for the detailed discussions and deep insight on my thesis.

I would like to extend my sincere appreciation to my colleague and friends Waqas Muhammed and Dr. Usman Ali for their support, motivation and advice.

Also would like to acknowledge Automotive Partnership Canada for providing the financial support for the project.

Finally, I would like to extend my profound gratitude to my family. I would also like to offer my thanks to my brother for his support and sacrifices. I would also like recognize my parents for their prayers and blessings, without which this document would not be possible.

Table of Contents

List of Figures

List of Tables

Chapter 1 Introduction

1.1 Motivation

As environmental issues become more important, countries around the world are introducing regulations to minimize the formation of greenhouse gases (GHG), especially carbon dioxide. The Canadian government has set in place regulations and is targeting 45-65% reduction in GHG emission by 2050 [1]. One of the major sources of GHG emissions, approximately 25%, is the automotive sector [2]. Since the automotive sector contributes so much towards GHG emission, this sector is continuously under pressure to reduce its carbon footprint. Automotive companies can reduce the GHG emission by applying multiple approaches, one by reducing the vehicle weight, and two by improving the efficiency of the vehicle [3].

Fuel consumption is reduced by approximately by 5.7% - 7.4%, if the weight of the vehicle is reduced by 10% [4]. Wrought magnesium is considered one of the strong contenders for vehicle light-weighting due to its high stiffness–to-weight ratio and low density when compared to traditionally-used automotive materials such as aluminum and steel. However one drawback of using wrought magnesium is its reduced formability due to its Hexagonal Close Packed (HCP) crystal structure. Currently the use of magnesium alloys are limited to die cast structural components. Components such as instrument panel beams are currently being produced using magnesium alloys [5][6].

In order to utilize magnesium to manufacture fatigue critical components for automotive applications, manufacturing processes such as hot forging can be used. High strength in automotive magnesium alloys components can be achieved using die-casting method but due to the presence of pores and other casting defects, reasonable ductility cannot be achieved. Thus to manufacture fatigue critical components methods such as hot forging can be utilized [7].

1.2 APC Project Overview

A lower control arm was selected as the focus of this research under the Automotive Partnership Canada (APC) program (APCPJ 459269-13) due to the need for appropriate fatigue strength and the significant potential weight benefits. In order to investigate the forging of a magnesium control arm, a multidisciplinary collaboration between Ford Motor Company, Multimatic Inc, CanmetMATERIALS and University of Waterloo was initiated. The scope of the research project is to build a knowledge base for three different forgeable magnesium alloys, AZ80, ZK60 & AZ31 including an understanding of the development of the microstructure, the appropriate manufacturing process and conditions, fatigue and fracture behaviour for both small- and full-scale forgings.

The project's main two objectives are to design an optimum control arm and provide forging process guidelines for the use of magnesium alloys in the automotive industry. The author's general role is to develop a numerical model for forging process and specify conditions that can be used to forge the designed control arm using magnesium alloys.

1.3 Objectives:

The objectives for this research include:

i) Create and validate a model using the commercially available finite element software DEFORM 3D of the forging process to produce a magnesium control arm from AZ80 and ZK60. DEFORM 3D (v11.1) is a finite element simulation software specially designed for simulating bulk deformation and has capability to model the material anisotropic behaviour using built-in material models [8].

ii) Design an appropriate preform shape that can be used to forge the control arm in a single step.

iii) Identify the process limits during forging, including tolerances on the preform geometry and sensitivities to forging process parameters such as forging temperature and ram speed.

Chapter 2 Literature Review

Magnesium alloys possess excellent structural properties and are lightweight when compared with other commonly used metals. But due their Hexagonal Close Packed (HCP) crystal structure and limited active slip systems at room temperature, they have poor cold workability, minimizing their usefulness. Increasing the temperatures above 250 ^{o}C, additional slip systems become activated, improving the workability of magnesium alloys [9].

2.1 Deformation Mechanisms During Forging

In order to homogenously deform magnesium and its alloys, five independent slip systems must be activated [9]. In magnesium and its alloys at room temperature the basal slip system is the dominant slip system [9] because of its lower critical resolved shear stress (CRSS) when compared to the other slip systems such as prism and pyramidal [3][10][11][12], as shown in Figure 2.1-1. [13]. At room temperature, the slip system such as prismatic and pyramidal inhibit formability due to their high CRSS value.

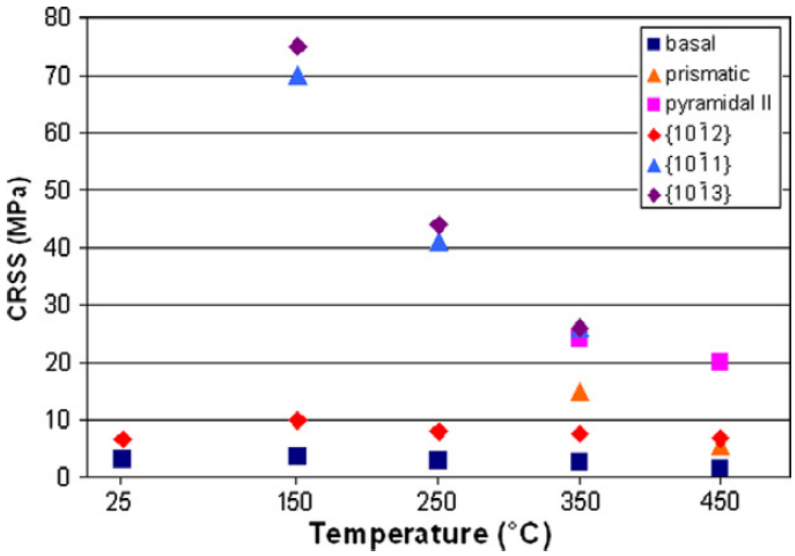

Figure 2.1-1: Critical resolve shear stress of different slip system in magnesium alloys [14].

Extension and contraction twins are the most common twins observed in magnesium and its alloys [13][15]. Figure 2.1-2 shows all of the slip and twining systems in an HCP crystal structure such as magnesium. The hexagonal lattice is extended along the crystallographic direction and the crystal lattice is reoriented to 86.3^o during extension twins. On the other hand, the lattice contracts in the crystallographic direction and crystal lattice reorient by 56.2^o during contraction twinning [13].

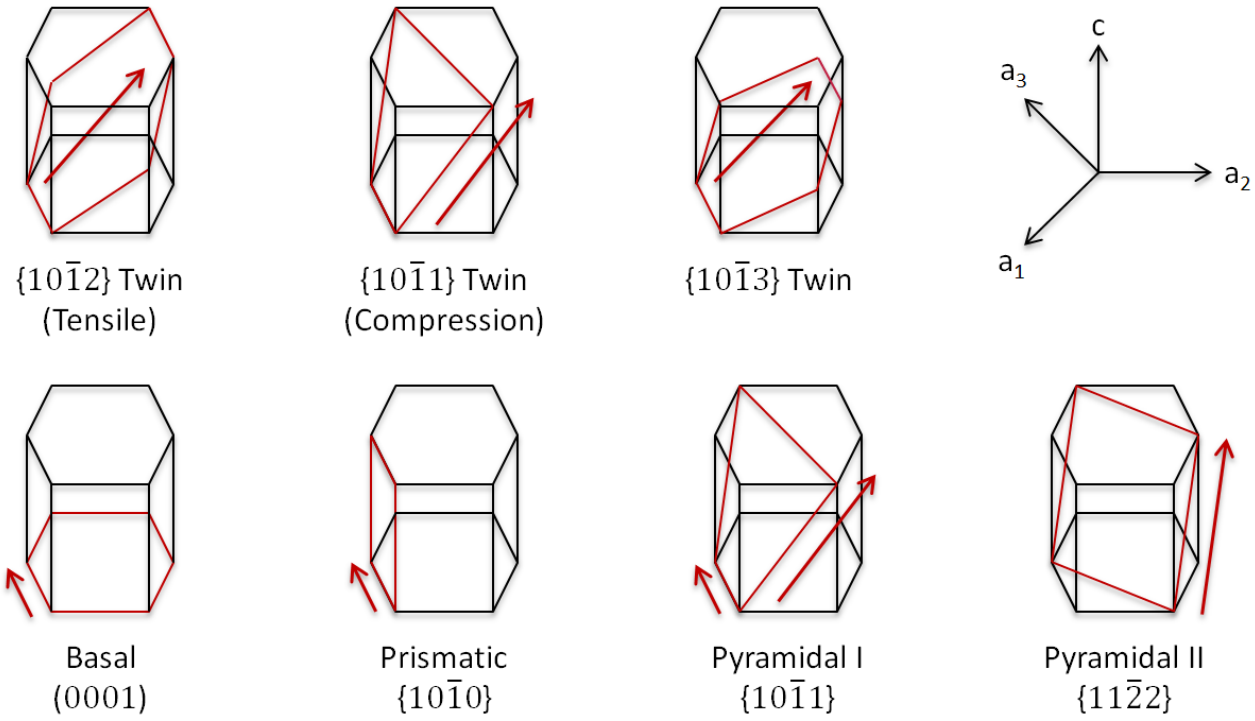

Figure 2.1-2: Slip and twining systems in HCP magnesium alloys [14].

In order to successfully achieve homogenous deformation in magnesium alloys, five independent slip systems need to be activated. As seen from Figure 2.1-1, as the deformation temperature increases more slip system become active. Thus, at high temperature, the magnesium alloy can be more easily and successfully deformed [14].

Experiments were performed to determine the effect of forging on cast AZ80 alloy. The tensile and strain controlled fatigue tests proved that forging showed significant improvement in strength, ductility and fatigue life of cast AZ80 alloy[16]. Similar effects were witnessed during forging of extruded AZ80 alloy at elevated temperatures at different strain rates in a semi-closed die. Forging showed substantial enhancement in mechanical and fatigue properties of extruded AZ80 due to

grain refinement and texture enhancement [17]. Studies on closed die forging of AZ80-F alloy had shown that best mechanical properties were obtained at lower temperature (250 ^{o}C) and higher forging rate. It was also observed that the mechanical strength decreases while elongation increases with increase in forging temperature [18].

Forging of cast ZK60 alloy at high temperature showed marginal improvement in mechanical properties such as 75% improvement in ductility [19]. While the semi-closed die forging of extruded ZK60 alloy shows significant improved in the mechanical and fatigue properties [20].

Research on forging of extruded AZ31 at high temperature, resulted in significant improvement in the maximum yield, ultimate tensile strength and the fatigue life when compared with the extruded material [21][22]. Successful forging of cast AZ31 were also done at multiple temperatures using both open and closed dies, resulting in improvement in mechanical properties as well as the fatigue life.

2.1.1 Yield Function – Hill's Coefficient

Due to highly textured magnesium wrought alloy's HCP crystal structure, anisotropy will play a critical role during deformation. This means that modeling of the forging operation needs to also include the anisotropic nature of the deformation that occurs. DEFORM 3D contains isotropic and multiple anisotropy models (yield functions) that can be used to model systems such as the deformation of magnesium. These models include: Von Mises, Hill's quadratic (6 coefficients), Hill's quadratic (R values), and Hill's quadratic (polycrystalline) and Lankford coefficient (R value) [24][25]

.

The Von Mises yield function is the DEFORM 3D default setting for isotropic materials. The yield functions with R values (strain ratios) are not suitable for bulk deformation. According to the developers of DEFORM 3D [8], R values are ideal for small reduction of thickness along the axial direction. This leaves two options, 'Hill's quadratic - 6 coefficients', and 'polycrystalline yield

functions' for modelling anisotropic behaviour in DEFORM 3D. 'Hill's quadratic six coefficients' requires the normal and shear yield stresses in the longitudinal and two transverse directions. The 'polycrystalline yield function' requires these six coefficients as well as texture details. In this project texture evolution is not modelled, polycrystalline yield function cannot be used.

In the literature, wrought AZ80 was successfully modeled using 'Hill's quadratic 6 coefficients' and then compared with full scale trials by Kobold et al. [26]. Verification of this model was also performed previously in the current research program when the coin forging simulations were compared with the actual forged coin samples by Yu [24]. 'Hill's quadratic 6 coefficients' were therefore selected as other sophisticated models were not applicable, and 'Hill's quadratic 6 coefficients' models anisotropy with acceptable accuracy.

In order to calculate the 'Hill's anisotropic coefficient', uniaxial compressive and shear yield stress values are required for a range of temperatures and strain rates. In early 1977, Meyer and Hartmann [27] used a specimen geometry shown in Figure 2.1-3 to measure the shear yield stress.

This test geometry was further improved by Meyer et al. in 1994 [28] and since then many successful studies have been carried using this test geometry specimen to determine the shear properties for different materials [24][29][30]. In his thesis, Yu [24] verified that the shear hat specimen geometry specimens with $\frac{r_1}{r_2} = 0.975$, as shown in the Figure 2.1-3 below, provided a good measurement of shear stress using compression testing [24]. Forged coin and I –beam specimens shapes were compared with the simulation results using anisotropic material properties and the results were reasonably well captured by the model.

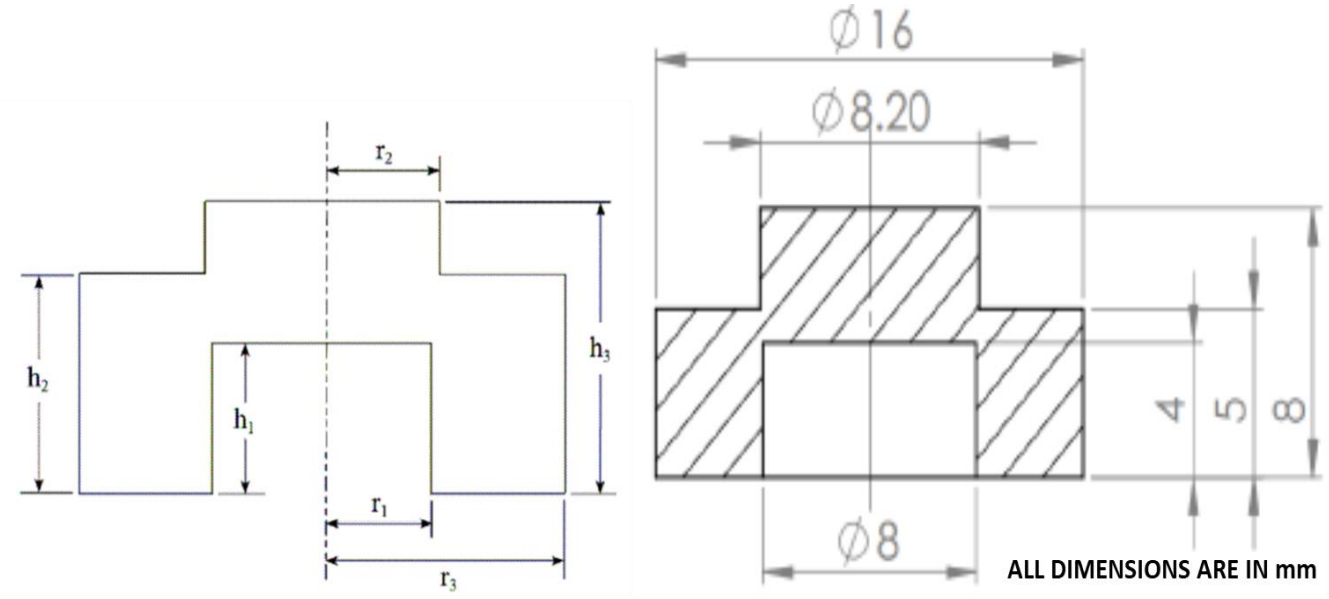

Figure 2.1-3: Shear hat specimen with dimensions [24].

'Hill's quadratic 6 coefficient' [31] equation is shown below in Equation 1:

$$F(\sigma_{22} - \sigma_{33})^2 + G(\sigma_{33} - \sigma_{11})^2 + H(\sigma_{11} - \sigma_{22})^2 + 2L\sigma_{23}^2 + 2M\sigma_{31}^2 + 2N\sigma_{12}^2 = 1 \quad (1)$$

Where σ_{ij} are material stresses in MPa. Uniaxial shear and compression tests are needed to determine the constants F, G, H, L, M, N as per the following equation. X, Y & Z are the compressive yield stresses while R, S and T are the shear yield stresses, where X= σ_{11}, Y=σ_{22}, Z=σ_{33}, R = σ_{23}, S = σ_{13} and T = σ_{12}.

$$\begin{aligned} 2F &= \frac{1}{Y^2} + \frac{1}{Z^2} + \frac{1}{X^2} \\ 2G &= \frac{1}{Z^2} + \frac{1}{X^2} + \frac{1}{Y^2} \\ 2H &= \frac{1}{X^2} + \frac{1}{Y^2} + \frac{1}{Z^2} \end{aligned} \quad (2)$$

$$2L = \frac{1}{R^2},\ 2M = \frac{1}{S^2}, 2N = \frac{1}{T^2} \quad (3)$$

For an isotropic material (Von Mises), the coefficients would be F=G=H=1 and L=M=N=3 [26]. However, in DEFORM 3D, the pre-set values for these coefficient are 0.5 and 1.5 respectively. So in order to input the coefficient into DEFORM 3D, the calculated coefficients are divided by 2. The calculated coefficients in equation 2 and 3 have units of MPa^2 and by using the conversion proposed by Finnie and Heller [32] as given by equations below are converted to a dimensionless form. The modified equation for coefficients F, G, H, L, M, N and the modified 'Hill's quadratic equation' are shown below.

$$\overline{\sigma_0}^2 = \frac{1}{3}((\sigma_{11})^2 + (\sigma_{22})^2 + (\sigma_{33})^2 \tag{4}$$

$$\begin{aligned} F &= \overline{\sigma_0}^2 \left(\frac{1}{(\sigma_{22})^2} + \frac{1}{(\sigma_{11})^2} - \frac{1}{(\sigma_{33})^2}\right) \\ G &= \overline{\sigma_0}^2 \left(\frac{1}{(\sigma_{11})^2} + \frac{1}{(\sigma_{33})^2} - \frac{1}{(\sigma_{22})^2}\right) \\ H &= \overline{\sigma_0}^2 \left(\frac{1}{(\sigma_{33})^2} + \frac{1}{(\sigma_{22})^2} - \frac{1}{(\sigma_{11})^2}\right) \\ L = \frac{\overline{\sigma_0}^2}{(\sigma_{23})^2},\ M &= \frac{\overline{\sigma_0}^2}{(\sigma_{13})^2}, \qquad N = \frac{\overline{\sigma_0}^2}{(\sigma_{12})^2} \end{aligned} \tag{5}$$

2.1.2 Forging Process Design & Modelling of Hot Deformation of Magnesium

A process in which compressive force is used to form a metal into a shape using a die or other tooling is called forging [33]. Although the processes has been used since 5000 BC, it was during the Second World War that magnesium alloy forging found its first substantial usage [34][35], due to a shortage of aluminum. The successful use of magnesium alloys in the aerospace industry [34] has renewed interest in the forging of magnesium alloys for use in automotive applications. This is due to its superior specific strength and fatigue properties relative to aluminum [36]. Magnesium alloys can be forged using a number of different types of forging presses, including hydraulic presses, drop hammers etc. [37][38].

Effect of multi-directional multi-step forging was studied by Miura et al. [39] on the mechanical properties of AZ61 alloy. Increased in material strength was observed due to grain refinement agreeing with the Hall-Petch relation.

Forging is a process that requires prototyping and trial and error design to ensure that the right starting geometry and die design is chosen, so that the final forged part geometry and component properties can be realized. The process design starts with the design and shape of the final component but also takes into consideration the forging equipment available, behaviour of the material, forging properties, and the tolerance to be achieved [37]. For relatively simple components, the final shape can be achieved using a single stage forging operation, but usually for a complex geometry a multi-stage forging process is required as shown in Figure 2.1-4 below [38].

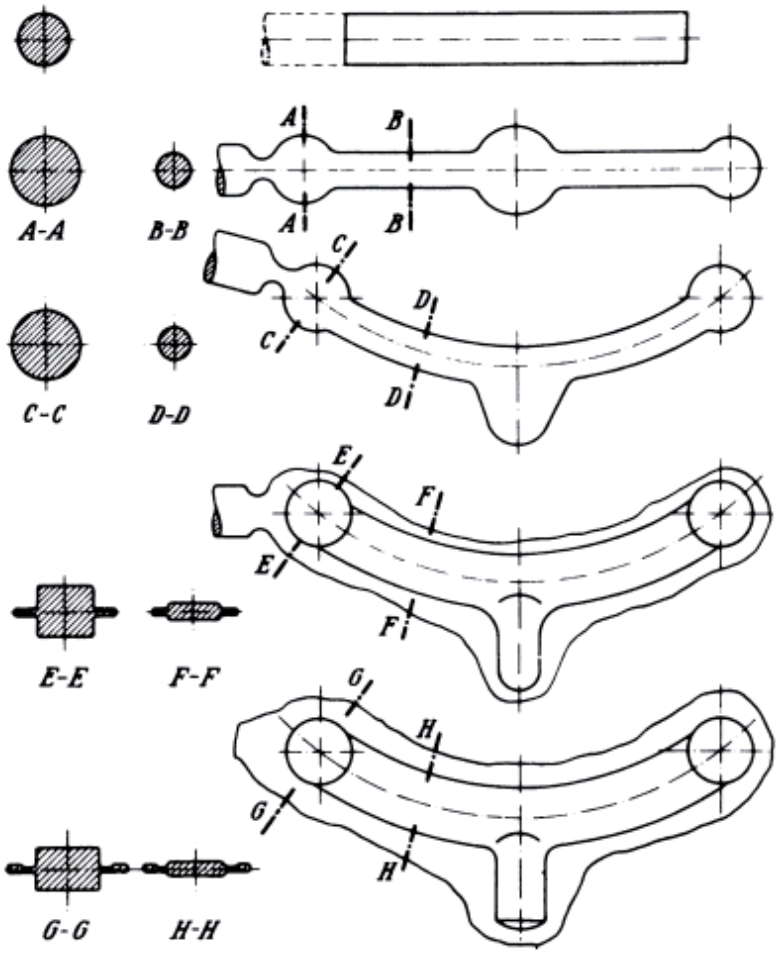

Figure 2.1-4 : Multiple stage forging process [35].

The time and cost associated with the forging process design can be significantly reduced by proper use of finite element (FE) simulations. Many researcher have performed geometric comparison after forging to the model predicted geometries for magnesium alloys and found that the model geometry matched the forged specimen [7][24][43][44]. Researchers like Vaxquez and Altan simulated a process for forging of an engine connecting rod using a refined and optimized finite element model in DEFORM 3D [42]. Critical parameters such as die filling, defects such as cracks, load requirements, and final shape of the magnesium alloy component, can be predicted by utilizing finite elements simulation models [26][38][43][44]. Utilization of computational simulation by the designer provides them with confidence that the forging process results and preform design can be predicted and optimized prior to manufacturing the tooling required for forging. Researchers have designed lab scale samples and successfully compared the results with finite element simulations [42][43][44]. Pepelnjak [44] compared 3 different finite element simulation packages. Due to the large deformation observed in the forging process, a better simulation package is one with remeshing ability or ALE (Arbitrary Lagrangian Eulerian)/ CEL (combined Eulerian Lagrangian) such as DEFORM 3D. DEFORM 3D with anisotropic material model developed and documented by Kobold et al. [26] on an industrial scale component is used herein.

Yu [24] designed two different specimens, a rib-web based geometry for the 110 tonnes press to the symmetric I-beam geometry for the 500 tonnes press. The specimens were forged using three magnesium alloys, extruded AZ80, AZ31 & ZK60. DEFORM 3D was used to perform the simulation for forging process for both specimens. Forging samples were then used to validate the materials model by performing both the geometric and load comparison of the forged samples with simulation results at optimal forging conditions. The results prove that magnesium anisotropic properties were well captured by DEFORM 3D.

Multiple forging components have been successfully manufactured using both heated and non-heated dies, using multiple different techniques [40]. Simulations successfully predicted the location of flaws (cracks) in the drop forging process [40]. The forging process was optimised using simulations and successfully forged good quality components using multiple lighter strikes [40].

2.1.3 Damage Criteria

Ductile fracture is considered the main source of material failure in bulk deformation, and crack initiation is considered more important than crack propagation in the successful design of a forged component. DEFORM 3D have multiple models to predict failure including but not limited to normalized Cockroft and Latham, Rice and Tracy, Brozzo etc. Christianse et al. [45] and Rao [46], after reviewing number of ductile failure models, concluded that the normalized Cockroft and Latham model was one of the most reliable in predicting damage location. This method integrates the largest principal stress normalized by the effective stress integrated over the effective strain to determine the damage value.

In the equation below, $\boldsymbol{\sigma_{max}}$ is the maximum principal stress, $\overline{\boldsymbol{\sigma}}$ is the effective stress, effective strain is given by $\boldsymbol{\varepsilon_i}$, and the critical damage value is described by C. Any material with a damage parameter above this critical value is assumed to have failed, and therefore a crack has initiated.

$$\int_{0}^{\varepsilon_i(t)} \frac{\boldsymbol{\sigma_{max}}}{\overline{\boldsymbol{\sigma}}} \; \boldsymbol{d\varepsilon_i(t) \geq C} \qquad \textbf{(6)}$$

During numerical simulations, in order to model the cracked region, any element with the damage above the critical value (pre-determined value C assigned to material) is deleted during remeshing. Our interest is not in predicting the crack geometry but in keeping the maximum value below the critical value. Deform 3D allows the user to assign a value of zero to the "critical value" in the advance material tab, calculating the critical value without eliminating elements. This permits the user to compare the maximum damage value to an assumed critical value, estimated from experiments or determined from the literature.

Numerous studies have been performed using the Cockroft and Latham criterion. Different approaches have been used to predict the critical damage value for magnesium alloys. At strain rates of 0.001 to 0.1 s^{-1}, a critical damage value of 0.5 was proposed for ZK31 at 500 °C. For AZ80 at 400 ˚C, the critical value ranged from 0.26 to 0.46 from Kim and Lee [47], and Xue et al. [48]. Yu [24] was able to successfully predict the location of surface cracks in the simulation of flatbread samples subsequently observed during actual forging. The critical damage value used for AZ31

was 0.5 [47]. The damage value at the crack location was slightly above 0.5, as can be seen in Figure 2.1-5 [24].

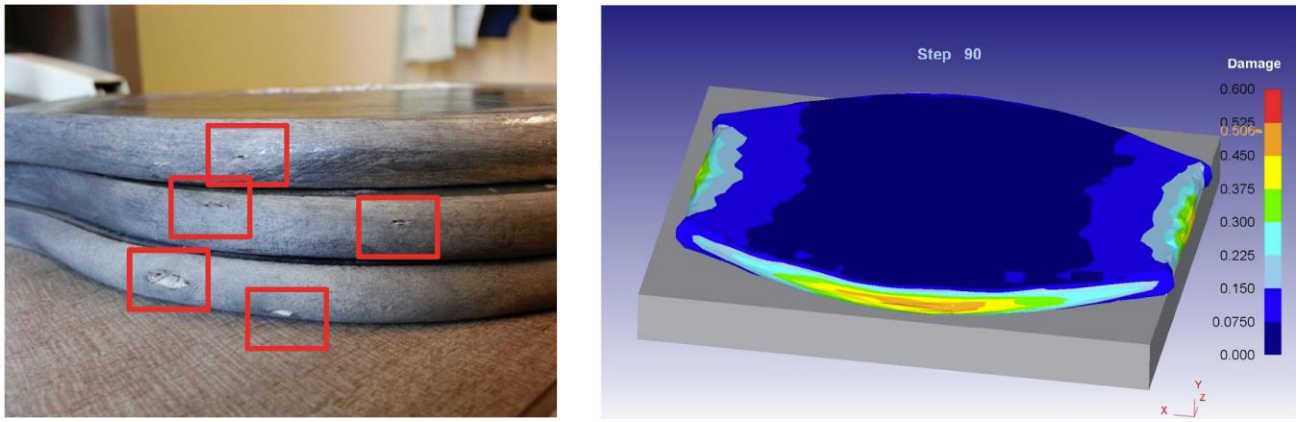

Figure 2.1-5: Surface crack prediction for the flatbread sample. [24].

Chapter 3 Material Characterization

In order to successfully simulate the forging process, material data is required: flow stress and anisotropy coefficients. Within this research project, other graduate students have characterized the compressive behaviour of the magnesium material for use in the models. Three magnesium alloys (AZ80, ZK60 and AZ31), each in two conditions, extruded and cast billets, were considered by the group. Only AZ80 and ZK60 in the extruded condition were considered herein. These had been identified earlier to be the most promising for full-scale forging based on the fatigue tests conducted on the I-beam forgings [16][19].

3.1 Compression Test (Flow Curves)

Compressive behaviour under uniaxial forging conditions was determined by performing uniaxial compression testing of cylindrical samples. A Gleeble machine was used to perform the uniaxial compression tests in both the extrusion (ED) and radial direction (transverse (TD) assuming rotational symmetry) in order to characterize the material and provide the flow curve. The samples were extracted as shown in Figure 3.1-1

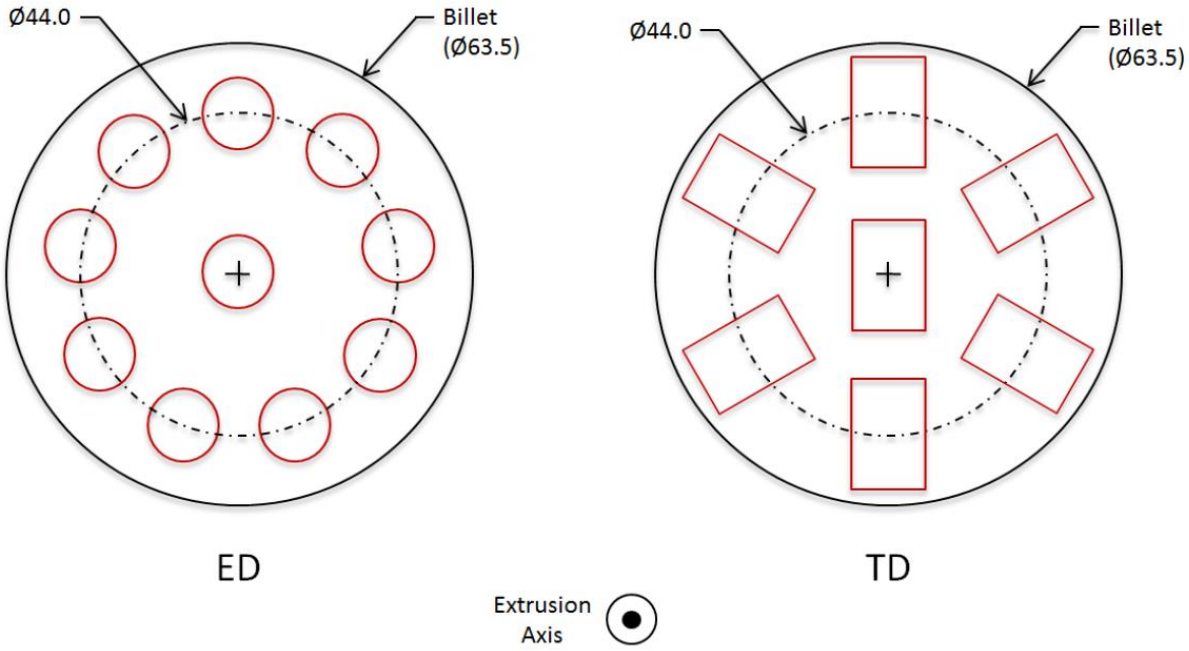

Figure 3.1-1: Orientation of sample extraction for Gleeble compression test [14].

All the compression tests were conducted by the forging group (Rick Wong performed testing on AZ31 [14], Paresh Parkash performed testing on AZ80 [49], and Amir Hadadzadeh [50] performed testing on ZK60). Tests were performed in the isothermal condition, with temperatures ranging from 300 ^{o}C to 500 ^{o}C, and at true strain rates of 10^{-3}/s to 1.0/s. The highest achievable rate was 1/s. The test system is shown below in Figure 3.1-2. The flow curves obtained from these experiments were used as the input for the DEFORM 3D material model, and are presented and discussed in Chapter 4.

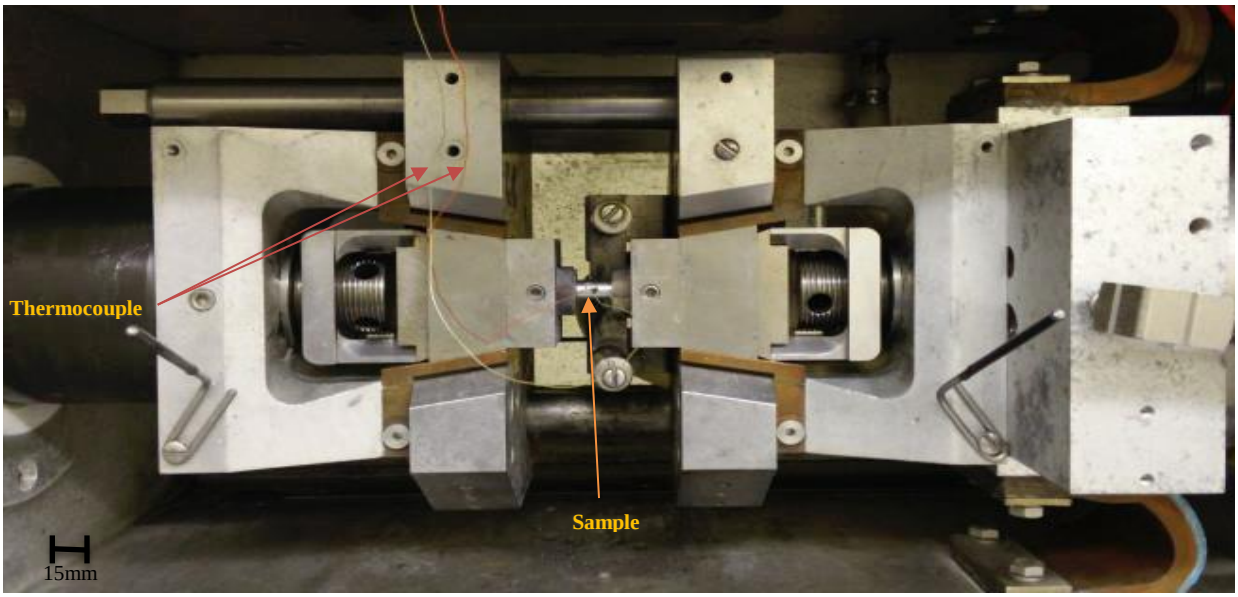

Figure 3.1-2 : Compression test Gleeble 3500 [24].

In Figure 3.1-3 below, the flow stresses at ε = 1 are plotted for the two magnesium alloys (AZ80 and ZK60) at different temperatures and strain rates of 1/s and 0.1/s. It was found that as the strain rate increases the stress increases for both materials. It was also seen that as the temperature increases the stresses decrease. The stresses for ZK60 for all strains and temperatures was higher than that of AZ80. As the temperature increases from 350 ºC to 450 ºC, the difference between stresses at the two strain rates decreases.

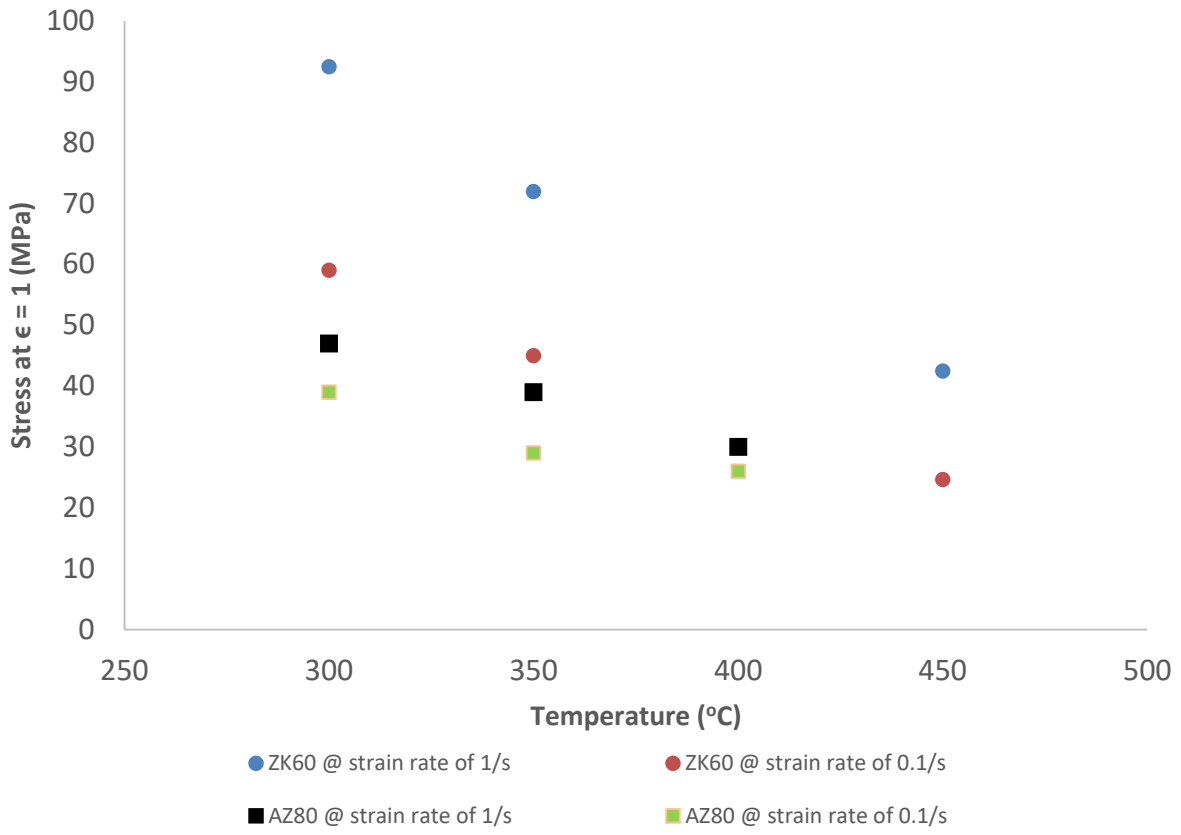

Figure 3.1-3: Flow stresses at ε= 1 for AZ80 & ZK60.

3.2 Shear Hat Testing

3.2.1 Specimen Design

The geometry selected and used by Yu [24] for the shear hat sample is shown below in Figure 3.2-1. The selection of this geometry was made keeping in mind that samples needed to be machined out of a 63.5 mm diameter billet and fit the test apparatus on the Gleeble 3500 [24]. Another notable benefit of selecting this profile was the ease of calculating the shear stress based on the load data and the shear zone area.

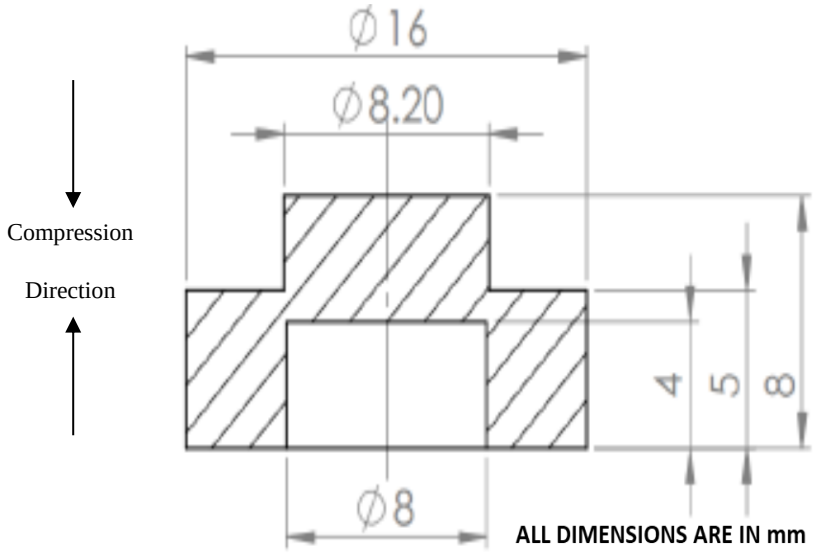

Figure 3.2-1 : Shear hat specimen geometry [24].

The shear hat specimens were machined out of 63.5mm diameter extruded materials for both extruded (ED) and transverse (TD) directions (assuming rotational symmetry). The samples were machined in such a way that the center of the extruded direction sample was located on the 44mm ring, and the shear zone of the transverse direction samples was located on the 44 mm ring, as shown in Figure 3.2-2. This was done in order to maintain consistency with the uniaxial compression test and to avoid any defects on the surface.

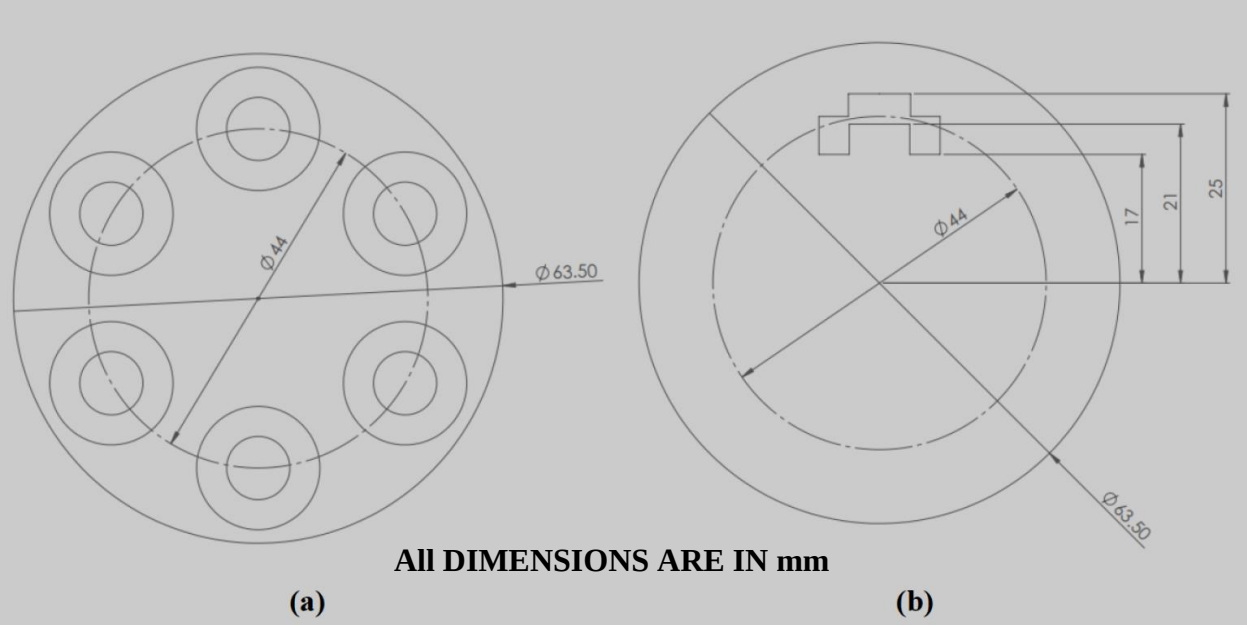

Figure 3.2-2: Extraction location for shear hat sample (a) Extruded (b) Transverse Direction [24].

3.2.2 Shear Hat Results – Gleeble

The Gleeble 3500 was used to perform the shear hat tests. The test matrix of the temperatures and strain rates to be used was selected based on recommendations from the forging and fatigue groups. The recommendations for best forging conditions were made based on processing maps and analyses performed on the forged coin and I-beam specimens. Shear hat tests by Yu [24] were only performed at one temperature for each alloy: AZ80 @ 400 ºC, ZK60 @ 450 ºC and AZ31 @ 500 ºC. Current tests were performed to expand the range of available data, at temperatures ranging from 300 ºC to 450 ºC, and at strain rates of 0.1/s or 1/s. Table 3.2-1 gives the test matrix for the shear hat test that were conducted herein.

Table 3.2-1: Test matrix for the shear hat tests.

Material	**Temperature (ºC)**	**Strain Rate (1/s)**	
		0.1	1
AZ80	300	●	●
	400	●	●
ZK60	300	●	●
	450	●	●

In order to assess the reliability and repeatability of the results, multiple samples were tested for each condition, as indicated in Table 3.2-1. Typical measured data is shown for two tests at one condition, for AZ80 at 300 ºC at 1/s strain rate, in Figure 3.2-3.

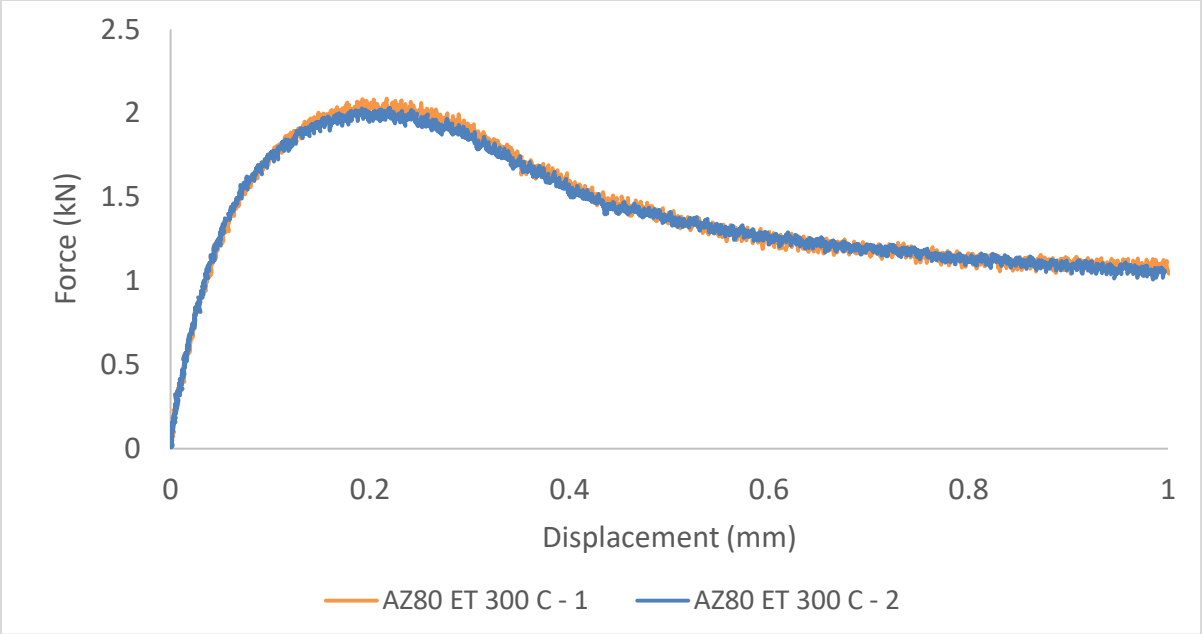

Figure 3.2-3: Shear hat test result for AZ80 @ 300 °C and 1/s showing repeatability.

The following equation was used to calculate the shear strain rate for each material:

$$\dot{\gamma} = \frac{v}{\Delta r} \text{ [51]} \quad \textbf{(7)}$$

In the above equation, υ is the Gleeble die displacement rate and Δr is the difference between r_2 and r_1 ($r_2 - r_1 = 0.1$mm). In order to achieve the required strain rate, the Gleeble die displacement rate was set as 0.01 mm/s and 0.1mm/s respectively.

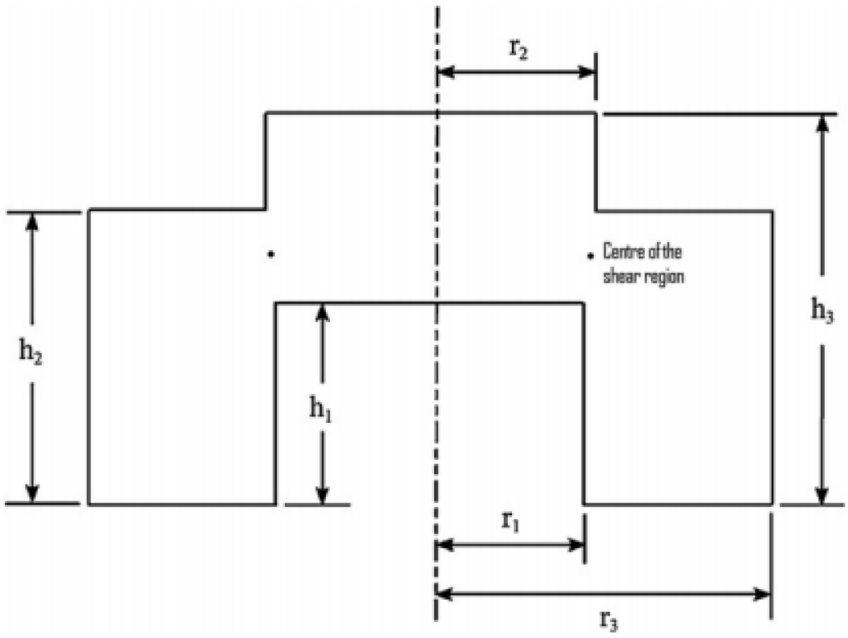

Figure 3.2-4: Shear hat specimen design [24].

The shear stress is the load divided by the shear zone area. Shear zone area is calculated using the cylindrical surface area formula:

$$A = 2 * \pi * \frac{(r_1 + r_2)}{2} * h \quad \textbf{(8)}$$

which uses the average of radius r_1 and r_2 and h was taken as 1 mm ($h_2 - h_1$). The measured maximum yield load was divided by the calculated surface area to obtain the shear yield stress.

Chapter 4 Mathematical Modelling Using DEFORM 3D

4.1 Material Models

Flow stress curves are required to perform isotropic simulations, and are used in conjunction with Hill's coefficients to perform anisotropic simulations.

Load (F) and displacement (Δh) are converted to true-stress-true strain using the following equation.

$$\sigma = \frac{F}{\left[\frac{\frac{\pi d_0^2}{4} h_0}{h_0 + \Delta h}\right]} \qquad \varepsilon = \ln\left(\frac{h_0 + \Delta h}{h_0}\right) \tag{9}$$

However, a correction is typically applied for barreling and ovaling. This was observed during uniaxial compression as a direct result of surface friction and material anisotropy. The flow curves were corrected using the methods proposed in the literature by Luan et al. [52]. The flow curve corrections were performed by the forging group (Rick Wong for AZ31, Paresh Parkash for AZ80, and Amir Hadadzadeh for ZK60) before the flow curves were used in DEFORM 3D.

Hill's coefficients were calculated using the three yield stress from the uniaxial compression tests (performed by Rick Wong for AZ31, Paresh Parkash for AZ80, and Amir Hadadzadeh for ZK60) and three shear yield stress values calculated using the shear hat tests.

In this project, since most of our billets were extruded in a cylindrical shape, rotational symmetry for mechanical properties was assumed. Rotational symmetry was also confirmed by the forging group after performing Gleeble testing. A coordinate system was chosen with the Z-axis along the extrusion direction, which was considered the line of symmetry of rotation. The other two directions, X & Y axis transverse directions, were orthogonal to Z – axis and perpendicular to each other [51]. Since rotational symmetry was considered, there was only a need to perform the uniaxial compression test and shear hat test in one of the two transverse directions and the extrusion direction. These uniaxial compression tests and shear hat tests were performed for each material

in both directions for each temperature and strain rate. The yield strength for both ED and TD direction are shown in the Table 4.1-1. Using the equation in section 2.2.2, Hill's coefficients were calculated. Figure 4.1-1and Table 4.1-2 below show the complete material model for AZ80 at 300 ^{o}C at 1/s strain rate. Results for the remaining material models can be found in Appendix A.

Table 4.1-1: AZ80 at 300 ^{o}C at 1/s - ED and TD direction stresses.

AZ80 at 300o C at 1/s		
	ED - Extruded Direction (MPa)	*TD - Transverse Direction (MPa)*
Yield Stress	*107*	*92*
Shear Yield Stress	*43*	*57*

Table 4.1-2: Hill's coefficient AZ80 @ 300 ^{o}C @ 1/s.

Hill's Coefficient - AZ80 at 300^{o} C at 1/s					
F	**G**	**H**	**L**	**M**	**N**
0.413	0.413	0.705	1.45	1.45	1.82

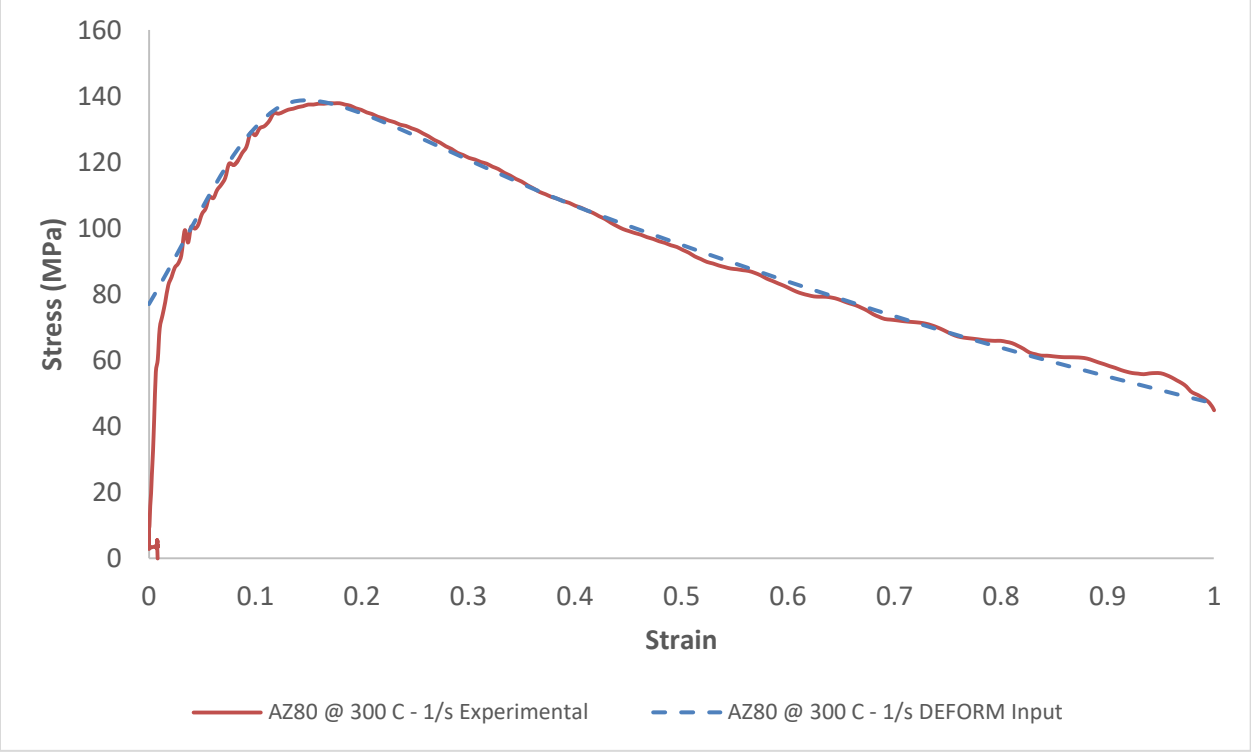

Figure 4.1-1: Flow stress curve for AZ80 300 ^{o}C at 1/s experimental [49] and simplified DEFORM 3D input.

In order to verify the use of Hill's coefficients and its effect, Gleeble experiments were simulated in DEFORM 3D. The method was:

1) First, a simulation was done for ZK60 at 450 ^{o}C at a strain rate of 1/s using the flow curve in the extruded direction (z axis) and Hill's coefficients calculated using the extruded axis as the primary axis. The axis of deformation was oriented along the z-axis, as shown in Figure 4.1-2.

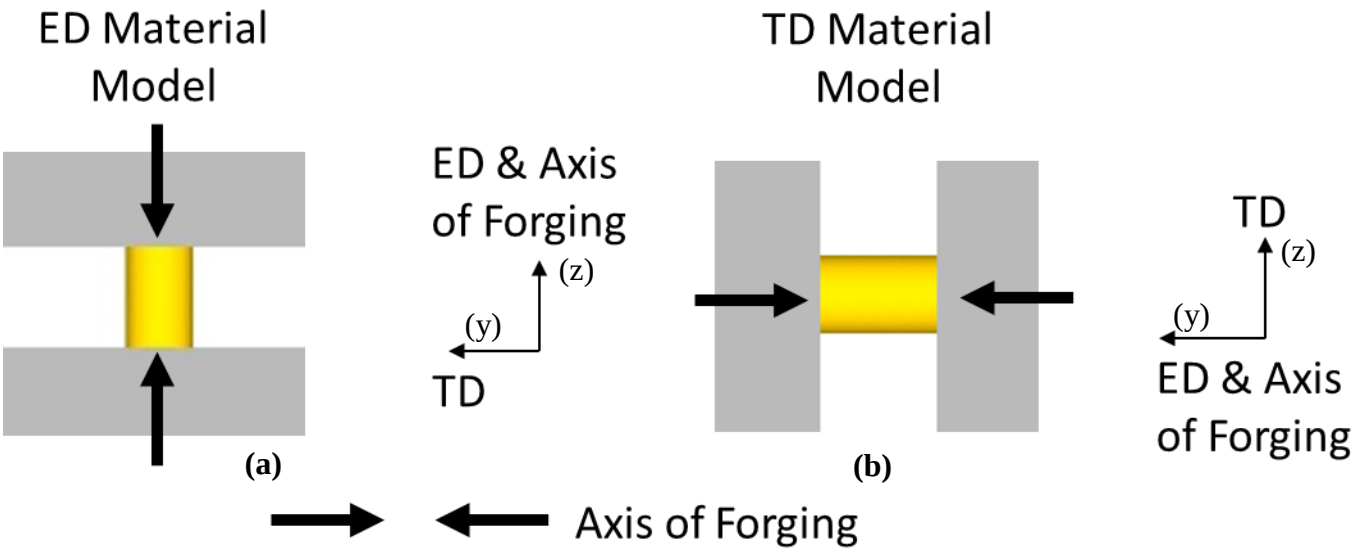

Figure 4.1-2: Simulation of Gleeble test in extrusion direction (a) Using ED material model (b) Using TD material model.

2) The second simulation was performed using the transverse direction flow curve and Hill's coefficients calculated considering the transverse direction as the primary direction. The axis of deformation was changed, oriented along the y-axis.

In both simulations, the specimen was compressed in the extruded direction, but the material model used was different. The results of both simulations were compared with the experimental compression in the extrusion direction, as show in Figure 4.1-3 below. A Similar experiment was performed in the transverse direction. The specimen was compressed in the transverse direction using both material model and the results were compared with the experimental compression in the transverse direction.

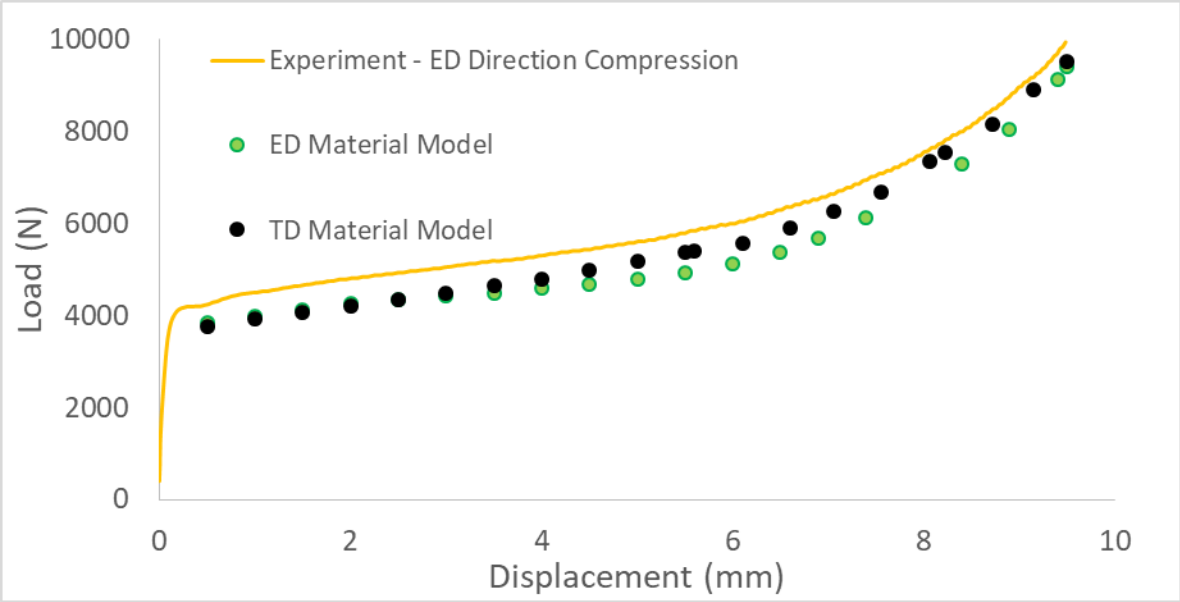

Figure 4.1-3: Gleeble experiment in ED direction ZK60 @ 450 °C, 1/s.

In Figure 4.1-3 & Figure 4.1-4 it can be seen that the experimental results and simulation results are similar. The predicted load matches that of both simulations, using either material model. Also Yu [24] had compared the coin and I- beam simulations with the forged specimens as shown in Figure 4.1-5. This suggests that Hill's model adequately captures the anisotropic effect of magnesium alloys.

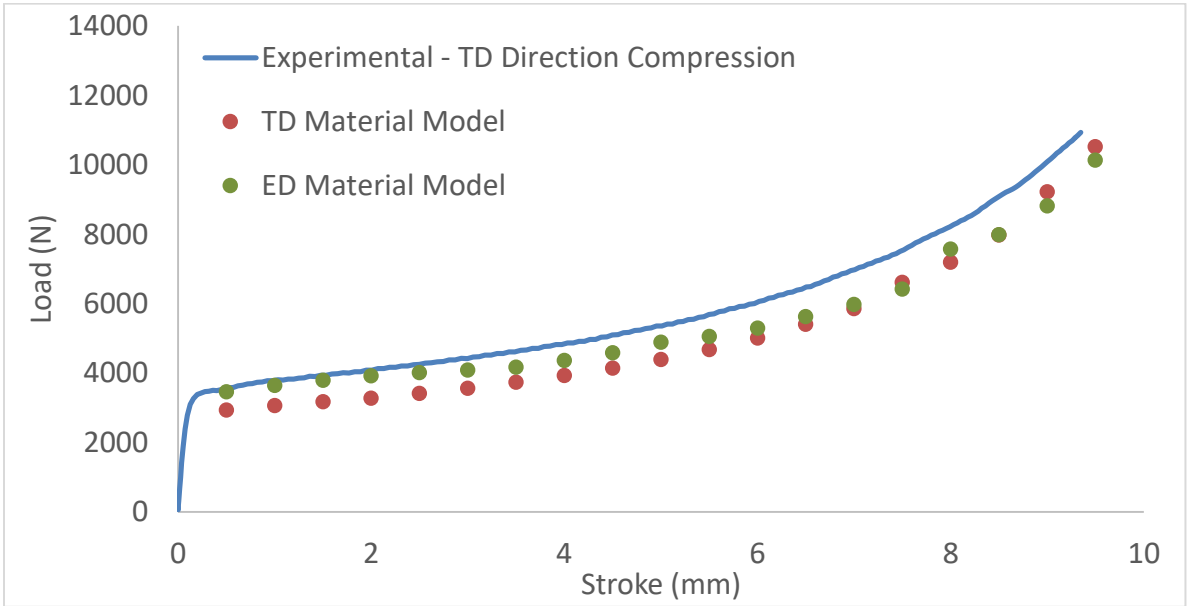

Figure 4.1-4: Gleeble experiment in TD direction ZK60 @ 450 °C, 1/s.

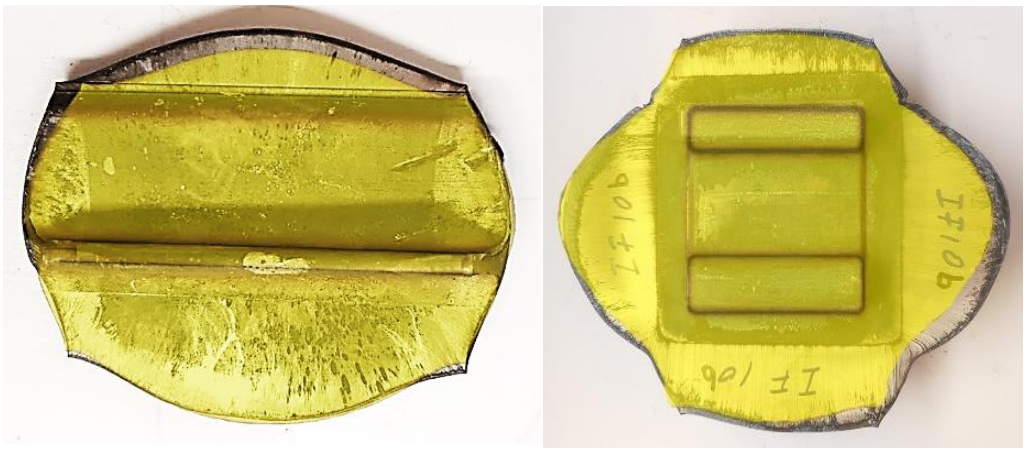

Figure 4.1-5: Coin and I beam simulation compared with forged specimen [24].

During the forging process simulation, DEFORM 3D keeps the anisotropic coefficients constant. In order to validate the material model, two forging samples were designed by Yu [24]: a rib-web based geometry for the 110-ton press Figure 4.1-6(a)); and a symmetric I-beam geometry for the 500 ton press Figure 4.1-6(b).

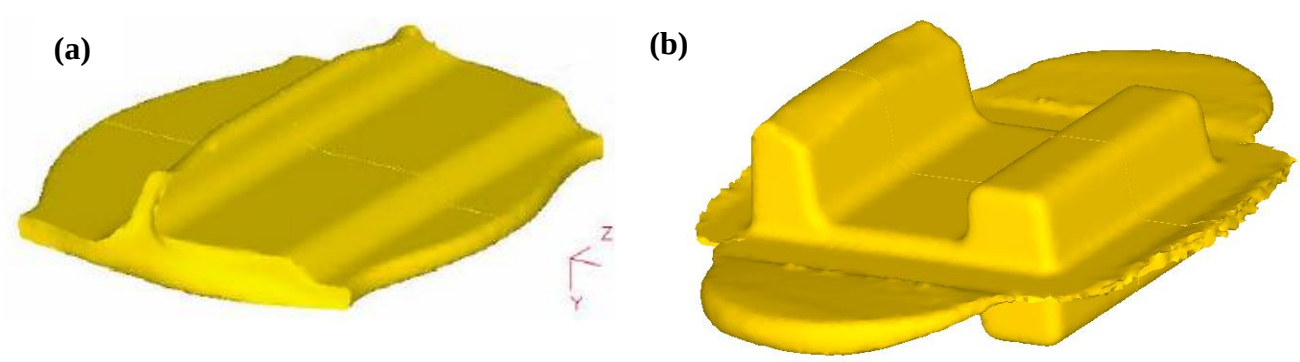

Figure 4.1-6: a) Coin forging specimen b) I - beam forging specimen.

These forging samples were used to validate the material model by performing both the geometric and load comparison of the forged samples with simulation results at only optimal forging conditions for each of the materials.

4.2 Numerical Parameters

In this project, DEFORM 3D was utilized to perform the forging simulation of the control arm. During the simulation, the billet was modelled as a plastic material. The dies were modeled as rigid, removing the need to mesh the dies, and thereby reducing the complexity of the simulation process. The flow curves and the 6 anisotropic Hill's coefficients obtained experimentally as discussed in the previous section were used to model the material. The Hill's coefficient remain constant for a given forging temperature and ram speed.

The number of simulation steps were set at five hundred with the step increment of 0.2 mm/step for the die displacement. The upper die stops when the distance between the upper and lower die reaches 3 mm, equal to the intended flash thickness. The step increment was selected after performing multiple trial runs ranging from 0.05 to 1 mm/steps. Too small of a time step results in a longer simulation time, while a large time step results in convergence errors and/or mesh distortion. The conjugate gradient solver was used with the direct iteration method. This method is recommended for simulation for very large problems and where a lot of contact exists between the die and the billet [8]. This method is also recommended for its ability to solve problems with a large number of elements in a reasonable time. The convergence error limit with the velocity error was set at 0.005, with the force error at 0.05. The nodal velocity/force divided for current iteration divided by the nodal velocity/force difference between current iteration and start of iteration procedure must be less than the velocity/force error limit.

The simulation was performed with the upper die assigned as the primary die and traveling at the specified velocity. Initial interference contact of 0.0001 mm was made between the bottom die and the preform. The upper die comes in contact with the preform as the die travels down.

The preforms were meshed with about 180K tetrahedron elements and placed on the bottom die by utilizing the drop function in DEFORM 3D. This function allows the preform to settle in the die with the use of gravity. In Figure 4.2-1 a typical forging process sequence is displayed. The global remeshing was enabled when the mesh interference depth was beyond 30%. A mesh sensitivity analysis was performed to determine the effect on load and final shape. The simulation

time for different preforms varied from 6 hrs to 9 hrs on a desktop computer (Intel Core i7 5600U CPU @ 2.6GHz, with 32GB Ram).

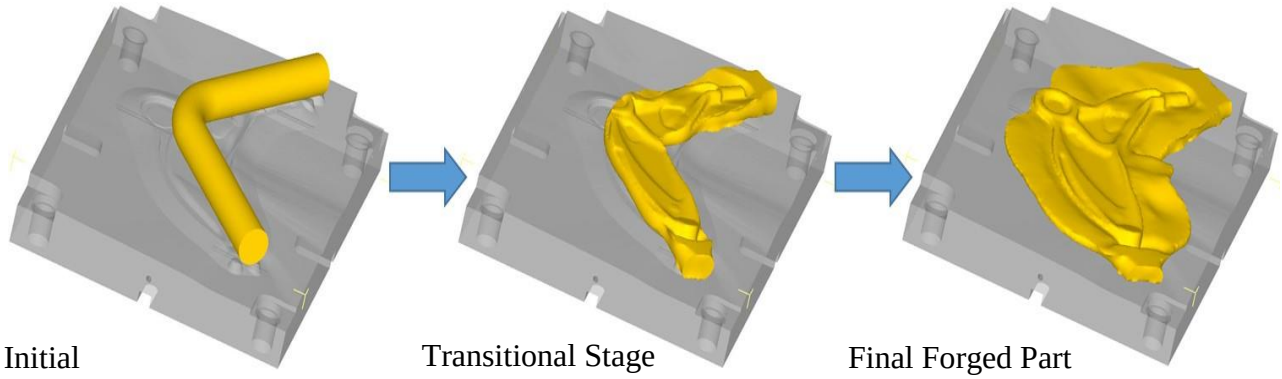

Figure 4.2-1: Forging process sequence for the control arm.

4.2.1 Mesh Sensitivity Analysis

A mesh sensitivity analysis was performed in order to select a mesh size that would provide accurate results within a reasonable computational time. A bent cylindrical preform was used to perform mesh sensitivity analysis using different element sizes. During the mesh sensitivity analysis, the other simulation parameters, such as material, ram speed, temperature and materials, were kept constant. As can be seen in Figure 4.2-2 and Table 4.2-1 below, increasing the number of elements does not significantly affect the forging load required, but almost doubled computational time. It was determined that an element size of 1.5mm, resulting in 180k elements and approximately 8.5 hrs of computational time, was acceptable. Increasing the number of elements to 300K, reducing the element size to 1.25 mm, took 14 hrs. Further increasing the number of elements to 350K, for an element size of 1 mm, gave a computational time of 24 hrs. The forging loads for these more refined analyses were 802 tonne and 805 tonne, respectively. Also decreasing the number of element from 180K to 100K reduced the load from 790 tonne to 745 tonne, and the computation time was decreased from 8.5 hrs to 6.5 hrs. This resulted in a difference of 6% in load and minor decrease in computation time. Based on this study it was shown that increasing the number of elements does not significantly change the predicted forging load (increases 3%). It was decided that 180,000 elements (typical) or a specimen with a volume of

4591 cm^3 (1.452 mm is the minimum element size) provided acceptable results for a reasonable computational time.

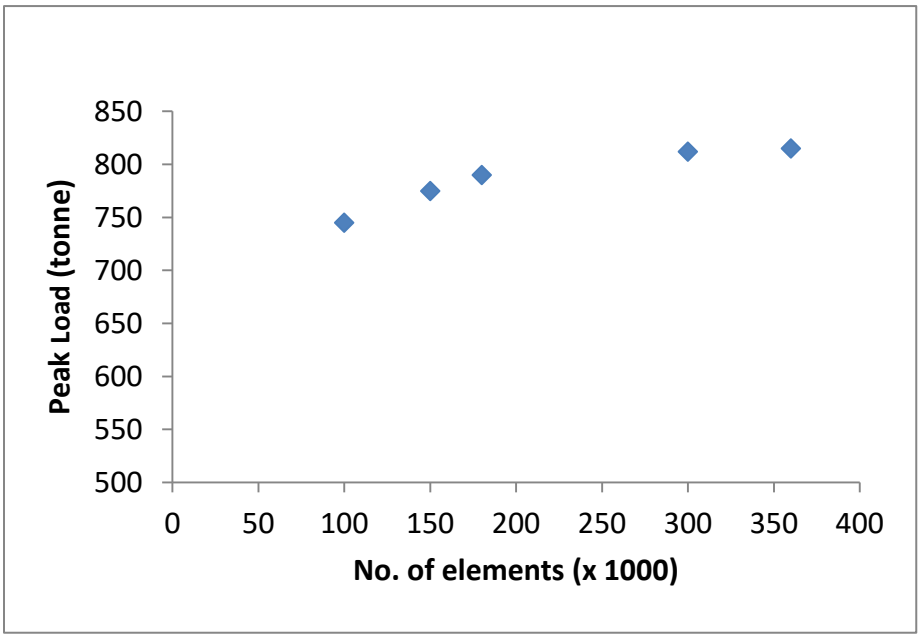

Figure 4.2-2: Mesh sensitivity analysis – no. of elements vs peak load.

Table 4.2-1: Mesh sensitivity analysis – no. of elements vs load vs simulation time.

# of Elements	Predicted Load (tonne)	Simulation Time (hr)
100 K	745	6.5
150 K	775	7
180 K (typical)	779	8.5
300 K	802	14
360 K	805	24

4.3 Boundary Conditions

All simulations were performed under isothermal conditions; the dies and preform temperature were kept the same and constant during the entire forging process. This seemed reasonable since the simulation shows that the forging process can be completed within 15 sec in all cases. Because of the small forging time, and because a heated die is used in the actual forging, it was assumed that no significant heat loss will be observed during forging. Also during the actual forging for coin and I-beam specimens, significant heat loss was not observed [24].

Graphite lubricant was used in all experiments conducted at CanmetMATERIALS. The value of friction coefficient was determined using the ring compression test for the graphite lubricant by Yu [24]. Therefore, a Coulomb friction coefficient of 0.2 was used to define the contact between the contacting surfaces in the present work.

Chapter 5 Forging Process Design

Forging is a complex process which is affected by various factors such as material, forging temperature, forging rate, die geometry, and preform design. The forging process design starts with the component design. The control arm was designed by Strong [53] and refined by Multimatic Inc to meet the manufacturer's requirements for packaging, stiffness, and strength. This component configuration was then used by Kodippili [54] to produce the die design in consultation with the author and Multimatic Inc.

In order to successfully design the forging process, the following must be considered:

I. Forging Equipment Constraints: The forging process will be carried out at the Natural Resources Canada (NRC) government lab CanmetMATERIALS located in Hamilton, Ontario. CanmetMATERIALS has two forging presses: a 1500 tonne press and a 1200 tonne press. The die needed to be designed such that it could fit into either press and would require a total forging load less than 1500 Tonnes.

II. Complex components like the control arm are usually forged using a multistage forging process [35]. A blocker die is used to distribute the material as required and more than one finisher dies are used to achieve the required shape and tolerance. In order to eliminate the need for multiple dies for this research project, it was decided to forge the control arm using a single stage forging process from a preform shape created using one or more different processes.

III. Preform shape needed to be designed such that it could formed from readily available material shapes, with existing equipment.

IV. Based on fatigue testing from forged I-beam samples previously conducted in this research program [16], it was determined that the strain in critical regions needs to be at least 125%, to achieve favourable material properties.

V. The component needed to be completely formed (complete die fill) with no forging defects such as fold lines.

A simulation matrix is shown in Table 4.3-1 for the parametric studies that are performed in order to understand the effect of different parameters on the forging process.

Table 4.3-1: Parametric studies simulation matrix.

Parametric Studies	**Material**	**Flash Width (mm)**	**Temperature (°C)**	**Friction Coefficient (μ)**	**Strain Rate (1/sec)**
Flash Width	ZK60	10 5 2	450	0.2	1
Temperature	AZ80	5	400 350	.02	1
Friction Coefficient	AZ80	5	400	0.05 0.1 0.3	1
Strain Rate	AZ80	5	300	0.2	1 0.1

5.1 Flash Geometry

During a closed die forging process, a necessary by-product is flash. Flash is excess metal that is squeezed out of the die cavity from the edges of the component geometry, during the forging operation. The flash is scrap and is trimmed off the finished forging after it is complete. For a complex forging process, the flash can account for as much as 10% - 50% by volume of the final component [55]. Based on the personal communications with Ron Champagne at Multimatic Inc (private communication, Feb 2017), 30% flash is an acceptable target based on their experience with forging aluminum.

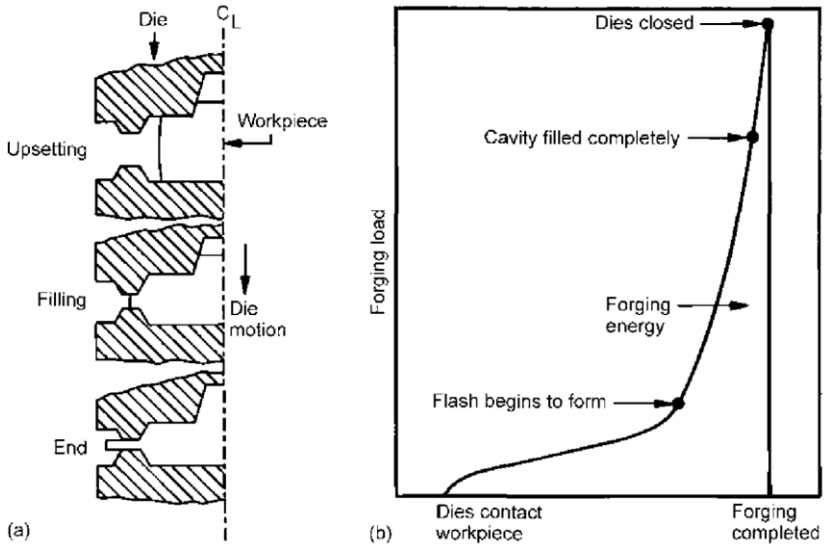

Figure 5.1-1: Typical axisymmetric forging sequence and load profile for forging process [55].

A simple axisymmetric forging process is illustrated in Figure 5.1-1. As can be seen, the initial load is very low as the billet is being deformed during the upsetting phase. The material starts to flow sideways, but in order to achieve complete die fill (force material into the cavities), this sideways material movement must be restricted. This restriction is achieved using a small gap, by having a flash land at the parting line of the part. Figure 5.1-2 shows a schematic of a forging, including the flash that forms and the flash land. As the dies closes, some material is extruded into the gutter through the flash land. As the gap between the dies decreases, it becomes more difficult for material to flow into the gutter through the flash land, thus increasing the pressure inside the die cavity. This is a result of increased friction, restriction, and other forces [55]. It is this increased pressure that forces material to flow into the die cavities. As this is happening, the forging load keeps increasing, reaching its peak after complete die fill is achieved, when the only option for material flow is across the flash land.

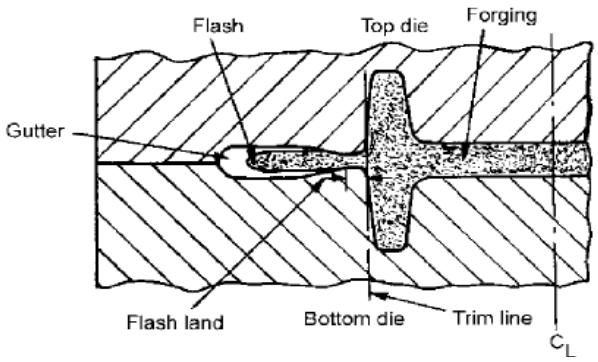

Figure 5.1-2: Schematic of a forging operation showing the flash formation [55].

Selecting a suitable dimension for the flash land is critical for the forging process. A poor choice can lead to incomplete die fill or excess forging load. Increasing the flash width increases the press load and the pressure inside the die. Yu selected 11.6 mm as the flash land width for the I-beam forging specimen [24]. In order to explore the effect of flash width, the author studied different flash land widths for the I-Beam. Simulations were conducted for ZK60 @ 450 °C at 1/s. The flash width was varied from 11.6 mm, shown in Figure 5.1-3, to 5 mm and 2 mm.

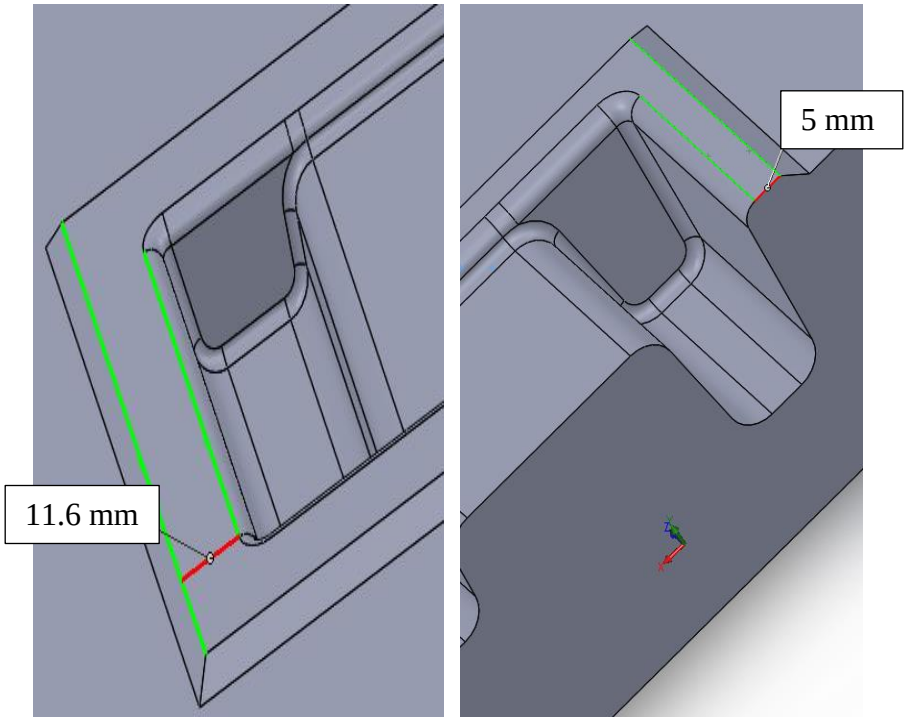

Figure 5.1-3: Schematic showing I-beam flash width changes from 11.6 mm to 5mm.

As expected, the load decreases as the flash width decreases. This can be seen in Figure 5.1-4 below. The maximum forging load for 11.6 mm flash width was around 10,000 N, but decreased to around 3,000 N for a flash width of 5 mm, and 1,800 N for a flash width of 2 mm. However, for a flash width of 2 mm, the die was not completely filled, as can be seen in Figure 5.1-5. The geometry of the final control arm is not as extreme as in the I-beam. The ribs are taller and narrower in the I-beam geometry, making it harder to fill compared with the control arm design. It was therefore decided to use a flash width of 5 mm for the final control arm forging to minimize the press load while still achieving complete die fill.

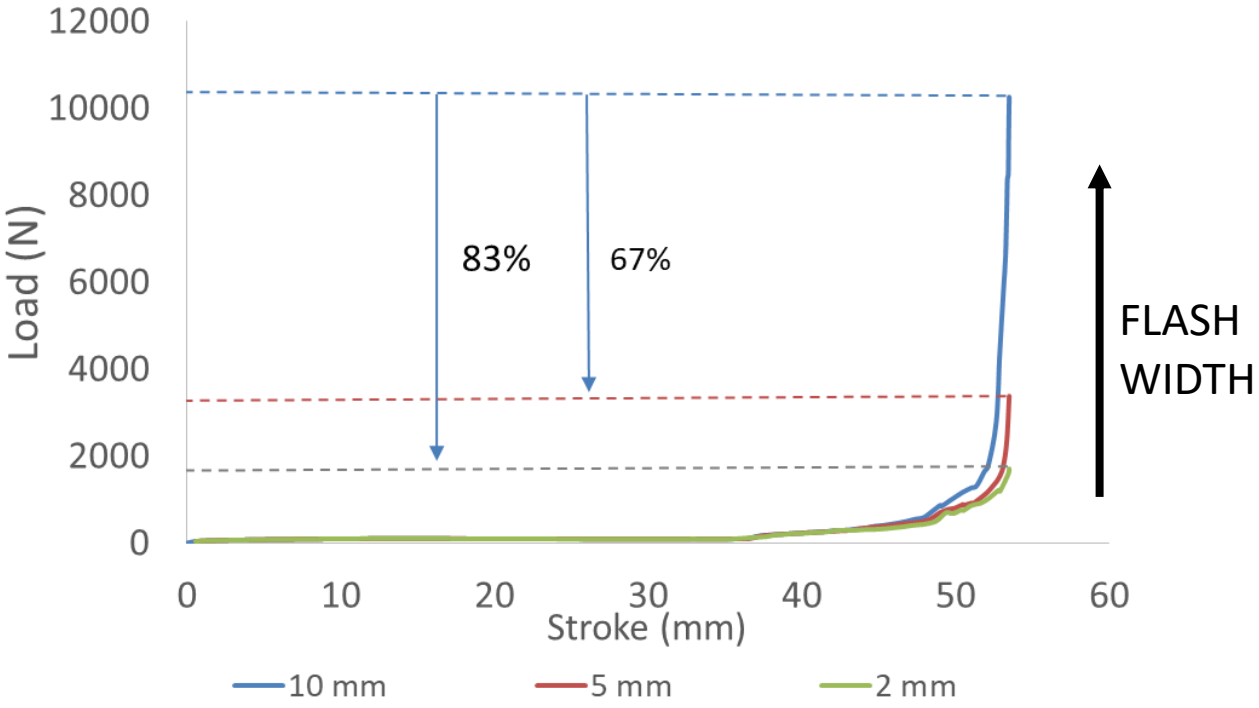

Figure 5.1-4: Model-predicted load Vs stroke graph for different flash width for an I-beam forging.

FLASH WIDTH 2 MM

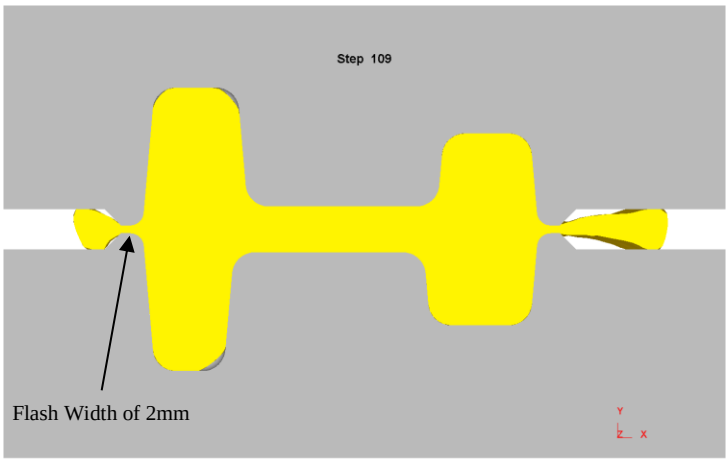

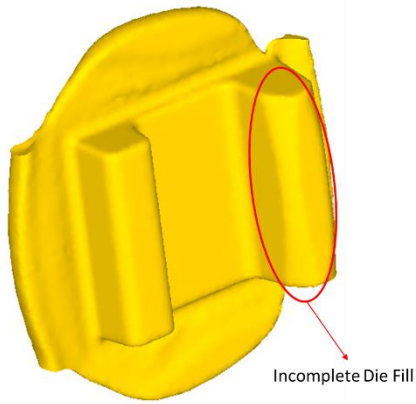

Figure 5.1-5: Final I-Beam simulation for flash width of 2 mm.

5.2 Temperature

Magnesium alloys, due to their HCP crystal structure and limited active slip systems, have poor workability at room temperature. Additional slip systems become active as the temperature increases above 250 °C, increasing its workability [10][11]. The Gleeble 3500 machine available at the University of Waterloo was used to perform uniaxial compression tests at 0.001/s, 0.01/s, 0.1/s and 1/s strain rate at temperatures ranging from 300 ^{o}C to 500 ^{o}C by the forging group [49][50]. This measured data was taken and processed for input into DEFORM 3D to represent the material constitutive behaviour during forging. Figure 5.2-1 below shows the resulting flow curve‘s for AZ80 at 350 ^{o}C and 400 ^{o}C at a strain rate of 1/s.

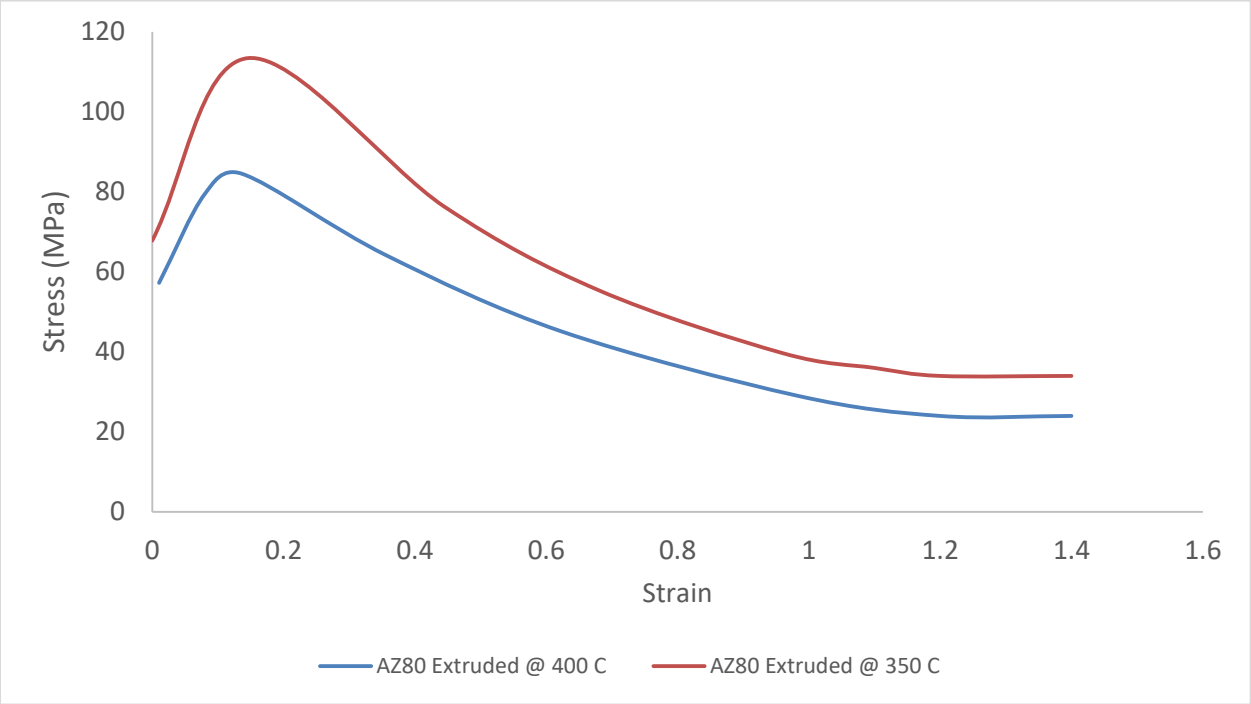

Figure 5.2-1: AZ80 flow curves input for DEFORM 3D at 350 ^{o}C & 400 ^{o}C @ 1/s [49].

As can be seen in the Figure 5.2-1 the stress decreases as the temperature increases. A decreasing trend in stress value after a threshold strain can be seen in Figure 5.2-1. This reduction in stress with increase in strain is associated with dynamic recrystallization [49]. As the material completely recrystallizes, a steady stress value is achieved. The steady stress value at 350 ^{o}C at 1/s was 34 MPa, decreases to 25 MPa at 400 ^{o}C at 1/s, a decrease of approximately 40%. This implies a 40% reduction in forging load.

A bent cylindrical preform billet was used to perform the forging simulation to analyze the effect of temperature. The simulation was performed on AZ80 in the isotropic condition, using a friction coefficient of 0.2, and a temperature of 350 ^{o}C or 400 ^{o}C. As expected, the maximum forging load decreases as the temperature increases, as seen in Figure 5.2-2. The load decreased from 4820 tonnes to 2270 tonnes, which is approximately 50% lower. Complete die fill was achieved at both temperatures. The difference between the flow stresses at a strain of 1 was 40% compared with the 50% difference in the forging load. This larger difference observed in the forging load can be due to the fact that difference between the flow curves at less than 1% strain is more than 40%.

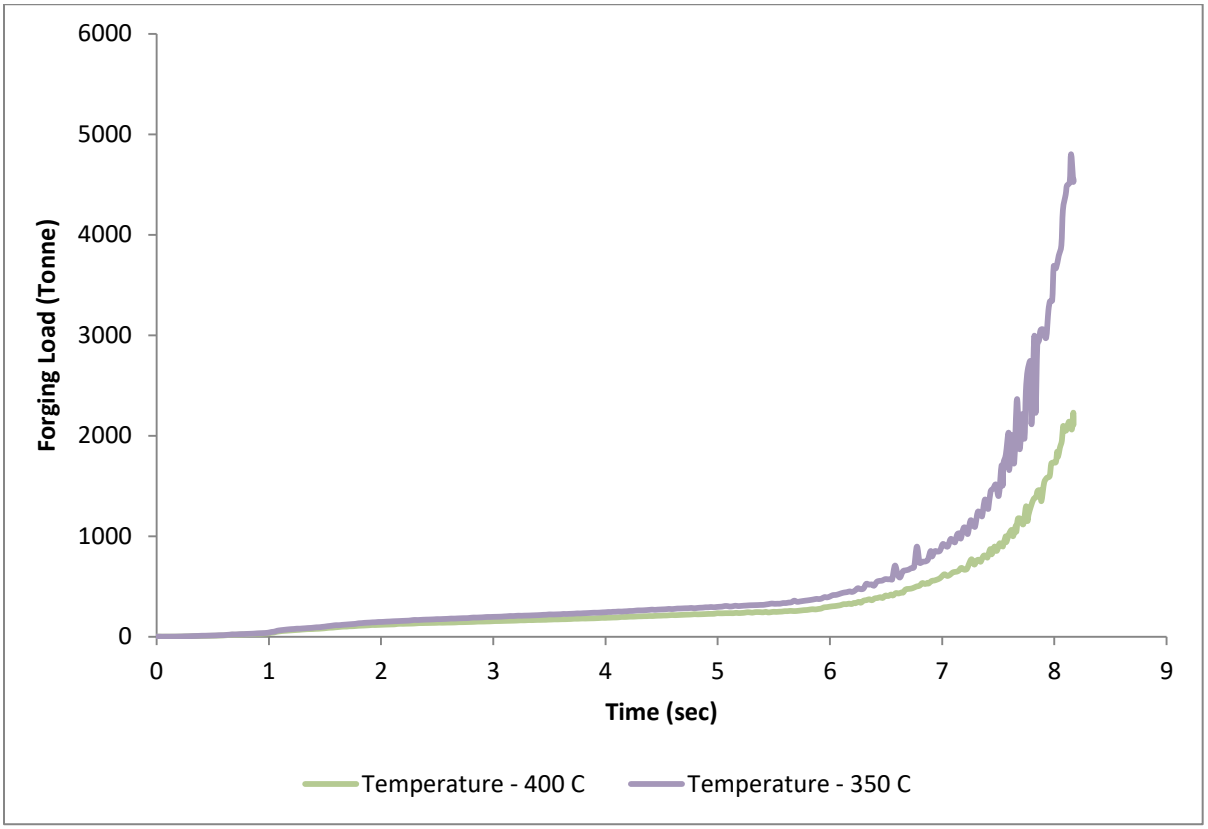

Figure 5.2-2: Load vs time for AZ80 at 350 ^{o}C and 400 ^{o}C.

5.3 Effect of Friction Coefficient

As the material deforms during the forging process due to the forging load, the material starts to flow and friction becomes significant. The friction between the die and the forging material plays an important role in determining forging load, die stress, and wear. Friction needs to be properly characterized in order to predict the forging load accurately and model the effect of different lubricants. In 1956 Kunogi [56] developed a ring compression test to be used to develop maps of friction factor for a forging process; this was further developed by Male and Cockroft [57]. The ring-shaped specimen is compressed, and the effect on the inner diameter is used to estimate the friction factor.

During this project, ring compression tests were performed at CanmetMATERIALS using the 500-ton hydraulic press and simulations were performed by Yu [24] using DEFORM 3D. All experiments and simulations were carried out under an isothermal temperature of 400 °C, and at a strain rate of 10 mm/min or 400 mm/min. Two different types of lubrication, graphite or boron nitride, were applied to the samples before heating them up to 400 ºC. In the simulations performed by Yu [24], the material AZ31 was assumed to be full plastic and isotropic, and a Coulomb friction coefficient from 0 to 1 in increments of 0.1 were used. The results obtained by Yu [24] are shown in Figure 5.3-1 and Figure 5.3-2 below.

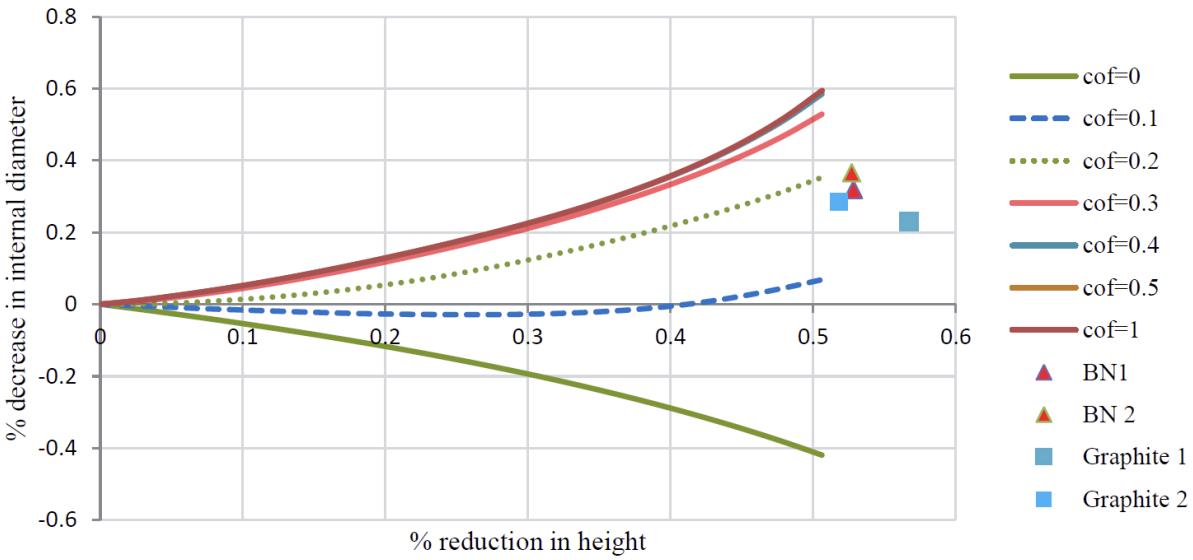

Figure 5.3-1: Calibration curves at 10 mm/min for AZ31 [24].

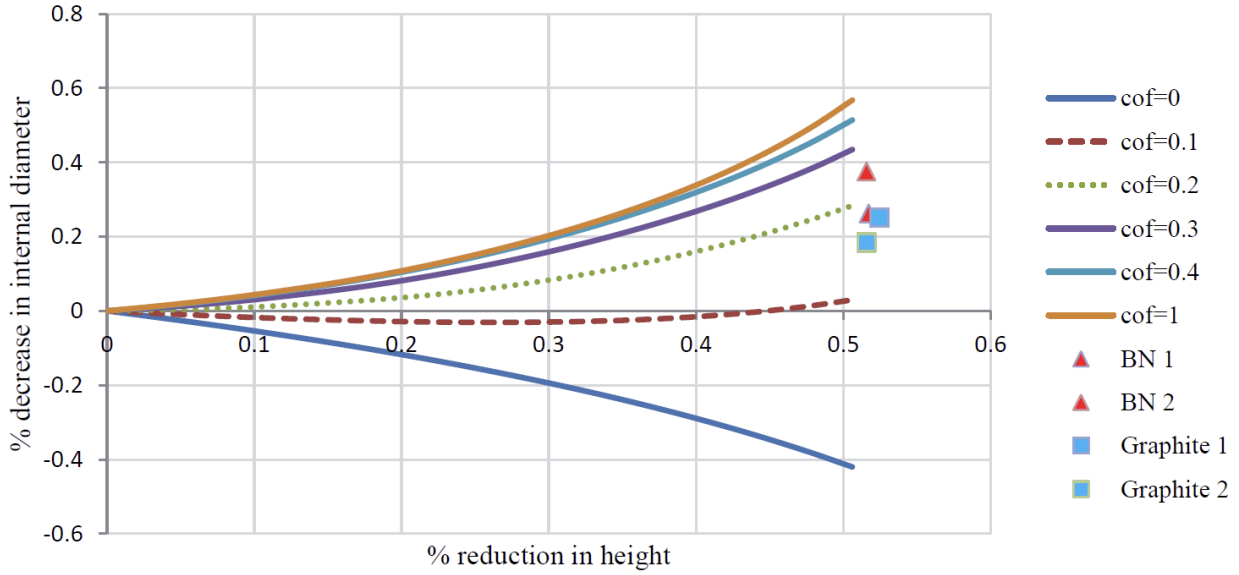

Figure 5.3-2: Calibration curve at 400 mm/min for AZ31 [24].

Graphite lubricant was selected for use in the actual forgings due to its ease of use and effectiveness. Graphite was also the cheapest option. By comparing his simulations with the experimental results, Yu concluded that the best friction coefficient to use for the model simulation was 0.2.

Friction between the work piece and die can play an important role in achieving die filling and determining press load. Based on this, it was decided to perform a sensitivity analysis for the friction coefficient for the control arm forging. The friction coefficient was varied from 0.05 to 0.3, while keeping other forging parameters, such as ram speed, temperature, material, and preform geometry, constant. The simulations were done using the anisotropic material model for AZ80, extruded at 400 °C at 8 mm/sec, using a bent cylindrical preform. As expected, there was a correlation between the coefficient of friction and the press load. As shown in Figure 5.3-3, the load decreased as the friction coefficient was decreased.

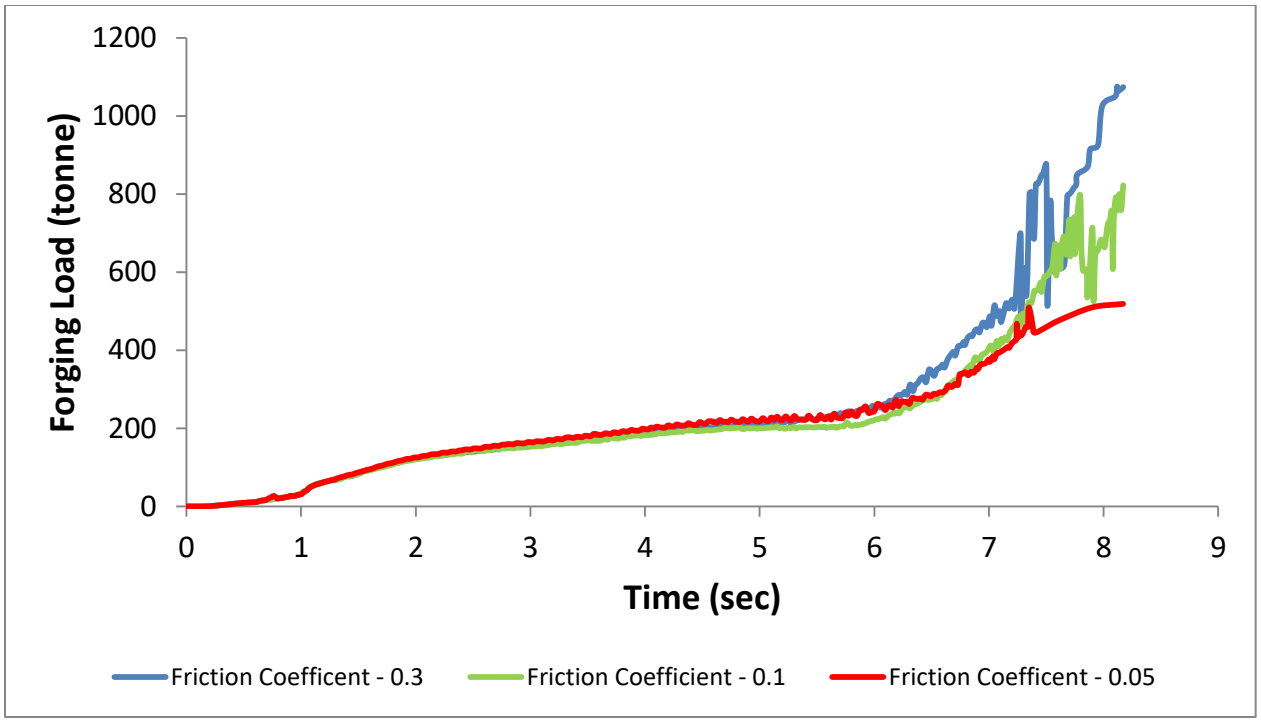

Figure 5.3-3: Model predicted load vs time for different friction coefficients for AZ80 @ 400º C at 8 mm/sec.

The forging load was 1200 tonnes for a friction coefficient of 0.3, decreased to 800 tons when the friction coefficient was changed to 0.1, and further decreased to 500 tons when the coefficient was further reduced to 0.05. Complete die fill was achieved for all friction coefficients except for a friction coefficient of 0.05, for which the die was not filled completely, as can be seen in the Figure 5.3-4.

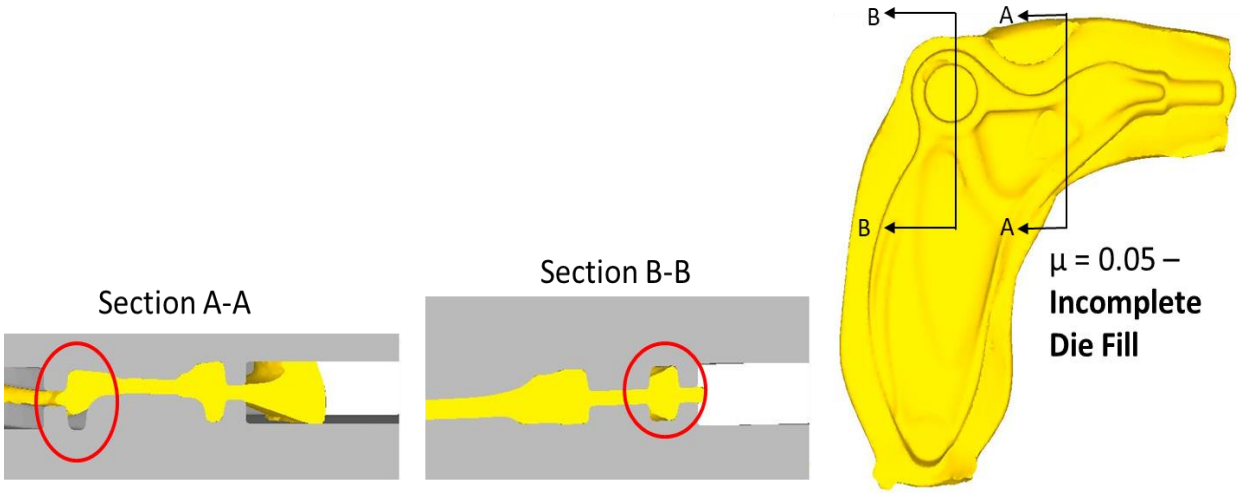

Figure 5.3-4: Simulation results for AZ80 @ 400 ºC at 8mm/s with friction coefficient of 0.05.

As can be seen, reducing the friction coefficient can reduce the forging load, but reducing it too much results in incomplete filling of the die based on previous testing. No attempt was made to modify the friction coefficient in the actual forgings.

5.4 Ram Speed

As can be seen in Figure 5.4-1 below, for AZ80 @ 300 ºC at a strain rate of 1/s and 0.1/s, the flow stress decreases as the strain rate is decreased. A simulation was performed with AZ80, in the isotropic condition, @ 300 ºC for two different ram speeds: 8 mm/sec or 1 mm/sec. For each ram speed, an average strain rate was calculated: the average strain rate at the end of the simulation across the whole specimen resulting from that ram speed. The ram speed of 8 mm/sec results in strain rate of 1/sec and the ram speed of 1 mm/sec result in a strain of 0.1/sec.

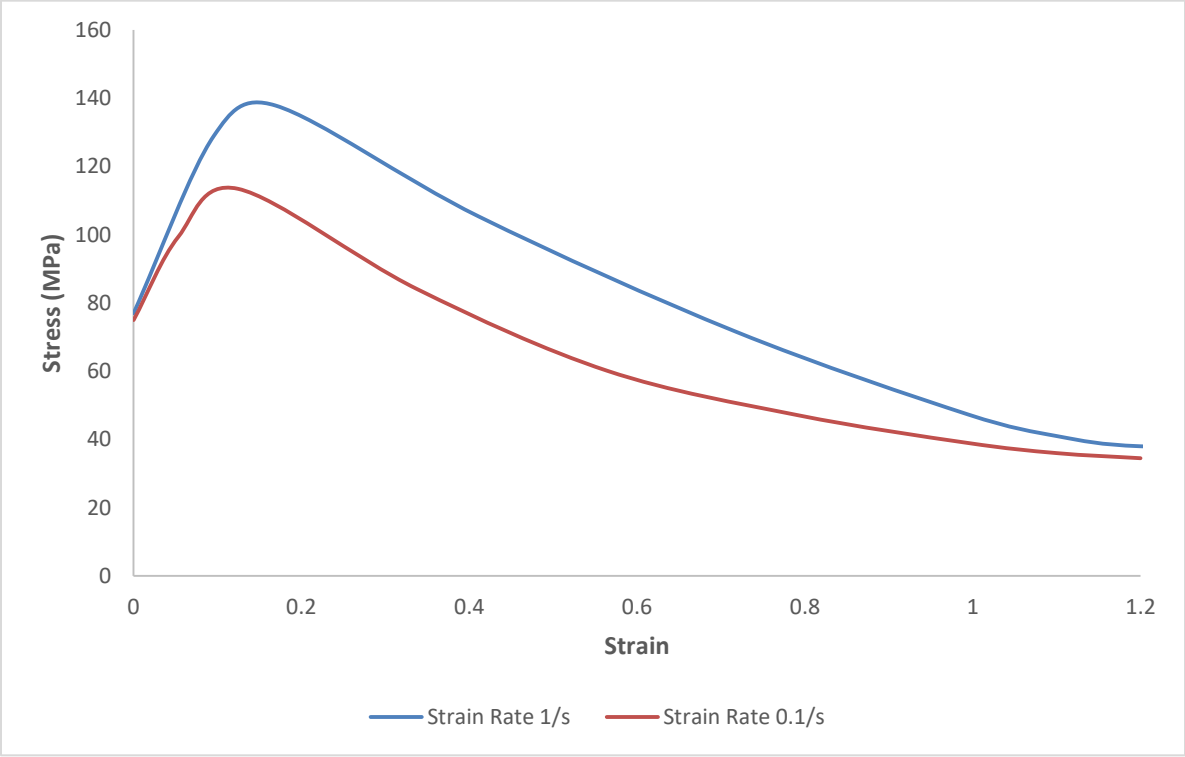

Figure 5.4-1: Extruded AZ80 flow curve @ 300 ºC [49].

It can be seen in the Figure 5.4-2 that reducing the ram speed results in reduction of forging load. The flow stress at strain of one is 38 MPa for strain rate of 1/sec and 34.5 MPa for the strain rate of 0.1/sec, a difference of 10%.

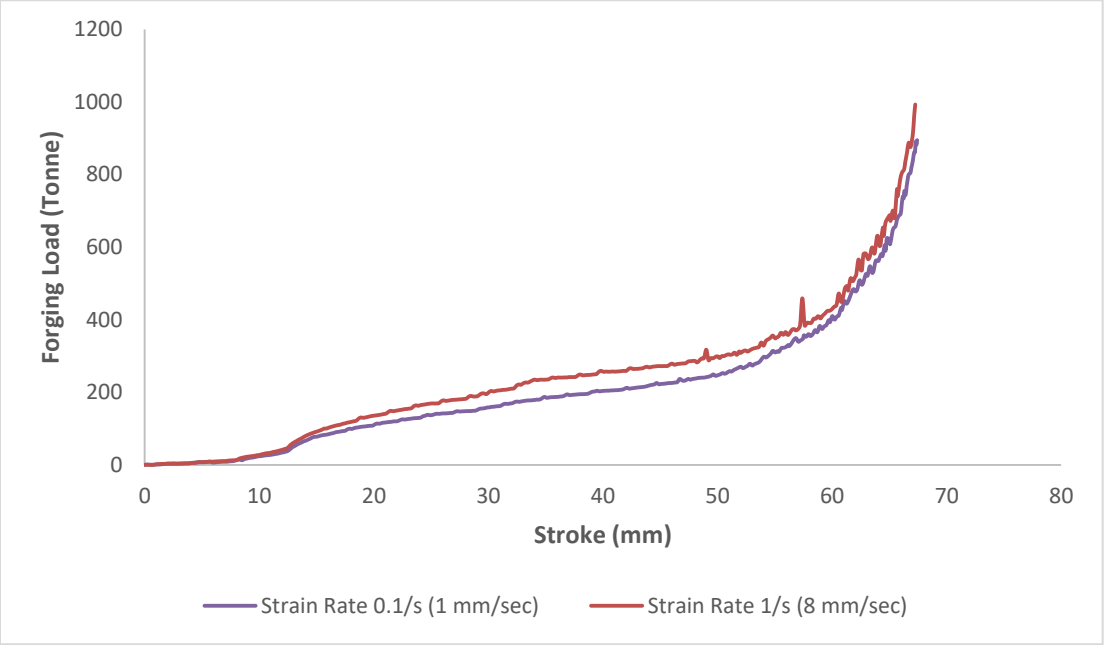

Figure 5.4-2: Simulated forging load - AZ80 at 300 °C with different ram speed.

On the other hand, forging load is reduced from 994 tonnes to 900 tonnes by changing the ram speed from 8 mm/sec (strain rate of 1/sec) to 1 mm/sec (strain rate of 0.1/sec).The difference of 10.4% in forging load compared to a 10% reduction in flow stress by reducing the strain rate. This implies a linear relationship between strain rate and forging load for the strain rates considered.

Chapter 6 Preform Design

A preform is the billet that is forged in single or multiple steps to achieve the final shape. According to the literature [55], the single stage forging process is rarely used in industry because of the large amount of flash produced to achieve complete die fill, and the large press load. Usually, multiple forging steps are used to bring the stock billet into the shape of the finished product. Single step forging processes are used only for simple geometries. Figure 6-1 show the typical forging sequence for a connecting rod.

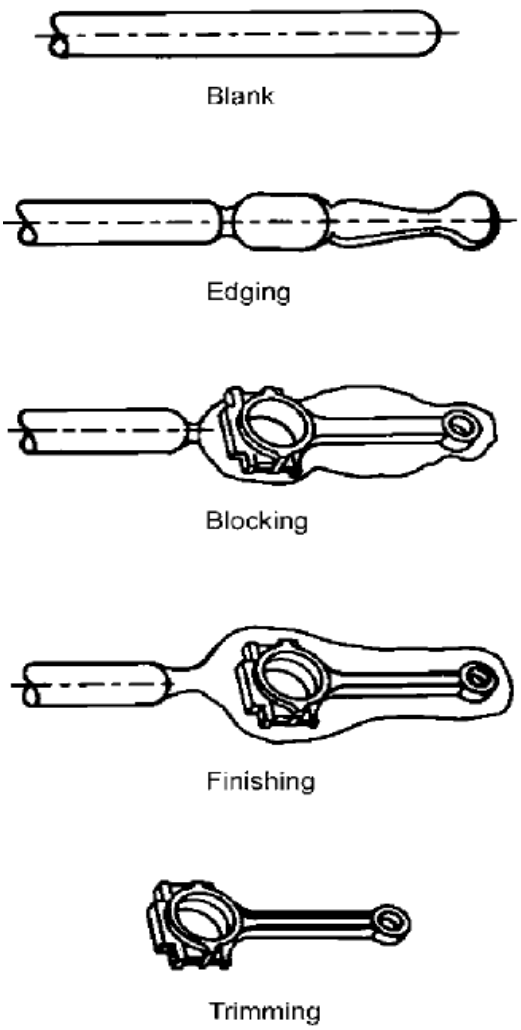

Figure 6-1: Typical forging sequence for a connecting rod [55].

It can be seen that a simple round rod was used as the starting point of the forging process for a connecting rod [55]. Further processes are carried out to distribute the material according to the final shape during the edging process. The blocking step is the last step before the final forging process. The blocking shape is usually a thicker version of the final shape with larger radii. After the final forging process, a trimming process is required to remove all the flash.

The starting point of the preform design is with the finished part geometry. A blocker geometry is then developed with thicker sections and larger radii. Usually, the final geometry is divided into multiple sections, the cross section volume for each section, including flash volume, is calculated. These are used to determine the initial billet radii for each section, as shown in Figure 6-2 [55].

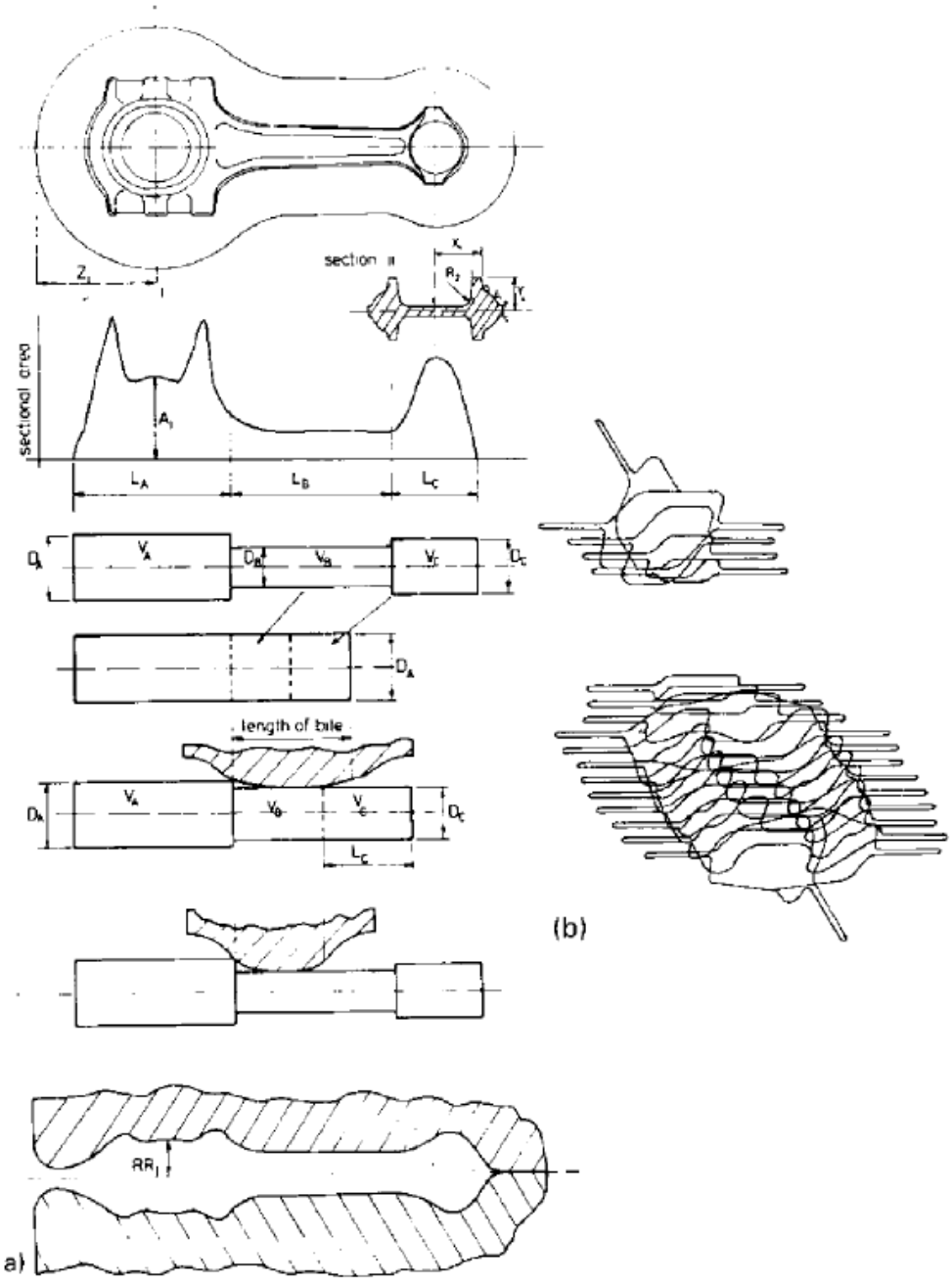

Figure 6-2: Forging sequence and billet mass distribution of a connecting rod [55].

For the control arm forging in the present work, multiple preform shapes were considered. They were evaluated for die fill, effective strain and press load.

Three major preform designs are discussed in more detail below and include: multi-section cylindrical preform, flat preform, and bent cylindrical preform. During the simulations, the preforms were dropped on the bottom die and the upper die was placed on top of the preform.

Contact was established between the upper die, lower die, and preform at the beginning of the simulation. A coefficient of friction, μ, of 0.2 was used for all simulations. The upper die travelled at a specified constant velocity towards the bottom die, forging the preform into the desired shape. The upper die was stopped when the flash thickness reached 3mm. The simulations were performed isothermally. Remeshing was activated at 0.7 of the element size. Approximately 180K tetrahedral elements, with minimum element size of 1 mm to 4.5mm, were used. Each simulation took approximately 6 to 9 hours on a desktop computer (Intel Core i7 5600U CPU @ 2.6GHz, 32GB Ram). All preform designs were evaluated using both AZ80 and ZK60 extruded material.

The anisotropic material model was used to perform all simulations. The model included a flow stress curve and Hill's coefficients as previously detailed in Chapter 4, Table 4.1-2 and Figure 4.1-3. The Hill's coefficient remain constant for a given temperature and strain rate, as this is one of the limitations of DEFORM 3D.

6.1 Multi-Section Cylindrical Billet

The first billet was designed based on the technique suggested in Chapter 14 of "Product design for Manufacturing and Assembly" [55]. In this chapter, a preform for a connecting rod was designed by first sectioning the connecting rod along its length, identifying appropriate cross sections, and bending the preform as required to get a suitable mass distribution.

Utilizing this approach, a multi-section cylindrical billet was designed for the control arm. The three major cross sections were created for the final control arm design by Kodippili, Figure 6.1-1 [54].

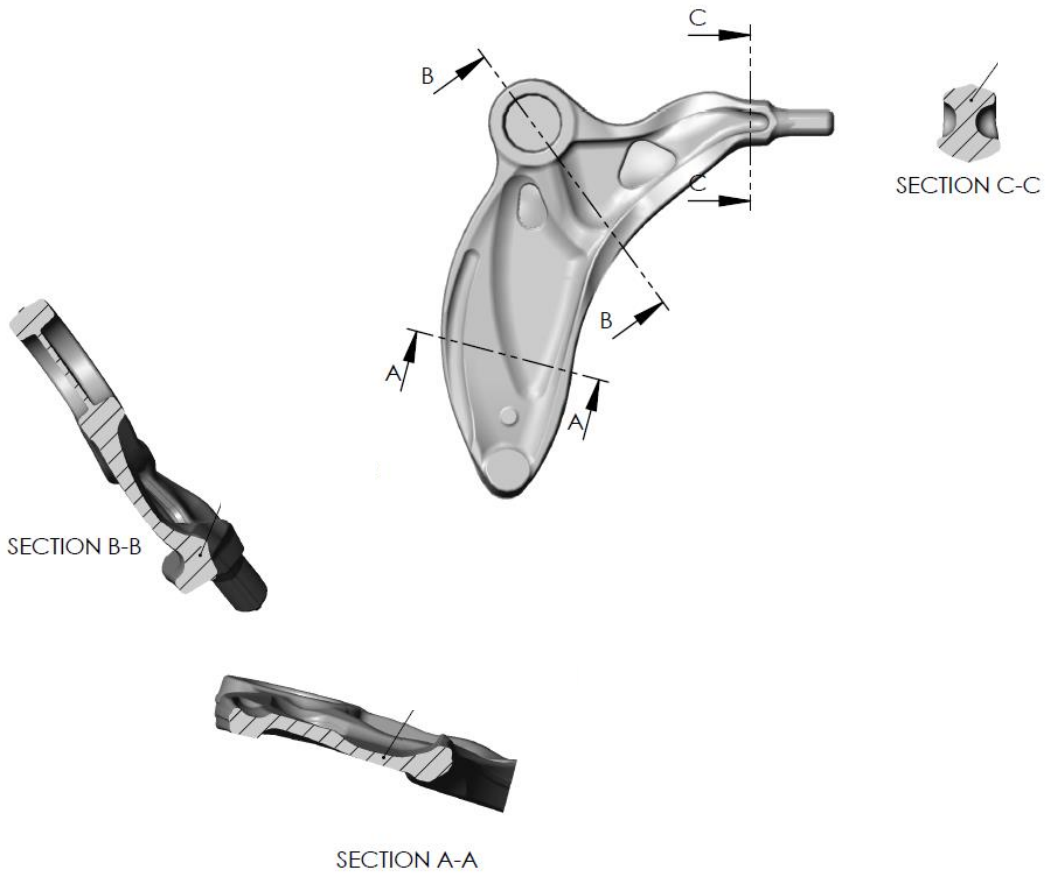

Figure 6.1-1: Key sections of the final control arm [54].

The areas in each section of the control arm were then converted into a circular cross section. The designed preform is shown in Figure 6.1-2. It has three circular cross sections, the end cross-sections have the same diameter and a larger diameter is used at the center to fill the maximum area at cross section B-B on the control arm, Figure 6.1-2. The preform was then bent to approximate the curvature of the control arm, as shown in Figure 6.1-2. The preform shape based on this technique resulted in minimal flash formation, as mass was distributed according to the cross-section of the control arm.

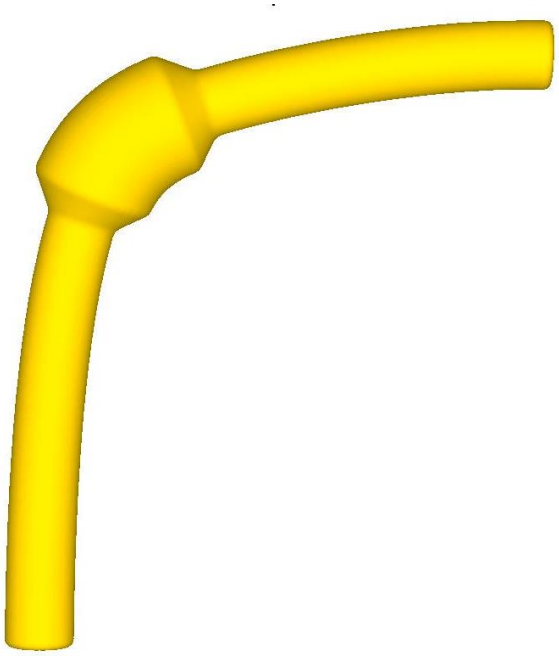

Figure 6.1-2: Multi section designed billet.

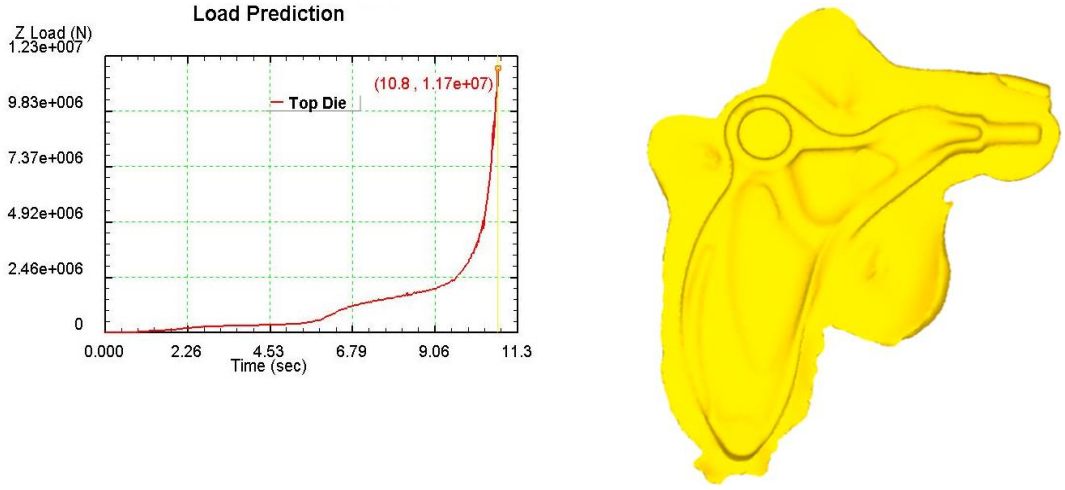

Figure 6.1-3: Shape and load vs time graph of the multi section billet for AZ80 @ 400 ºC at 8 mm/sec.

After the simulation was performed, it was observed that complete die fill was achieved. As can be seen in Figure 6.1-3, the forging load for AZ80 @ 400 ºC forged at 8 mm/sec was 1170 tonnes. This preform design completely satisfied most of the constraints for this project except for the ease of preform manufacturability. After multiple discussions with design engineers at Multimatic Inc, it was determined that this shape could be achieved by passing the billet through a sequence of rollers and then using a bending operation. This is not feasible for the few samples required for

this research project. Therefore, this design was not considered further for this project. This might be a viable option for a normal production run.

6.2 Flat Plate Billet

Considering the cost associated with preparing a multi-section cylindrical billet, other preform shapes were considered. One of the options considered was a flat plate billet. This could reduce manufacturing cost while still minimizing flash. The idea behind the flat plate billet was to design a shape that somewhat resembled the final shape so that it could be forged into the final shape without too much force required and could easily be machined out of a flat plate.

After several iterations of the design and multiple simulations, a final shape was achieved, Figure 6.2-1. Detailed drawings are shown in Appendix B. The flat plate billet had a volume 130% of the final control arm.

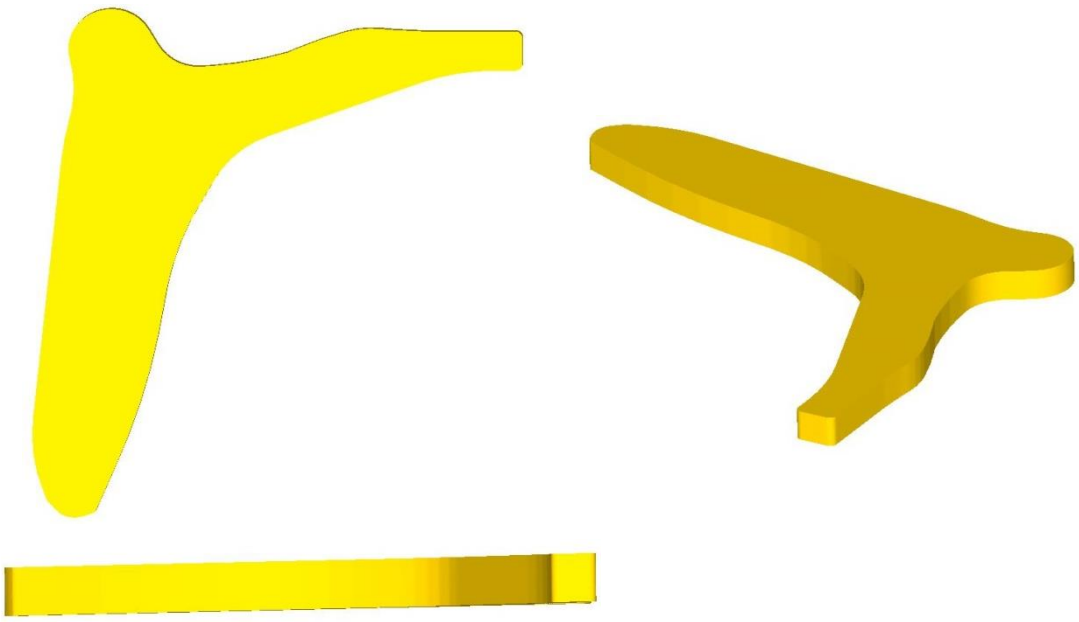

Figure 6.2-1: Flat plate billet.

The final forged shape can be seen in Figure 6.2-2. The load and effective strain are shown in Figure 6.2-3 and Figure 6.2-4, respectively.

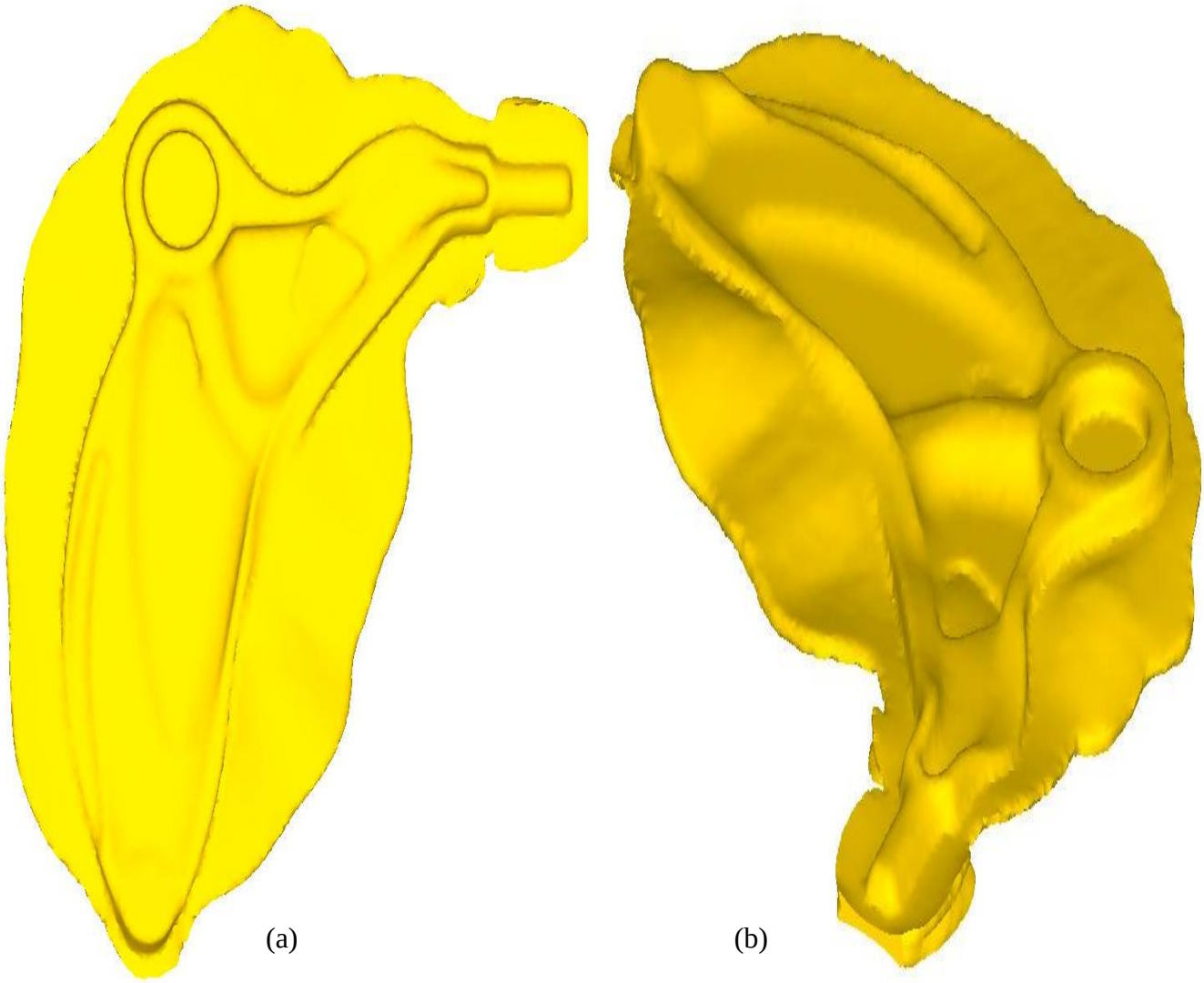

Figure 6.2-2: Forged shape for the flat plate billet - AZ80 @ 400 ^{o}C using 8 mm/sec, (a) front (b) back.

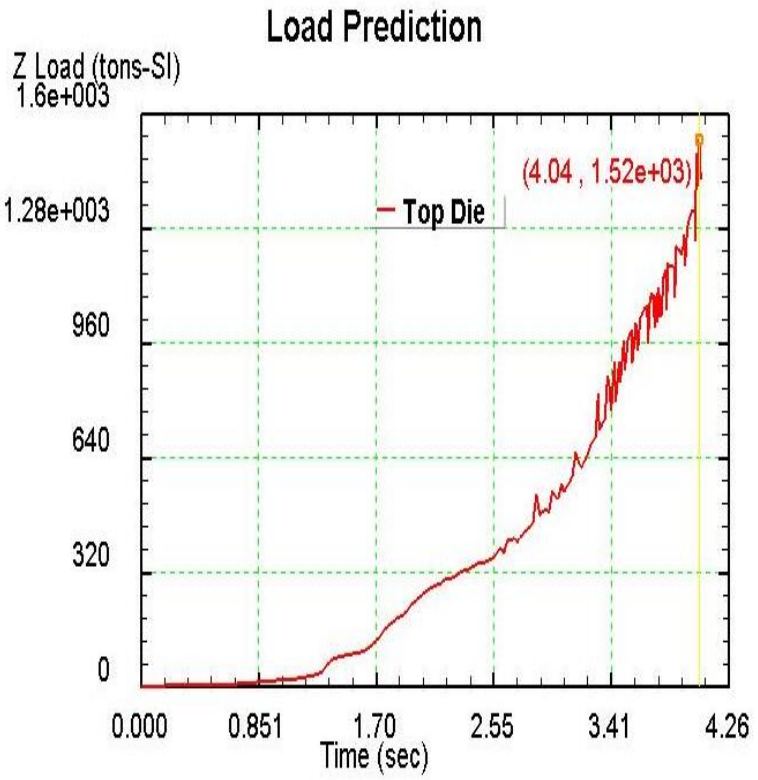

Figure 6.2-3: Load vs time graph for flat preform using AZ80 @ 400 °C at 8 mm/sec.

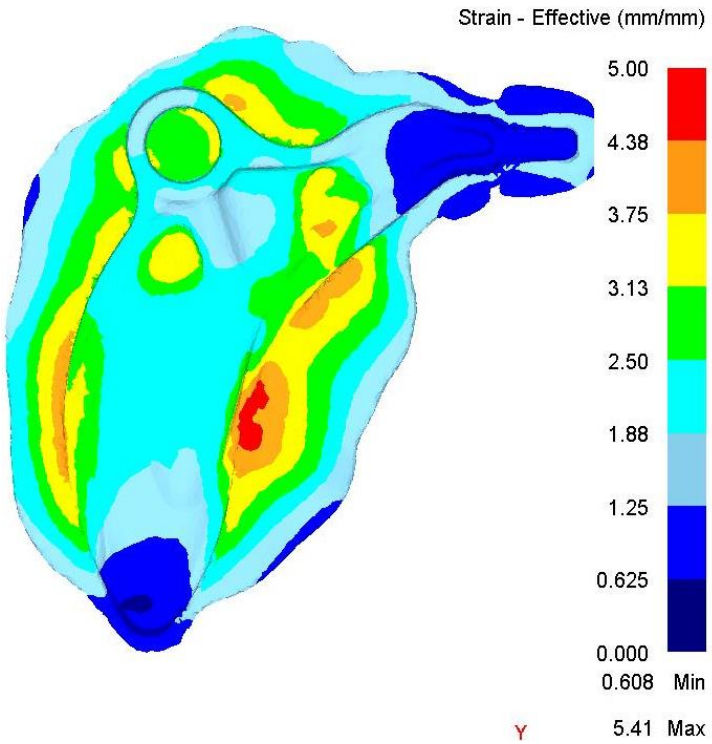

Figure 6.2-4: Effective strain for forged flat preform using AZ80 @ 400 °C at 8 mm/sec.

As can be seen from Figure 6.2-3, the load for the flat billet was around 1500 tonnes. The flat billet met most of the constraints set out for the project (Chapter 5) except for two issues. Since the shape of the preform closely resembled the final forged shape, insufficient deformation was induced during forging. This resulted in insufficient induced strain in critical control arm regions. After performing multiple testing on the forged I–beam specimens [16][19], it was determined that minimum effective strains needed was 125% to achieve acceptable forged properties, especially in critical regions. As can be seen in Figure 6.2-4, the effective strain was below 125% in the bushing and ball joint areas.

After performing further research and talking with Luxfer MEL Technologies, the supplier of our magnesium alloys, it was determined that a flat rolled sheet with the dimensions required to machine this shape was not readily available. This configuration was therefore dropped from further consideration in this project.

6.3 Bent Cylindrical Billet

Another option that was considered was to use a simpler bent cylindrical billet. After further detailed discussions regarding preform design within the research group, it was decided to design a preform that can be more easily formed while still minimizing flash. However, due to the small number of samples to be forged during this research, it was decided to give less weight to flash minimization.

A bent cylindrical preform was selected, and the specific geometry chosen based on engineering judgement and a series of simulations, as shown in Figure 6.3-1.

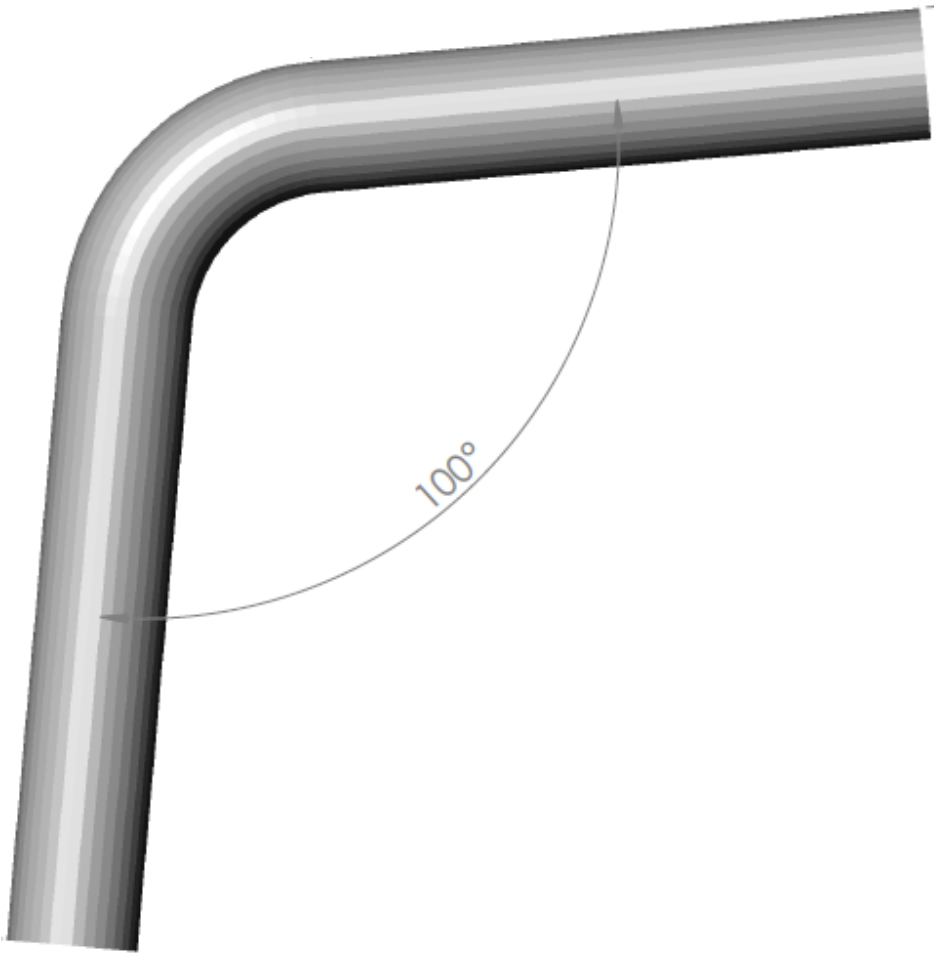

Figure 6.3-1: Bent cylindrical preform.

It was decided to use a diameter of 63.4 mm for the cylindrical preform as this was readily available from Luxfer MEL Technologies. In order to perform simulations, a solid model of the bent billet was created with a bend angle of 100°. Load, effective strain, and damage graphs are shown in Figure 6.3-2 and Figure 6.3-3 for extruded AZ80 at 400 ºC and 8 mm/s.

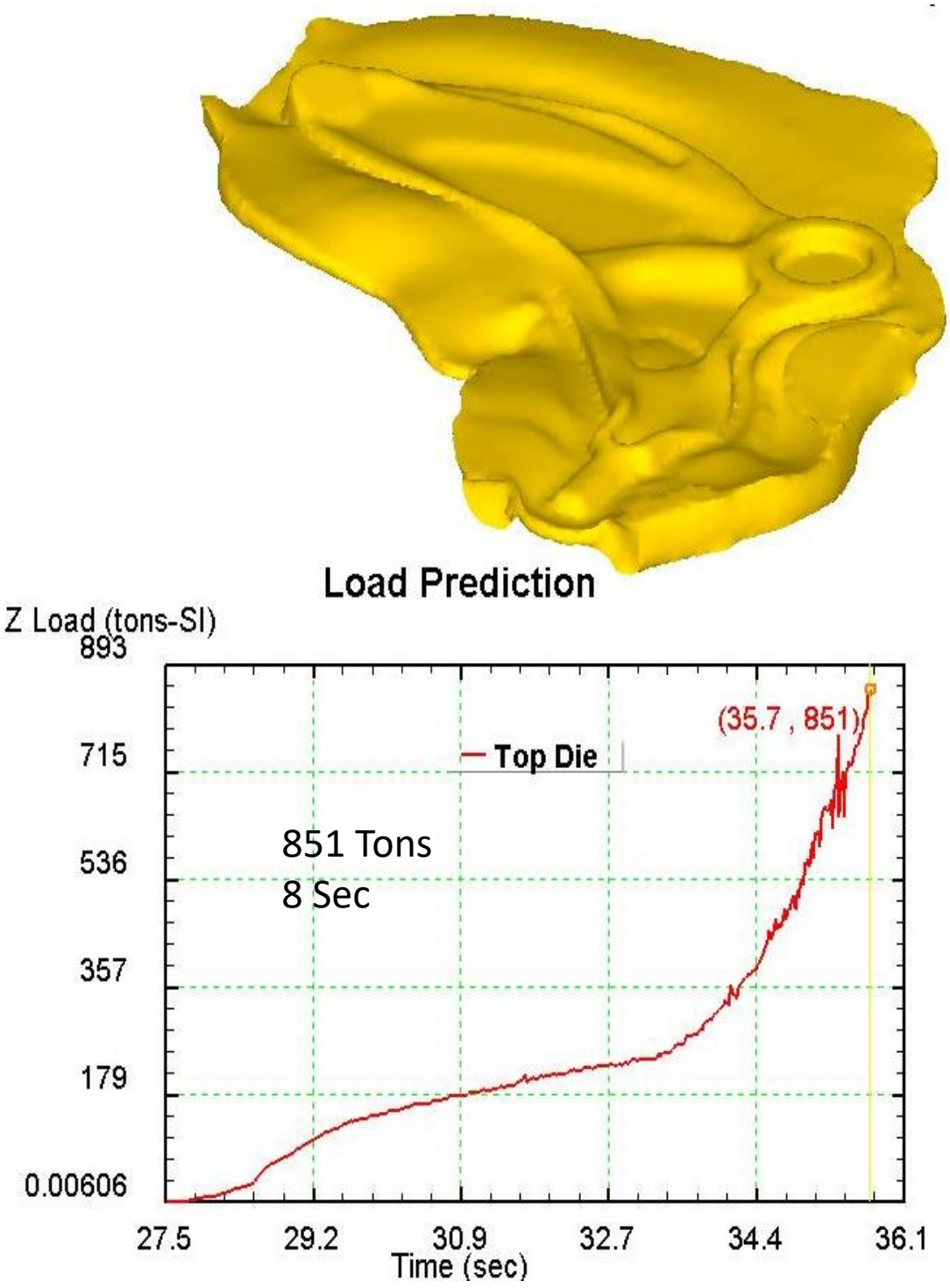

Figure 6.3-2: Load graph for cylindrical billet for extruded AZ80 @ 400 °C at 8 mm/sec.

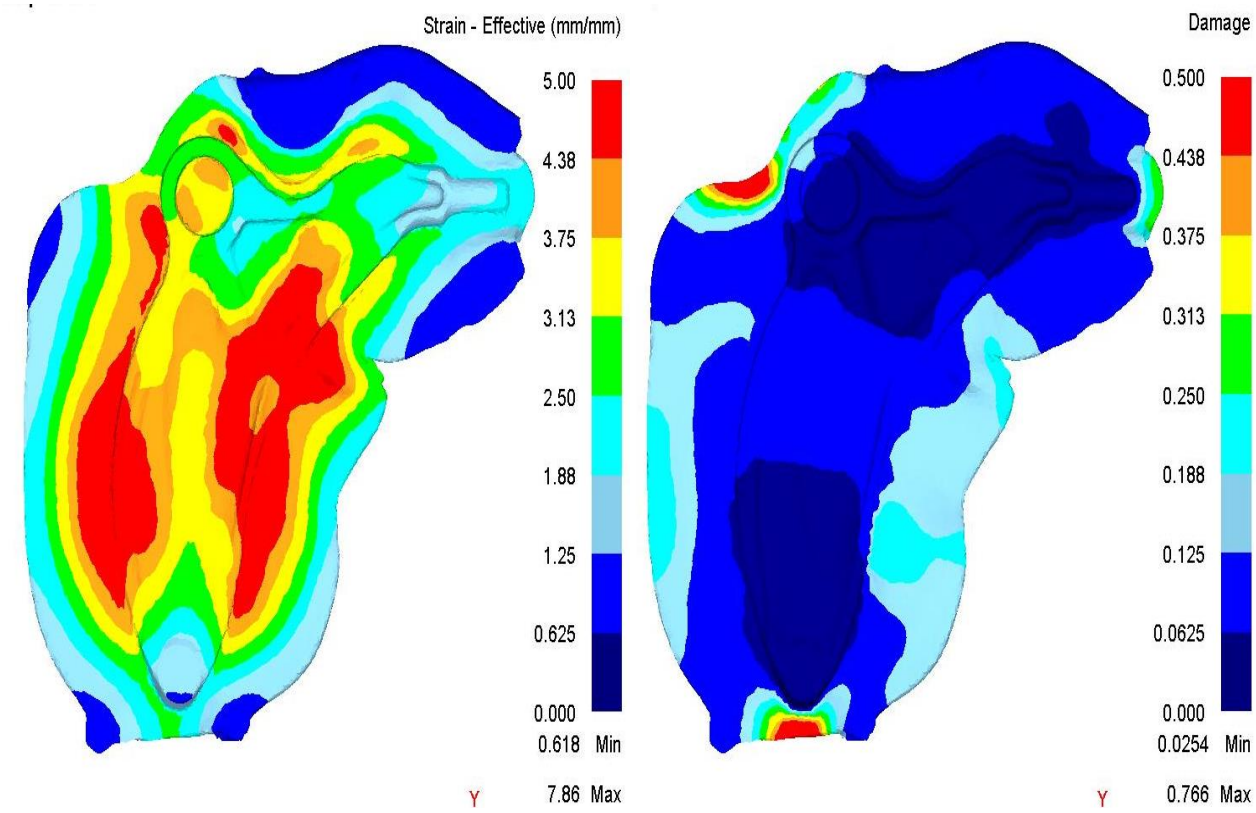

Figure 6.3-3: Model-predicted effective strain and damage distribution for extruded AZ80 @ 400 ºC at 8 mm/s.

As can be seen in Figure 6.3-2, the maximum predicted load for the bent cylindrical billet for extruded AZ80 at 400 ºC at 8 mm/sec was 850 tonnes. The forged billet also met the minimum effective strain criteria. The minimum strain in the critical area such as bushing was observed to be around 188%, more than the minimum acceptable value. The damage value in the forged specimen was below 0.125, as can be seen in Figure 6.3-3, which is below the value for crack initiation (0.5). The cylindrical billet satisfied all the project constraints, but there was significant material lost in the form of flash: 250% versus the 30% desired. This was deemed acceptable for the project, and different preform designs or machining the ends could be done to improve this situation for production.

6.4 Final Preform Design

6.4.1 Comparison & Selection

As mentioned in the previous section, there were multiple design constraints in this project. The preforms were designed and analysed against these constraints. Some of the constraints included:

1) The forging operation would be performed with a single closed die using one stroke.
2) The maximum load during forging was 1500 tonnes, which corresponded to the CanmetMATERIALS press to be used for the forging.
3) The preform shape should be simple and easy to form from the extruded magnesium cylinders available.
4) After forging, the control arm should not show any evidence of under-filling in any locations, or damage, and the effective strain in critical areas needed to be greater than 125%.

6.4.2 Preform Geometries Considered (Summary)

Many different preform geometries were considered during the project taking these constraints into account. From this, three preform geometries were considered and discussed in subsequent sections. These preform geometries included: 1) Multi-section cylindrical preform, 2) flat plate preform, and 3) Bent cylindrical preform, as shown in Figure 6.4-1.

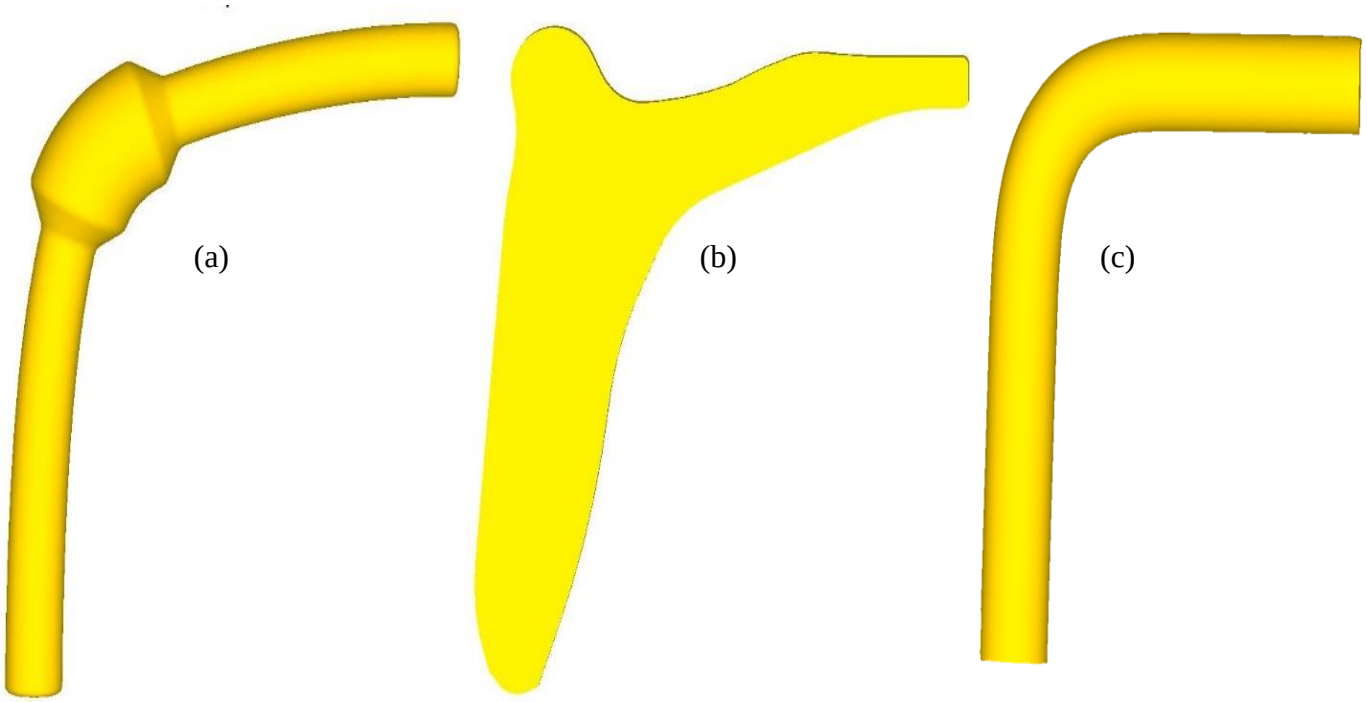

Figure 6.4-1: Different preform geometries. (a) Multi-section cylindrical preform, (b) Flat plate, (c) Bent cylinder.

A multi-section billet, with optimized material distribution was the first preform considered. It met most of the project criteria the load was less than 1500 tonne, completely filled the die and optimised material lost. The major drawback was the complex geometry of the preform, which required multiple manufacturing steps. The next preform considered was the flat plate. The preform shape was close to the final shape. But the simulation showed that the forging load was within limit but the effective strain was less than required. The last preformed designed was a bent cylindrical preform. The simulation showed a load within the limit. The cylindrical billet was freely available and only required a three point bending operation to achieve the desired shape. The drawback was that it was not optimised for material usage. Since only a few samples needed to be forged during this testing phase it was decided to ignore the waste of material. The preliminary analysis of these three preforms was at the beginning of this chapter (Chapter 6).

6.4.3 Detailed Analysis

A detailed analysis was performed on the selected preform. The cylindrical bent billet was created in Solid Works and imported into DEFORM 3D. The final die set model was designed and provided by Kodippili [54] and imported into DEFORM 3D. This differed from the die used in the previous section in the following ways: the dies were updated to accommodate minor changes made by Multimatic Inc to the control arm design, locating pins were added to locate the billet on the die consistently, and the gutter area was extend to the edges of the dies. The billet was placed on the locating pins of the lower die, as shown in Figure 6.4-2.

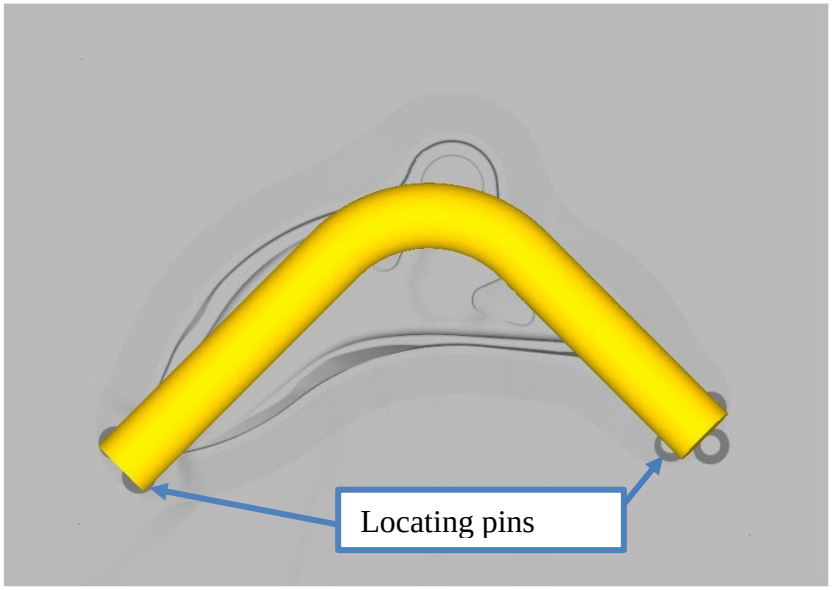

Figure 6.4-2: Bent cylinder placed on the lower die on locating pins.

The simulation setup is shown in Figure 6.4-3. The bottom and top die are considered rigid, and are shown in Figure 6.4-4 and Figure 6.4-5. In the simulation, the top die moves at constant velocity towards the bottom die, forging the control arm, until the flash thickness in the flash land area reaches 3 mm.

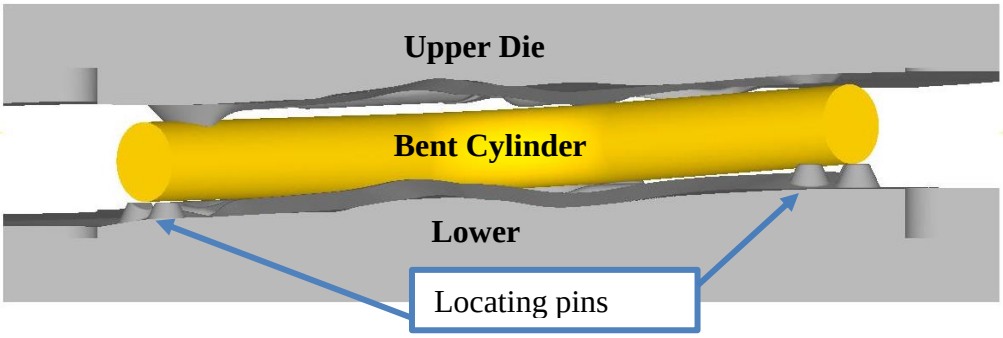

Figure 6.4-3: X-sectional view of the forging simulation setup in DEFORM 3D.

The coefficient of friction between the contacting surfaces was set to 0.2. Initially the contact was generated between the bottom die and the billet. All simulations were carried out using isothermal conditions.

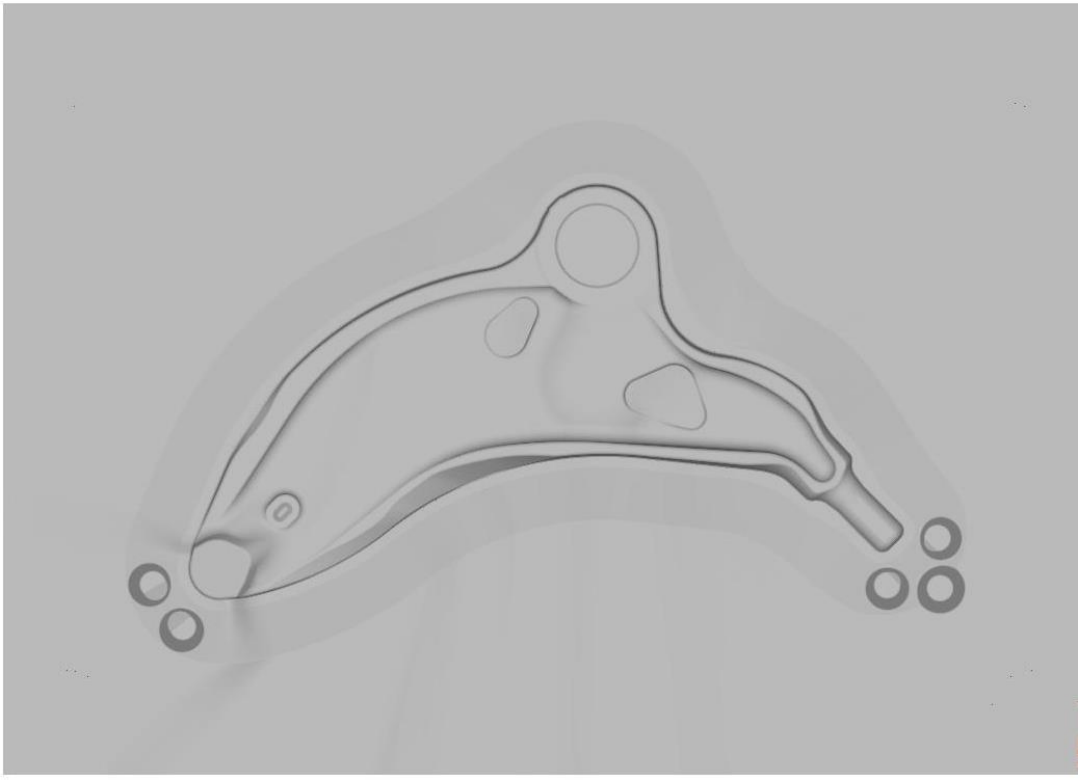

Figure 6.4-4: Lower die [54].

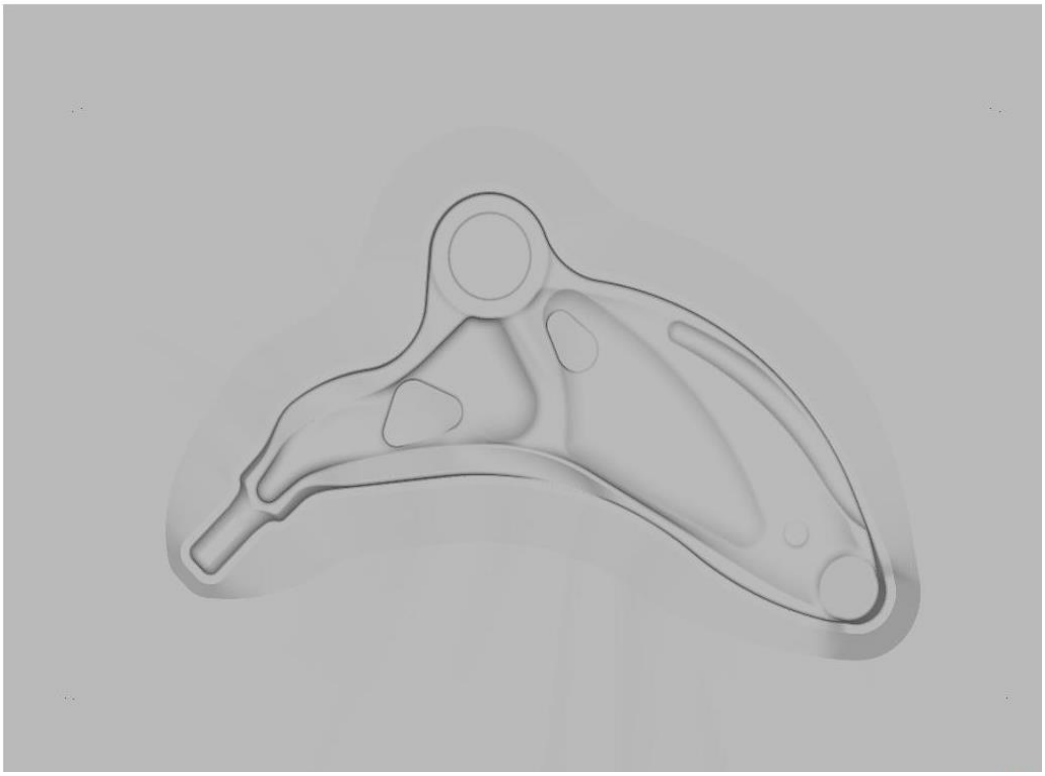

Figure 6.4-5: Upper die [54].

The bent billet was meshed with 200,000 tetrahedron elements. Due to the complex geometry of the control arm, remeshing was enabled for the distorted elements. The anisotropic material model was used. The meshed bent cylindrical billet is shown in Figure 6.4-6. Details of the numerical modelling were previously discussed in Chapter 4.

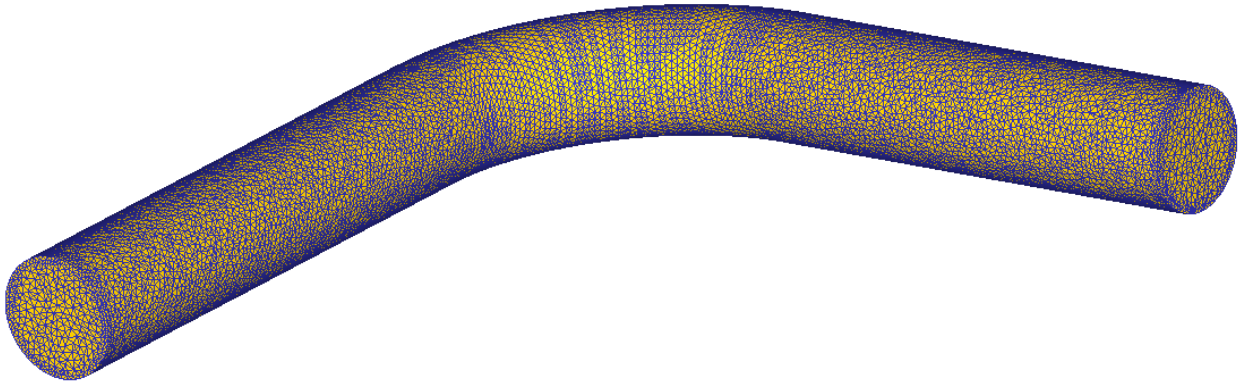

Figure 6.4-6: Meshed control arm.

6.4.4 Results

Initially, simulations were performed for AZ80 at 400 ^{o}C at 8 mm/sec.

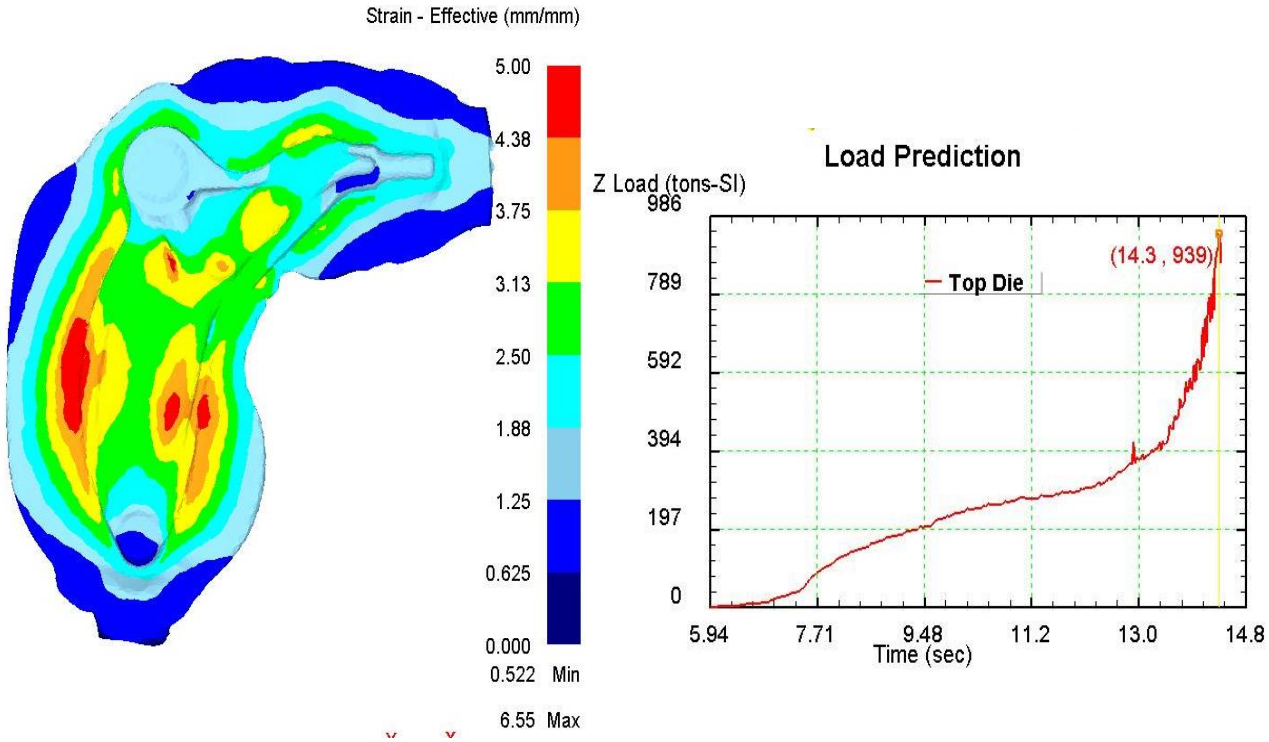

Figure 6.4-7: Simulation results of forged bent cylinder AZ80 @ 400 ^{o}C at 8 mm/sec.

The effective strain distribution and the press load are shown in Figure 6.4-7. The press load reached a maximum of 939 tonne and the effective strain in critical regions was found to be above the minimum effective strain of 125% (1.25 strain). Complete die fill was achieved, as can be seen from the contact nodes on the billet in the Figure 6.4-8. Contact nodes, shown in green, were observed over the entire control arm and the flash land, indicating that the entire area was in contact with the upper die.

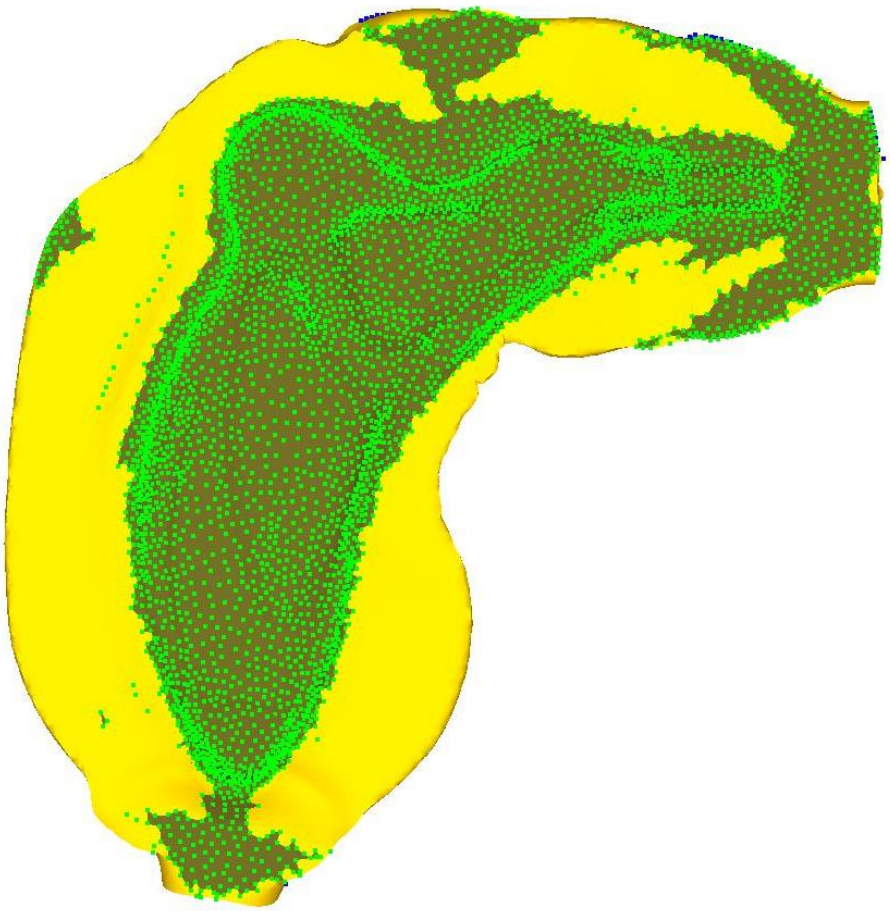

Figure 6.4-8: Simulated AZ80 @ 400 ºC - 8mm/sec contact pressure distribution.

Simulations were also performed at 300 ºC for both AZ80 and ZK60 at 8 mm/sec; these results are shown in Appendix C. The best structural and fatigue properties were achieved for these lower temperatures as per the analysis of the fatigue group [16][19] on the I-beam specimen samples previously forged [24].

Unfortunately, the predicted press loads for the control arm forged at 300 ºC and 8 mm/sec were too high: 1700 Tonne for AZ80 and 3220 Tonne for ZK60 as can be seen in Figure 6.4-9 and Figure 6.4-10 below. The equipment available for testing at CanmetMATERIALS has a maximum capacity of 1500 tonne.

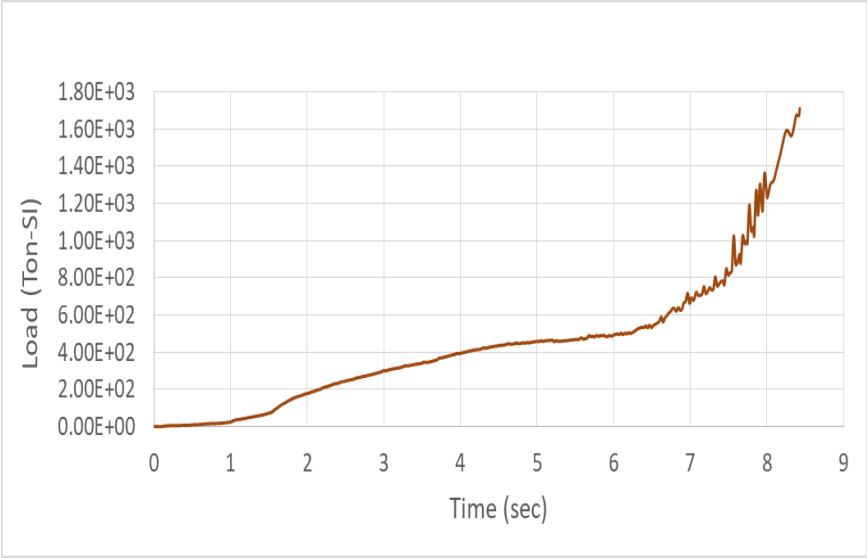

Figure 6.4-9: Simulation results for AZ80 @ 300 ºC at 8mm/sec.

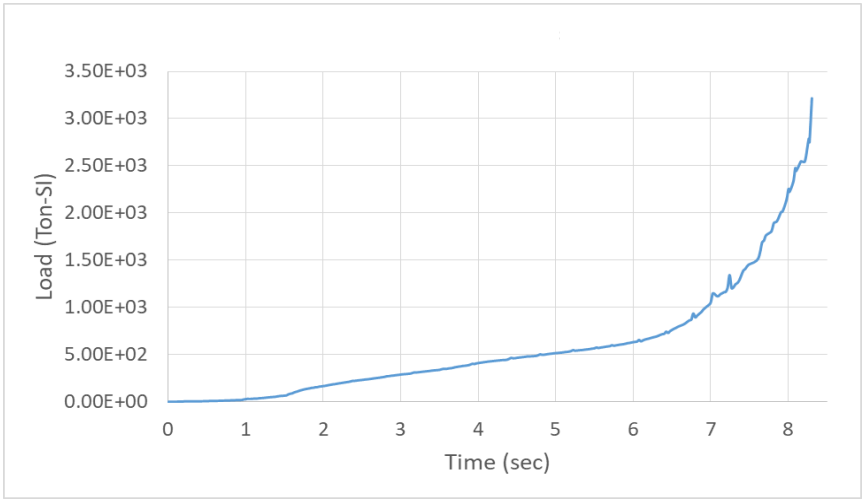

Figure 6.4-10: Simulation results for ZK60 at 300 ºC at 8 mm/sec.

Reducing the ram speed resulted in a reduced forging load. A constant ram speed of 1 mm/sec for ZK60 or 5 mm/sec for AZ80 @ 300 ºC resulted in acceptable predicted forging loads, as seen in Figure 6.4-11. The simulated forging load for AZ80 at 5 mm/sec was 1370 tonnes and for ZK60 at 1 mm/sec was 1420 tonnes. This means that the forging can be carried out with the currently available equipment at CanmetMATERIALS.

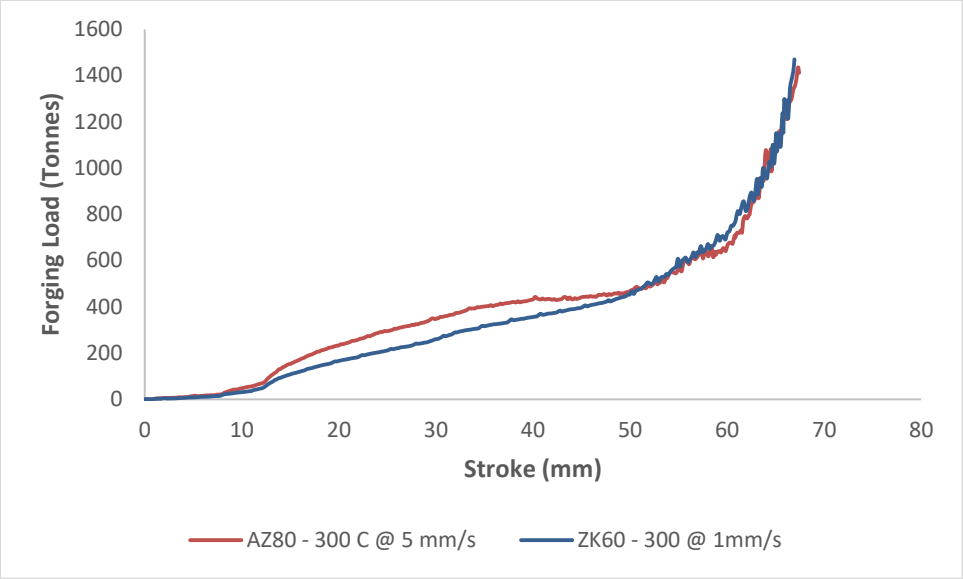

Figure 6.4-11: Forging load at ram speed, AZ80 at 5 mm/s, ZK60 at 1 mm/s @ 300 ºC.

An alternate way to reduce the press load is to use a two stage ram speed [58]. This technique was investigated here by applying it to the simulation of a two-stage forging process for extruded AZ80 at 400 ºC. Initially a ram speed of 8 mm/sec was used to simulate the forging of control arm until the stoke length of 60 mm was reached, and then the ram speed was reduced to 1 mm/sec for the remaining stroke length, from 60 mm to 67.4 mm. The load vs stroke graphs for both a constant ram speed of 8 mm/sec and the two-stage ram speed are plotted in Figure 6.4-12.

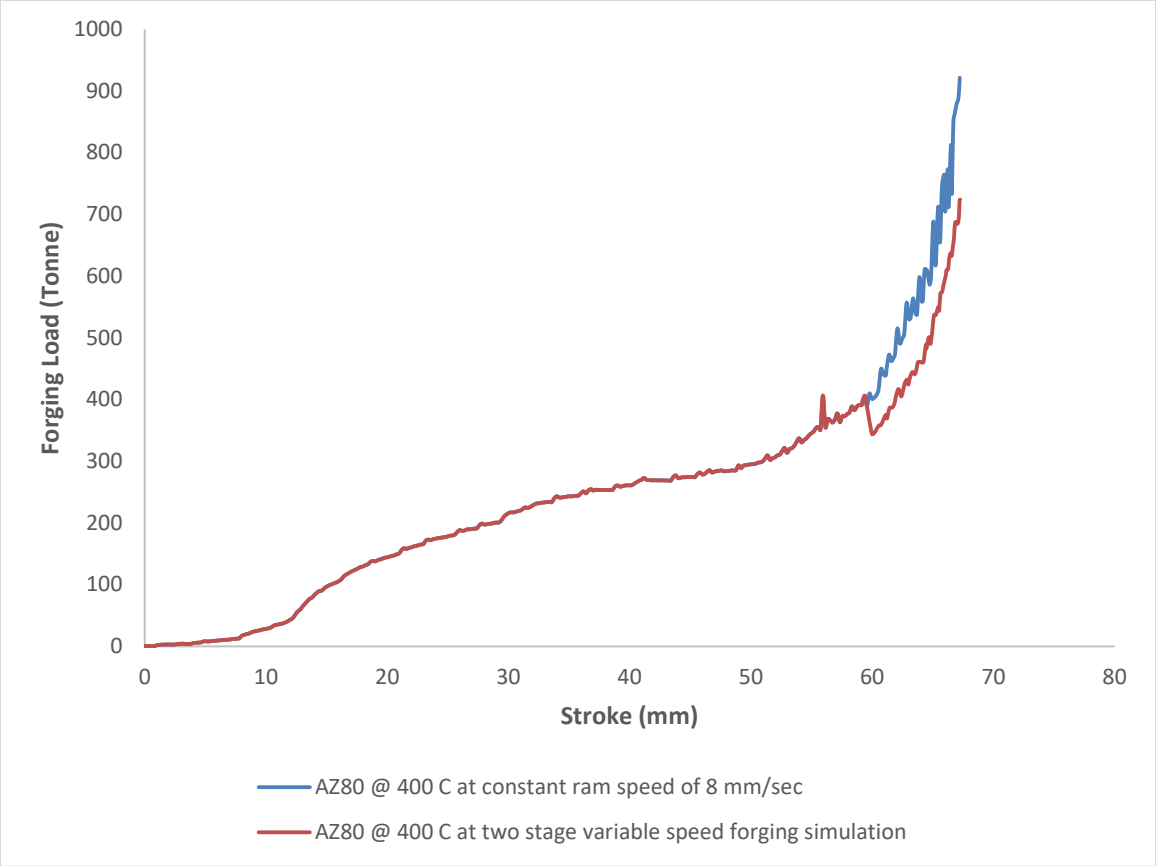

Figure 6.4-12: Load vs stroke graph for AZ80 @ 400 °C.

In the final forging stage from 60 mm to 67.4 mm, the load decreased from a maximum load of 921 tonne to 750 tonne, approximately 25%. This is consistent with the material model shown in Figure 5.4-1, as the strain rate decreases the material flow stress decreases. This techniques can be utilized to forge the control within the available resources and can result in significant saving of resources.

6.4.4.1 Verification of the Model

Based on the simulation results, the forging dies designed by Kodippili were manufactured by Multimatic Inc. The forging trials were performed at CanmetMATERIALS under the supervision of Jonathan Mckinley. The forging trials were performed on a 1200 tonne press available at CanmetMATERIALS. The bent cylindrical preform detailed in previous section was used to

perform the forging trials. Graphite lubricant was applied to both the dies and the billet at room temperature. The billet was than heated in an over to the desired temperature, AZ80 to 400 ^{o}C and ZK60 to 450 ^{o}C. The dies were also heated and maintained at the desired temperature throughout the forging using the heaters installed in the dies. The heaters were installed some distance below the surface of the dies along with the thermocouples. Since thermocouples were not installed at the surface of the dies, the dies were brought to the desired temperature and soaked for hours before the forging trial. This was done to bring the die surface temperature to the same temperature.

The forging trials were carried out under load control. The forging rate was 8 mm/sec at the beginning of the trial, but the press automatic slows down as the maximum load was approached. The forging trials were carried out using two materials, AZ80 and ZK60.

The result for ZK60 forging trial performed at the 450 ^{o}C is shown is Figure 6.4-13. A complete die fill was achieved and no visible surface cracks were observed. The graphite lubricant residual resulted in the dark surface finish on the control arm. The load, displacement versus time, data from the forging press was received from CanmetMATERIALS. Based on the displacement and time data received, simulation was performed using the same speed profile as an input for the top die movement. The speed profile can be seen in Figure 6.4-14.

Figure 6.4-13: Forging trial result for ZK60 forged at 450 ^{o}C.

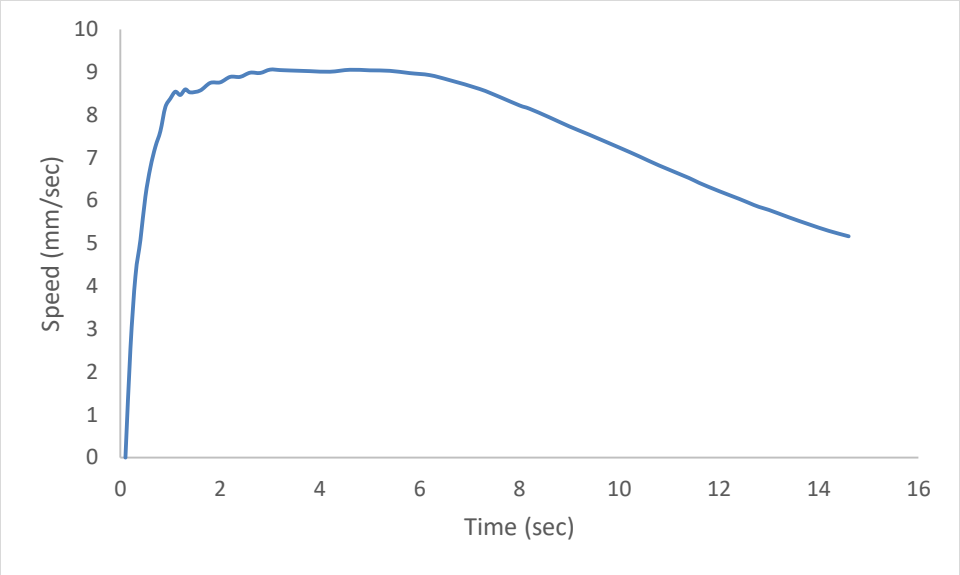

Figure 6.4-14: Speed profile used to perform simulation to repeat the forging trial performed at CanmetMATERIALS.

The load vs displacement results for both the simulation and actual forging trial were compared and results are shown in Figure 6.4-15. As can be seen in Figure 6.4-15, the simulation predicted the load reasonably well.

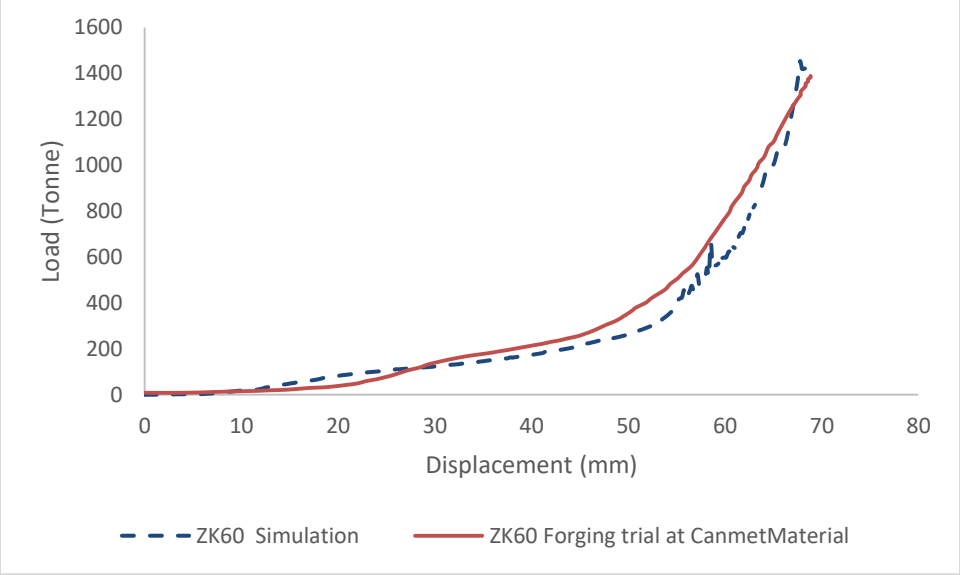

Figure 6.4-15: Load vs displacement - simulation results vs forging trial for ZK60.

A geometric comparison was also performed between the simulation and the forging trial. In Figure 6.4-16, the simulation result (yellow) is superimposed on the forging trial result photo. Since both the simulation and trial a complete die fill is achieved the visual comparison will focus

on the flash geometry. It must be noted here that the forging trial picture is take at an angle, which might result in some error when performing the geometric comparison. It can be seen in Figure 6.4-16, overall the flash geometry was captured pretty well with simulation, except in a couple of areas where the simulation was under predicting the flash. This can be attributed to the differences between the simulations and the actual forging trial parameters. In simulation, the entire process is considered isothermal, meaning no heat gain or loss was modeled during the forging process. The dies and billet were kept at the same temperature of 450 ^{o}C. On the other hand, during forging trial, the dies and billet were heated up to the temperature. The dies were kept close to the temperature with the help of the installed heaters but once the billet is removed from the furnace and placed on the die, no temperature control is available for the billet. Also the heat generation experienced during the forging process is not captured in simulation. This can result in increase in the material temperature which could result in easier material flow. In simulation a constant friction coefficient of 0.2 was used, while in forging trial this could vary based on the amount of graphite lubricant applied and the effectiveness of the lubricant to maintain the friction coefficient of 0.2 as the temperature changes. This could also result in decrease in friction coefficient, allowing the material to flow move easily.

Figure 6.4-16: ZK60 geometric comparison with simulation. Yellow is the model-predicted final forged geometry overlaid on the actual forging.

The forging trial was also performed for AZ80 at 400 ºC. Simulations and material flow curve, predicted that AZ80 would be easier to forge than ZK60 alloy. But during the forging trial at CanmetMATERIALS with AZ80, the dies were not able to completely close. The press maxed out at 1400 tonne. In the case of AZ80, the simulation didn't predicted the results successfully. This discrepancy between the forging trial and the simulation load results may be attributed to the material flow curve accuracy and temperature differences, since the same simulation model successfully predicted the ZK60 forging.

6.4.4.2 Creating the Preform Geometry via Bending

The process of using a bent cylinder as a preform depends on readily achieving the desired bend angle. The easiest way of achieving the bend is using a three point bend fixture. Initially it was decided to use an existing three point bend fixture at the University of Waterloo to create the preform. The bending fixture is shown in Figure 6.4-17. The bending needed to be performed at temperature of around 400 ºC, and an appropriate furnace was not available. It was decided that the actual bending would be conducted at Multimatic Inc.

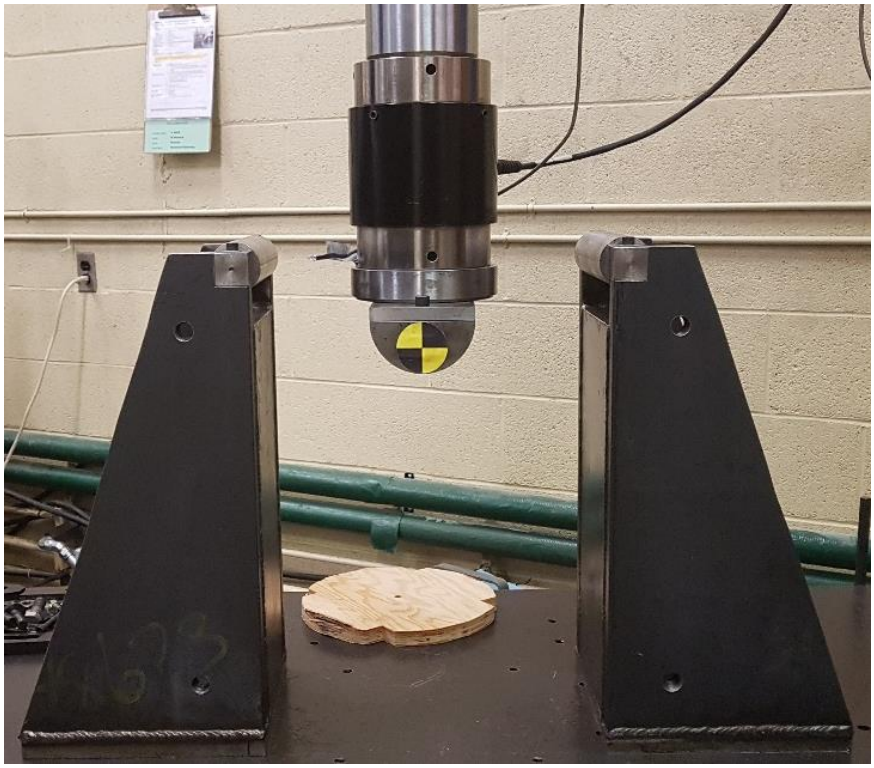

Figure 6.4-17: Bending fixture at University of Waterloo

Simulations, Figure 6.4-18, were performed to predict the load required, to assess whether cracking might occur, to simulate the strain distribution during pre-bending, and to verify the final shape. To achieve the required shape, a bend angle of 100^{o}, the centre roller needed to travel downwards a distance of around 110 mm. Due to magnesium's poor formability at low temperatures, it was decided to perform the bending at an elevated temperature of around 400 ^{o}C.

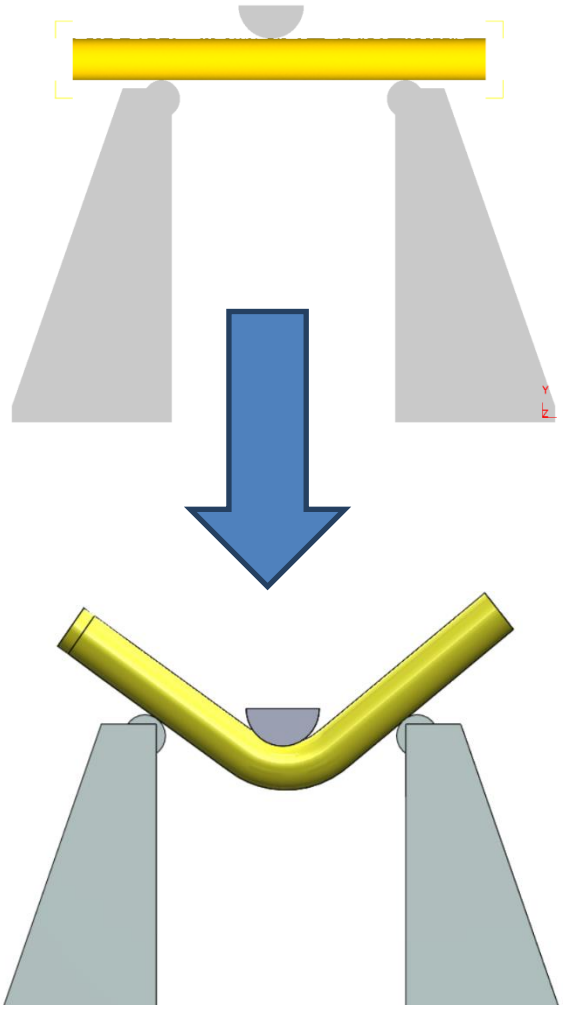

Figure 6.4-18: Schematic of the bending process

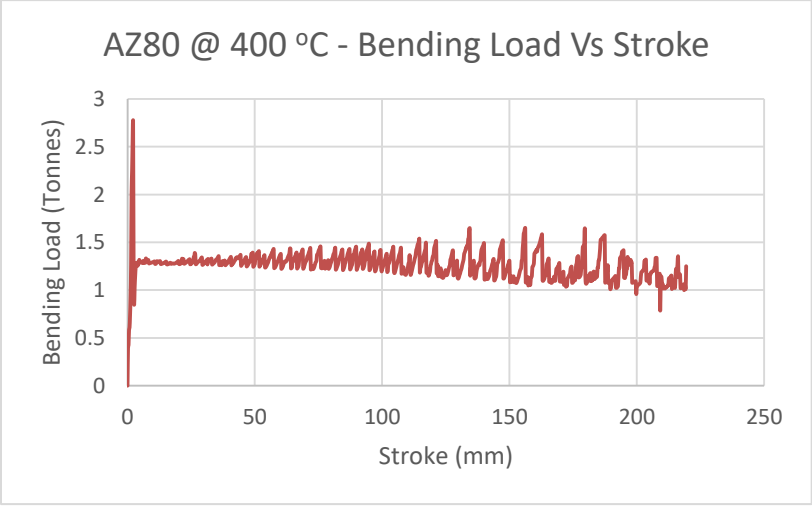

Figure 6.4-19: Extruded AZ80 @ 400 °C Bending Process Simulation

The simulation results show that it requires 1.25 tonne to achieve the bend angle of 100 degrees, as can be seen in Figure 6.4-19. The effective strain and damage distribution are shown below. It can be seen that the maximum damage value was 0.35, less than the limit of 0.5 for cracking as seen in Figure 6.4-20. Also, the effective strain was predicted in the bend region.

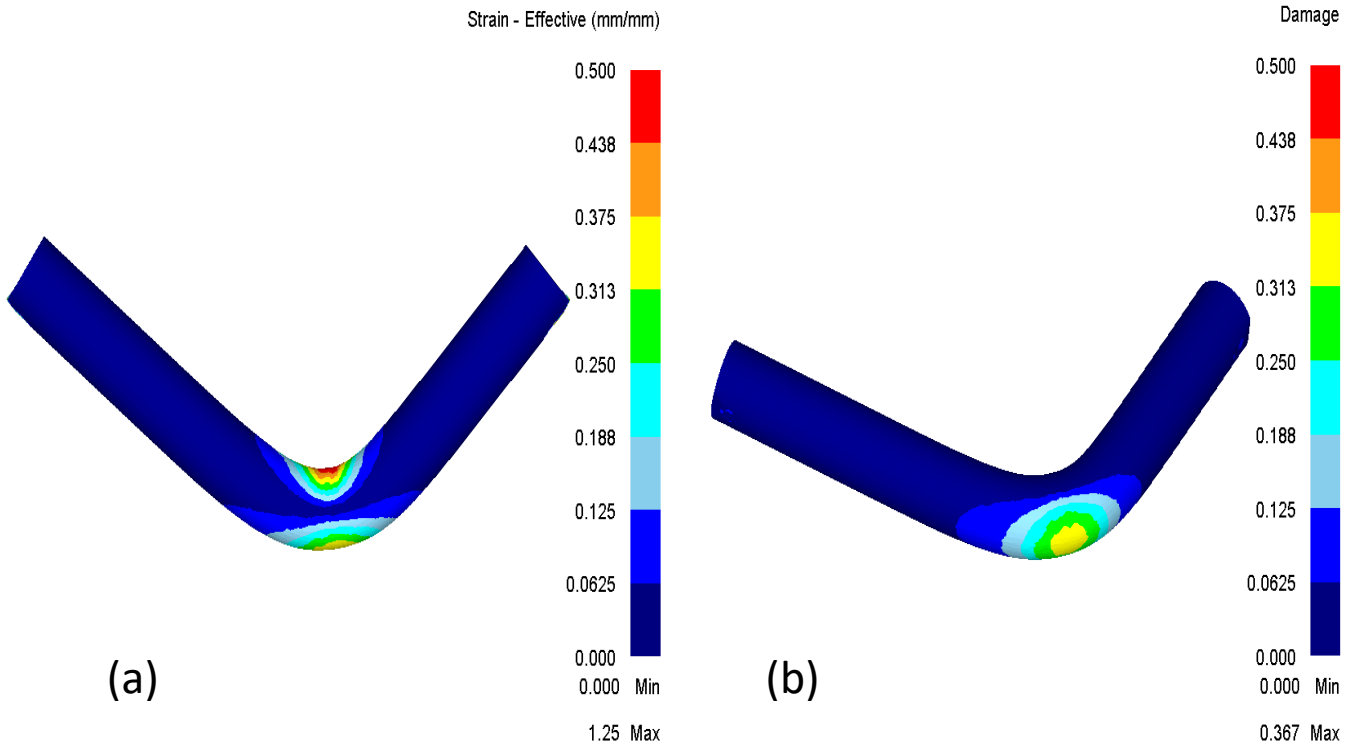

Figure 6.4-20: Effective strain and damage distribution form bending simulation

In order to develop the bent cylindrical preform for the forging runs, Multimatic developed a bending fixture and performed bending tests at an elevated temperature of 400 ^{o}C, as shown in Figure 6.4-21. The bent billet was formed against a gauge to make sure a bend angle of 100^{o} was successfully achieved, as shown in Figure 6.4-22

Figure 6.4-21: Preform bending process at Multimatic Inc

Figure 6.4-22: Checking bend angle against the bend gauge

In order to understand the effect of strain developed during the bending operation on effective strain of the forged part, a simulation of bending process was carried out followed by the simulation of the forging process. As can be seen in Figure 6.4-23 (b), the effective strain significantly increased in the forged part in which the bending process was performed prior to

doing the forging operation, as compared with one in which the preform shape was directly modeled and the forging simulation was performed, as seen in Figure 6.4-23. The increase in the effective strain can be attributed to the effective strain induced during the bending process.

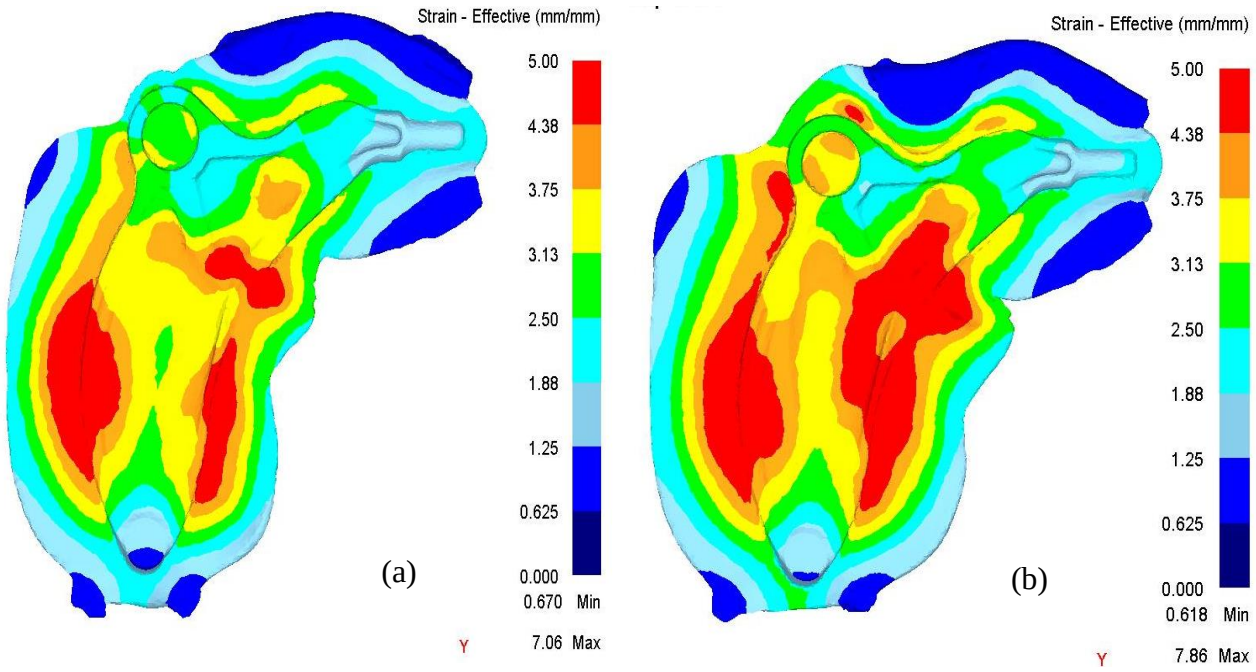

Figure 6.4-23: Model-predicted AZ80 at 400 °C (a) Effective strain distribution of forged part with bent preformed modelled in a CAD software (b) Effective strain distribution of the forged part with bent preform formed using a bending operation in DEFORM 3D

Chapter 7 Conclusions & Recommendations

7.1 Conclusions

In this project, a forging process was developed with the help of simulations using DEFORM 3D to forge a control arm using magnesium alloys. An anisotropic material model, which utilizes the compressive flow stress in one direction, and Hill's anisotropic coefficients, was used. Flow curves were generated by others, but shear hat tests were conducted at different temperatures and strain rates to calculate the necessary Hill's anisotropic coefficients at conditions shown in Table 3.2-1. Verification of the Hill's anisotropic coefficients was performed by simulating Gleeble tests in two orientations. Results of the simulation of the Gleeble test along with a comparison of coin and I-beam simulations [24] with the forged specimen shows that the Hill's anisotropic coefficient appropriately captures magnesium's anisotropy.

In order to understand the forging process in detail, several parametric studies were performed. The effect of ram speed, friction, temperature and different materials were considered. The required press load was a major concern. It is directly affected by the flow stress at strain equal to 1. The flow stress at strain equal to 1 increases with decreasing temperature. It can be seen in Figure 7.1-1 that there exists a strong correlation between the peak forging load (circles) and flow stress at strain of 1 (squares).

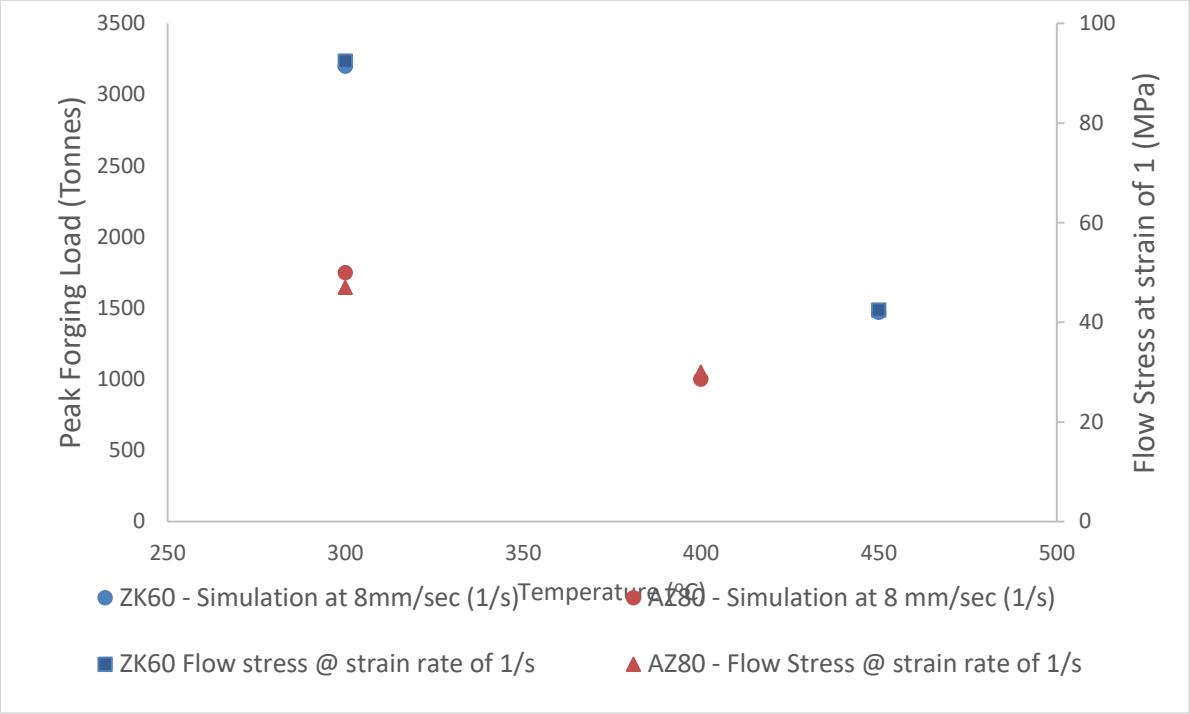

Figure 7.1-1: Model-predicted peak forging load, flow stress vs temperature.

Forging load is also influenced by the assumed friction coefficient; decreasing the friction coefficient decreases the press load by allowing the material to flow more easily. However, if the friction coefficient was reduced to about 0.05, the material doesn't flow into the all die cavities properly, resulting in incomplete die fill.

Since flow stress at a strain equal to 1 or above is lower for AZ80 than that of ZK60, the predicted press load is less as well. The dies were manufactured and forging trials were performed at CanmetMATERIALS on a 1200 tonne press. The control arm was successfully forged using ZK60 alloy. For AZ80, the press max out on load before completely closing. The simulation results were compared with ZK60 forging trials. The results comparison proves that the simulation model successfully predict the actual forging results. The unsuccessful forging of AZ80 can likely be attributed to accuracy of the AZ80 flow curves. This can also be effected by number of factors, such as, in simulation the coefficient of friction was kept constant at 0.2, while in forging trial this

can vary. Also all the simulation were performed in the isothermal conditions while in forging trial temperature can vary due to heat lost and heat generation due to mechanical work.

Several preform designs were considered in this project: the multi-section cylinder, flat billet, and bent cylinder. After considering each billet with respect to the project constraints, the bent cylindrical billet was selected as the best for this research project. The bent cylindrical billet completely fills the die, and the press load was observed to be below the 1500 tonne limit at 400 ^{o}C at 8mm/sec for both alloys. In industry, the lowest possible temperature at highest possible ram speed is preferred, to minimize costs while maximizing throughput. This also maximizes final material properties. For the alloys and component considered, temperatures below 400 ^{o}C for AZ80 and 450 ^{o}C for ZK60 will require lower ram speeds in order to forge a control arm within the capacity of the 1500 tonne press.

7.2 Recommendations

As forgings are completed at CanmetMATERIALS and more experimental data becomes available, further validation of the model is possible. Beside the load and shape comparison, other aspects of the forging need to be compared with simulation. For example, the critical dimension in the forged trial part can be measured and compared with simulation. The forged part also needs to be sectioned at various places and the micro hardness needs to be measured and compared with the effective strain distribution. This also needs to be compared with the benchmark component as previously done with the I-beam samples. Samples need to be extracted at various positions for fatigue testing and the results need to be compared with the benchmark results.

Recently, it was discovered that using the bent cylindrical billet with a 100^{o} angle results in a fold line (material from both sides come and fuse together). This will result in a material defect. This needs to be investigated. A number of solutions can be investigated. One is to change the bend angle, and a second is to pre-flatten the billet before being forged. Further simulations and experiments need to be performed to recommend a suitable solution.

After the unsuccessful AZ80 forging trial, questions were raised on the veracity of the flow curves for this alloy. The previous conducted compression tests need to be repeated. Simulations for AZ80 alloys need to be repeated using the new flow curves and calculated Hill's coefficients. The simulations results need to be then compared with the forged AZ80 control arm.

All the simulations for the control arms were performed under isothermal conditions. Consideration of non-isothermal conditions will more accurately model the experimental conditions and may improve the results, especially for simulations done at slow ram speeds. It takes longer for a forging to complete at slower ram speeds, resulting in more thermal losses to the surroundings.

Another limitation to the simulation process is the material model. The Hill's anisotropic coefficients used in the material model are provided for one strain rate and temperature. This is a

limitation of DEFORM 3D. It is recommended to develop a user routine or use other models [59][60] to take into account of thermal and strain rate effects over a wider range.

In order to reduce press load during the forging process, another method that needs to be investigated is to stop the forging process in the middle, remove the billet, trim the flash, reheat the billet, and place it back in the die to finish the forging process. It is recommended to perform a simulation to determine the effect of this method on the forging of the control arm.

A multi-section cylindrical preform was initially suggested, but was not implemented in this project due to the extra steps required to produce the preform. It is recommended to follow up on this shape before the start of any formal production cycle, since this shape reduces the material waste in the form of flash.

Another preform design method that was not considered in this project was to sand- or die-cast the preform shape before forging. Applying this method will eliminate the extra steps like bending, rolling etc in order to achieve the final preform shape. This should be investigated further, especially its effect on material waste and final forged properties.

Damage values from literature which were further validated using small scale and I-beam beam specimen were used to predict damage. In simulation and forging test result, the predicted damage was low. For more accurate results, it is recommended to obtain the critical damage value for the two materials, AZ80 and ZK60 using the method proposed by S.W. Kim and Y. Xue [61][62].

References

[1] "NSERC Magnesium Network", 2012, http://www.magnet.ubc.ca/

[2] Environment Canada, “Greenhouse Gas Emissions by Canadian Economic Sector” 2015, https://www.ec.gc.ca/indicateurs-indicators/default.asp?lang=en&n=f60db

[3] L. Cheah, C. Evans, A. Bandivadekar and J. Heywood, "Factor of Two: Halving the Fuel Consumption of New US Automobiles by 2035," MIT Laboratory for Energy and Environment, Cambridge, MA, 2007

[4] Americas Climate Choices. National Research Council. Washington, DC: The National Academies Press, 2011, www.nap.edu

[5] "National Highway Traffic Safety Administration (NHTSA)", 2012, https://www.nhtsa.gov/staticfiles/rulemaking/pdf/cafe/CAFE-GHG_Fact_Sheet.pdf

[6] A A Luo, "Wrought Magnesium Alloys and Manufacturing Processes for Automotive Applications," in SAE Technical Paper, 2005, pp. 2005-01-0734

[7] J. Yoon and S. Lee, “Warm forging of magnesium AZ80 alloy for the control arm in an automobile,” Journal of Automobile Engineering, vol. 229(13), pp.1732-1738, 2015

[8] DEFORM v11.1 system documentation, Scientific Forming Technologies Corporation, Columbus, Ohio, 2016

[9] Roberts, C.S., 1960. Magnesium and its Alloys. John Wiley, New York and London [robers 1960]

[10] Kelley, E.W., Hosford, W.F., 1968b. Plane-strain compression of magnesium and magnesium alloy crystals. Trans. Metall. Soc. AIME 242, 5–13.

[11] T. Obara, H. Yoshinga, S. Morozumi, {1122}〈1123〉 Slip system in magnesium, Acta Metallurgica, Volume 21, Issue 7, 1973, Pages 845-853, hhtps://doi.org/10.1016/0001-6160(73)90141-7

[12] Lou, X.Y., Li, M., Boger, R.K., Agnew, S.R., Wagoner, R.H., 2007. Hardening evolution of AZ31B Mg sheet. International Journal of Plasticity 23, 44–86.

[13] Waqas Muhammad (2014). Experimental Characterization and Constitutive Modeling of AZ31B and ZEK100 Magnesium Alloys for Monotonic and Reverse Loading Paths. UWSpace. http://hdl.handle.net/10012/8795

[14] Tsz Wun (Rick) Wong (2016). High Temperature Forging of AZ31B Magnesium Alloy. UWSpace. http://hdl.handle.net/10012/10694

[15] Yoo, M.H., 1981. Slip, twinning, and fracture in hexagonal close-packed metals, Metall. Trans. A 12, 409–418

[16] A. Gryguc, S.K. Shaha, S.B. Behravesh, H. Jahed, M. Wells, B. Williams, X. Su, Monotonic and cyclic behaviour of cast and cast-forged AZ80 Mg, International Journal of Fatigue, Volume 104, 2017, Pages 136-149, ISSN 0142-1123, https://doi.org/10.1016/j.ijfatigue.2017.06.038.

[17] A. Gryguc, S. K. Shaha, S. B. Behravesh, H. Jahed, M. Wells, and B. Williams, "Compression Behaviour of Semi-closed Die Forged AZ80 Extrusion," Characterization of Minerals, Metals, and Materials. 2017, pp. 361–369, 2017.

[18] Kurz G, Clauw B, Sillekens W, Ketzug D (2009) Die forging of the alloys AZ80 and ZK60. In: Magnesium technology—TMS 2009, San Francisco, California

[19] S. M. H. Karparvarfard, S. K. Shaha, S. B. Behravesh, H. Jahed, and B. W. Williams, "Microstructure, texture and mechanical behavior characterization of hot forged cast ZK60 magnesium alloy," J. Mater. Sci. Technol., 2016.

[20] S. M. H. Karparvarfard et al., "Characterization of Semi-Closed Die-Forged ZK60 Mg Alloy Extrusion," Magnes. Technol. 2017. Springer Int. Publ., pp. 329–334, 2017.

[21] A. Gryguc, S. K. Shaha, H. Jahed, M. Wells, B. Williams, and J. McKinley, "Tensile and fatigue behaviour of as-forged AZ31B extrusion," Frat. ed Integrita Strutt., vol. 10, no. 38, pp. 251–258, 2016

[22] D. Toscano, S. K. Shaha, B. Behravesh, H. Jahed, and B. Williams, "Effect of forging on the low cycle fatigue behavior of cast AZ31B Alloy," Mater. Sci. Eng. A, 2017

[23] D. Toscano, S. K. Shaha, B. Behravesh, H. Jahed, and B. Williams, "Effect of Forging on Microstructure, Texture, and Uniaxial Properties of Cast AZ31B Alloy," J. Mater. Eng. Perform., vol. 26, no. 7, pp. 3090–3103, 2017.

[24] Guo Yu (2016). Forging specimen design for Mg alloys. UWSpace. http://hdl.handle.net/10012/10690

[25] Ali, U., Odoh, D., Muhammad, W., Brahme, A., Mishra, R. K., Wells, M., & Inal, K. (2017). Experimental investigation and through process crystal plasticity-static recrystallization modeling of temperature and strain rate effects during hot compression of AA6063. Materials Science and Engineering: A, 700, 374-386.

[26] D. Kobold, G. Gantar, and T. Pepelnjak, “Finite element analysis of magnesium AZ80 wrought alloy anisotropic behavior during warm forging,” Mechanika, vol. 18(3), pp. 251-258, 2012.

[27] Y. Bai and B. Dodd, Ed., Adiabatic shear localization: occurrence, theories, and applications. Waltham, MA: Elsevier Ltd, 2012.

[28] L.W. Meyer and E. Staskewitsch, “Adiabatic shear failure under biaxial dynamic compression/shear loading,” Mechanics of Materials, vol. 17(2), pp.203-214, 1994

[29]E. El-Magd and M. Abouridouane, “High speed forming of the light-weight wrought alloys,” in 1st International Conference on High Speed Forming, Dortmund, Germany, 2004

[30] J. Peirs, P. Verleysen, J. Degrieck, and F. Coghe, “The use of hat-shaped specimens to study the high strain rate shear behavior of Ti-6Al-4V,” International Journal of Impact Engineering, vol. 37, pp.703-714, 2010

[31] R. Hill, “A theory of the yielding and plastic flow of anisotropic metals,” Proceedings of The Royal Society of London. London: The Royal Society, 1948, pp.281-297

[32] D.W.A. Rees, Basic Engineering Plasticity, Elsevier, pp. 339-367, 2006

[33] Rajput, R. K. A textbook of manufacturing technology: Manufacturing processes. Firewall Media, 2007

[34] M. K. Kulekci, "Magnesium and its alloys applications in automotive industry," International Journal of Advanced Manufacturing Technology, no. 39, pp. 851-865, 2008

[35] S. Kalpakjian and S. R. Schmid, Manufacturing Processes for Engineering Materials (5th Edition), Upper Saddle River, NJ: Pearson Education, 2008

[36] B. A. Behrens, I. Pfeiffer and J. Knigge, "Forging technology for magnesium alloys," in Advances in wrought magnesium alloys, Philadelphia, PA, Woodhead Publishing, 2012, pp. 376-389

[37] B.L. Jenkins, S.I. Oh, and T. Altan, “Investigation of defect formation in a 3-station closed die forging operation,” Annals of CIRP, vol. 38, 1989

[38] H.S. Valberg, Applied Metal Forming Including FEM Analysis. New York: Cambridge University Press, p.275, 2010

[39] Miura H, Matsumoto K, Kobayashi M (2015) Multi-directional forging of AZ61 Mg alloy using die under decreasing temperature conditions. In: The 10th international conference on magnesium alloys and their application, Jeju, Korea

[40] A. Gontarz, Z. Pater, and K. Drozdowski, “Hammer forging process of lever drop forging from AZ31 magnesium alloy,” Metalurgija, vol. 52, pp.359-362, 2013

[41] W.J. Kim, H.W. Lee, J.P. Park, M.G. Kim, and U.S. Yoon, “Forging of Mg-3Al-1Zn-1Ca alloy prepared by high-frequency electromagnetic casting,” Materials and Design, vol. 30, pp.4120-4125, 2009

[42] V. Vazquez and T. Altan, "Die design for flashless forging of complex parts," Journal of Materials Processing Technology, vol. 98, pp. 81-89, 2000

[43] Q. Wang, Z.-m. Zhang, X. Zhang and J.-m. Yu, "Precision forging technologies for magnesium alloy bracket and wheel," Transactions of Nonferrous Metals Society of China, no. 18, pp. 205-208, 2008

[44] T. Pepelnjak, R. Werkhoven, D. Kobold and K. Kuzman, "Analysis of Warm Magnesium Forging in Digital Environment," Journal of Technology of Plasticity, vol. 35, no. 1-2, pp. 13-23, 2010

[45] P. Christiansen, J. H. Hattel, and N. Bay, “ Modelling of damage during hot forging of ingots,” in Fifth International Conference on Steelsim, Ostrave, Czech Republic, 2013

[46] A.V. Rao, N. Ramakrishnan, and R.K. Kumar, “A comparative evaluation of the theoretical failure criteria for workability in cold forging,” Journal of Materials Processing Technology, vol. 142, pp.29-42, 2003

[47] S.W. Kim, and Y.S. Lee, “Comparative study on failure prediction in warm forming processes of Mg alloys sheet by the FEM and ductile fracture criteria,” ASM International 2013 Metallurgical and Materials Transactions B, vol. 45B, p.415, 2014.

[48] Y. Xue, Z.M. Zhang, and Y.J. Wu, “Study on critical damage factor and the constitutive model including dynamic recrystallization softening of AZ80 magnesium alloy,” Science of Sintering, vol. 45, pp.199-208, 2013.

[49] Paresh Parkash, Phd Thesis in preparation, University of Waterloo

[50] Amir Hadadzadeh, Mary A. Wells, Analysis of the hot deformation of ZK60 magnesium alloy, Journal of Magnesium and Alloys, Volume 5, Issue 4, 2017, Pages 369-387, ISSN 2213-9567, https://doi.org/10.1016/j.jma.2017.09.002

[51] Y. Bai and B. Dodd, Ed., Adiabatic shear localization: occurrence, theories, and applications. Waltham, MA: Elsevier Ltd, 2012

[52] J. Luan, C. Sun, X. Li, and Q. Zhang, “Constitutive model for AZ31 magnesium alloy based on isothermal compression test,” Materials Science and Technology, vol. 30, no. 2, 2014

[53] Alexander Strong (2016). Optimization of Forged Magnesium Structural Automotive Components. UWSpace. http://hdl.handle.net/10012/10692

[54] Tharindu Abesin Kodippili, MASc Thesis in preparation, University of Waterloo

[55] Boothroyd, Geoffrey, editor. “Chapter 14” Product Design for Manufacturing and Assembly. Marcel Dekker, Inc, 2002.

[56] Mahito KUNOGI, A New Method of Cold Extrusion, Transactions of the Japan Society of Mechanical Engineers, Released March 28, 2008, Online ISSN 2185-9485, Print ISSN 0029-0270, https://doi.org/10.1299/kikai1938.23.742

[57] Male, A.T., Cockcroft, M.G., 1965. A Method for the Determination of the Coefficient of Friction of Metals under Condition of Bulk Plastic Deformation. Journal of the Institute of Metals 96, Page 241, https://doi.org/10.1016/0043-1648(66)90161-X.

[58] Hailin He, Shiquan Huang, Youping Yi, Wanfu Guo, Simulation and experimental research on isothermal forging with semi-closed die and multi-stage-change speed of large AZ80 magnesium alloy support beam, Journal of Materials Processing Technology, Volume 246, 2017, (http://www.sciencedirect.com/science/article/pii/S0924013617301085)

[59] Muhammad, W., Mohammadi, M., Kang, J., Mishra, R. K., & Inal, K. (2015). An elasto-plastic constitutive model for evolving asymmetric/anisotropic hardening behavior of AZ31B and ZEK100 magnesium alloy sheets considering monotonic and reverse loading paths. International Journal of Plasticity, 70, 30-59.

[60] Kang, J., & Muhammad, W. (2016). Measurement of Plastic Strain Ratio Using Digital Image Correlation. Journal of Testing and Evaluation, 45(5), 1587-1600.

[61] S.W. Kim, and Y.S. Lee, “Comparative study on failure prediction in warm forming processes of Mg alloys sheet by the FEM and ductile fracture criteria,” ASM International 2013 Metallurgical and Materials Transactions B, vol. 45B, p.415, 2014.

[62] Y. Xue, Z.M. Zhang, and Y.J. Wu, “Study on critical damage factor and the constitutive model including dynamic recrystallization softening of AZ80 magnesium alloy,” Science of Sintering, vol. 45, pp.199-208, 2013

Appendix A: Material Models

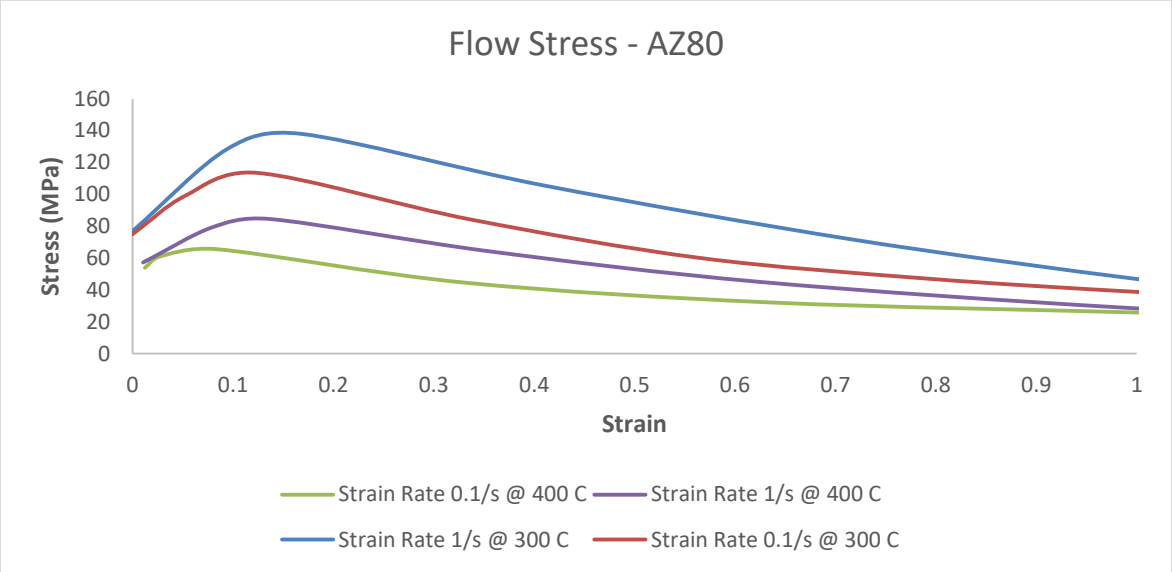

Figure A-1: Flow curve for extruded AZ80 [49]

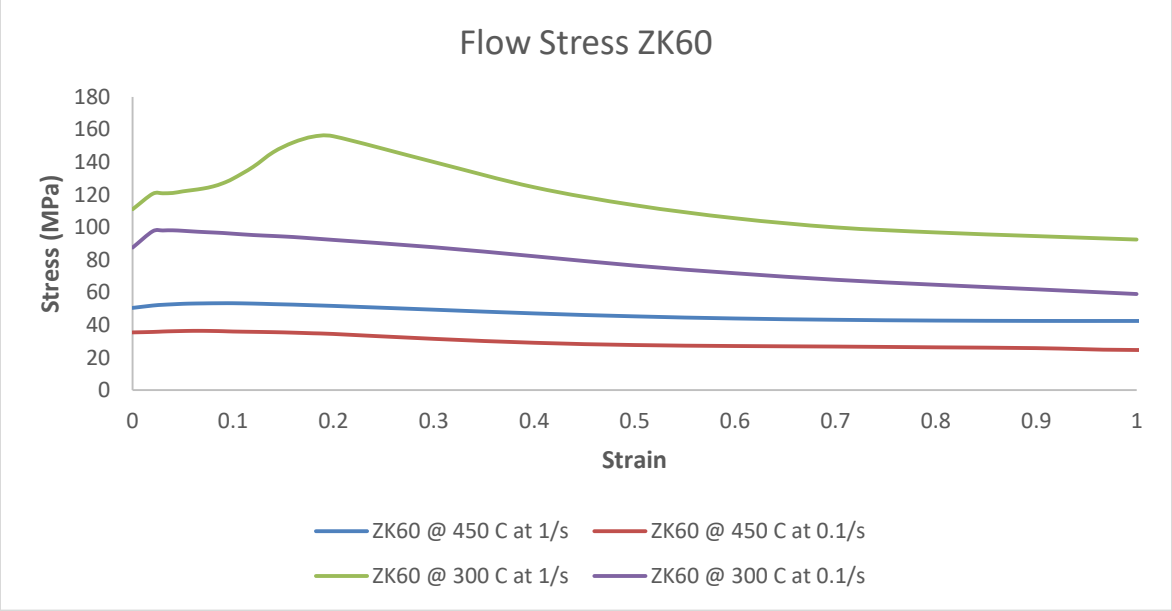

Figure A-2: Flow curve for extruded ZK60 [50]

Appendix B: Engineering Drawing for Preforms

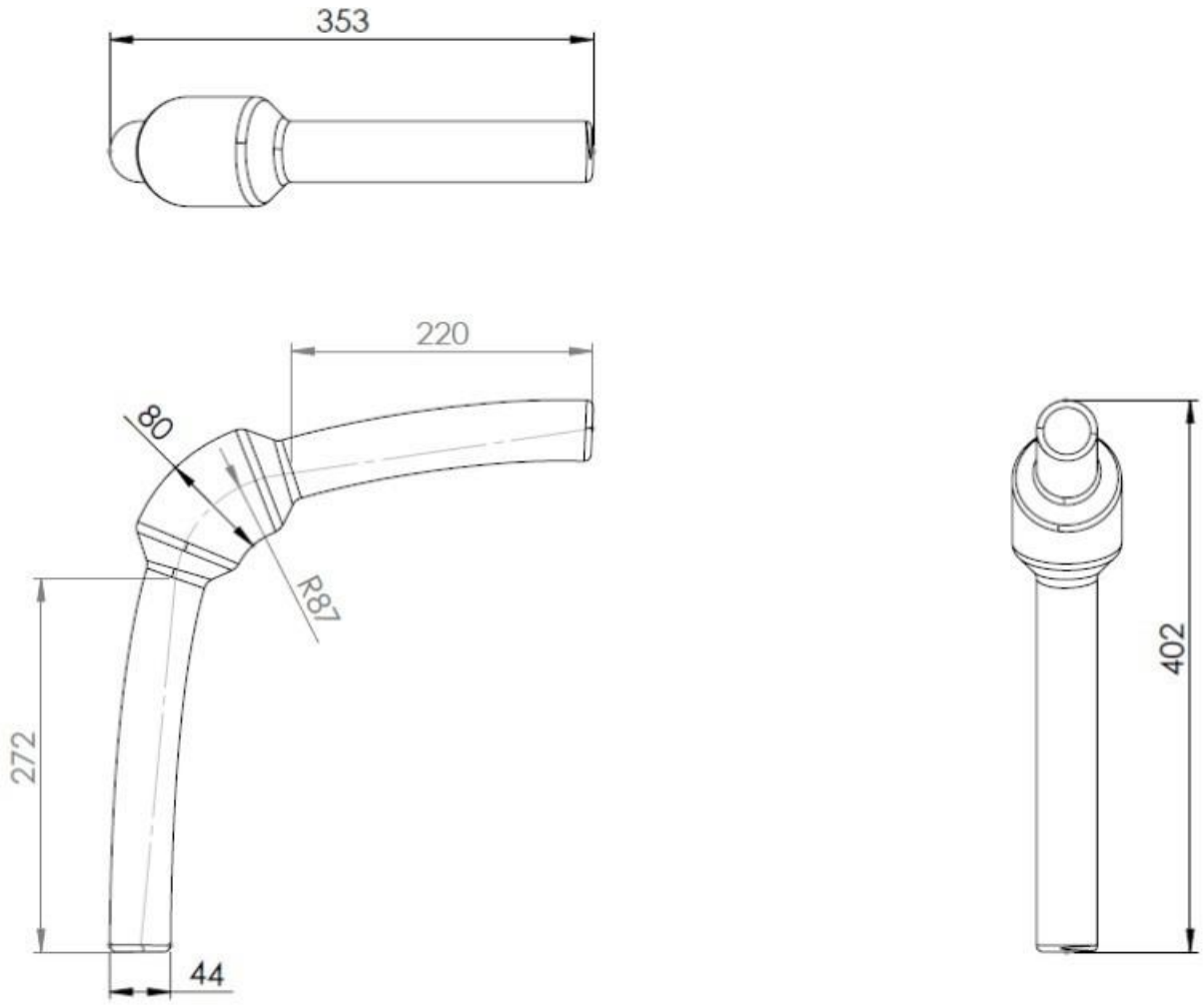

Figure B-1: Multi-section cylindrical billet drawing [54]

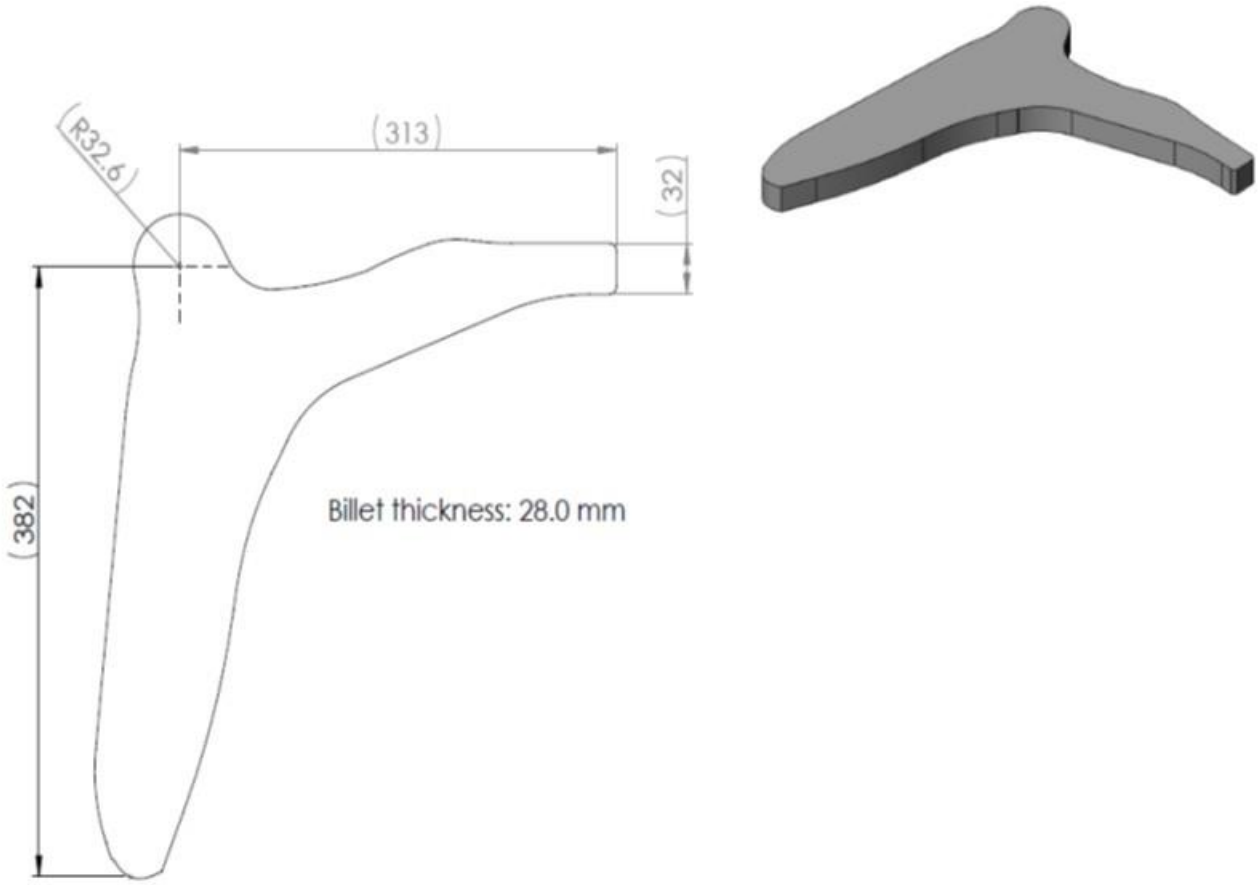

Figure B-2: Flat billet drawing

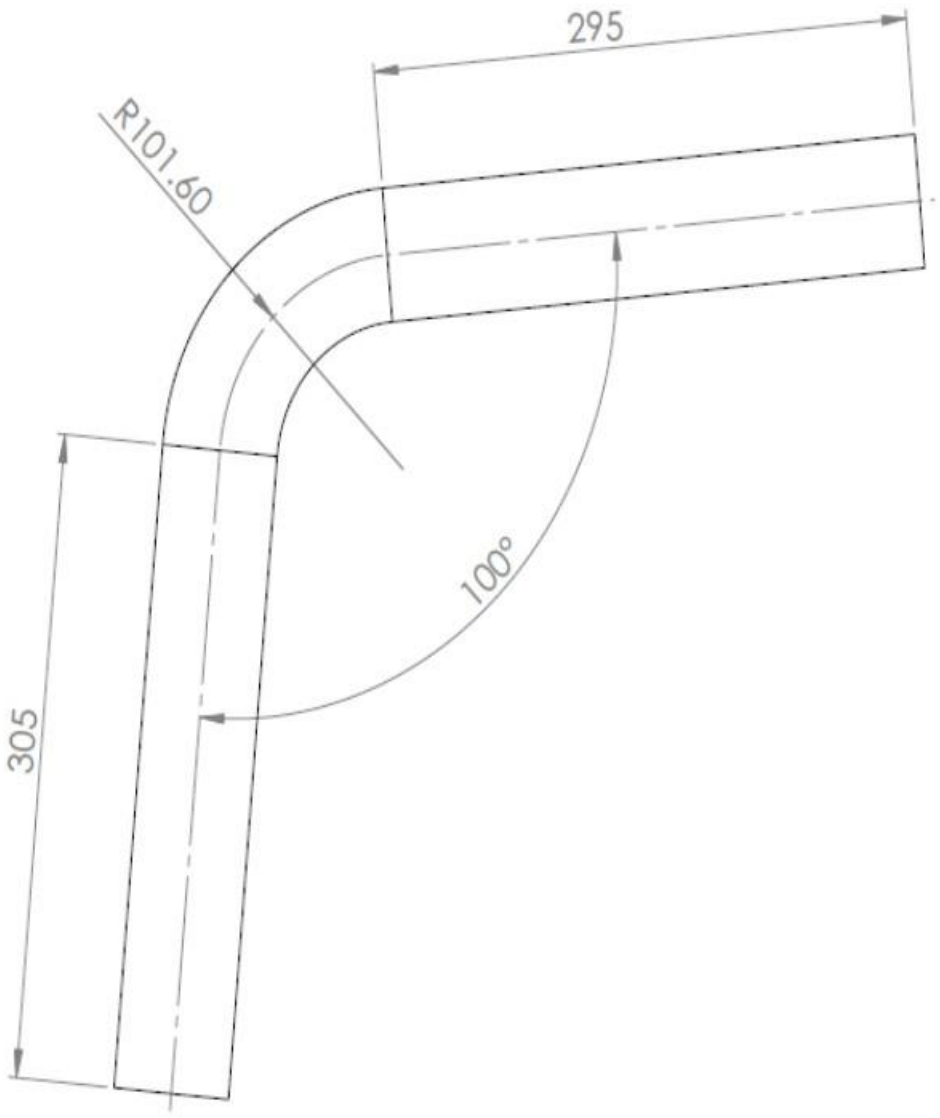

Figure B-3: Bent cylindrical billet drawing

Appendix C: Forging Simulation Results

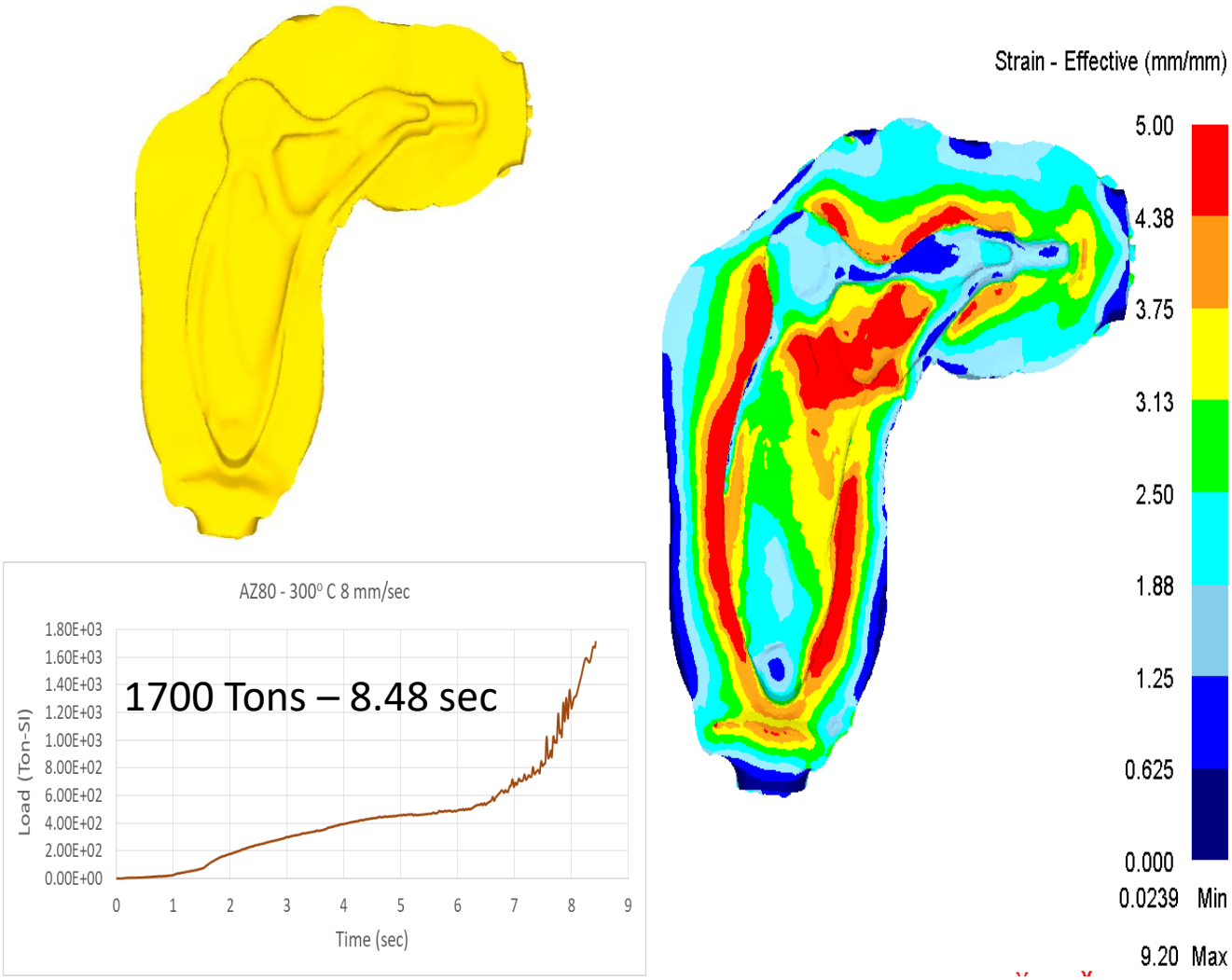

Figure C-1: Simulation results for AZ80 @ 300 °C at 8mm/sec

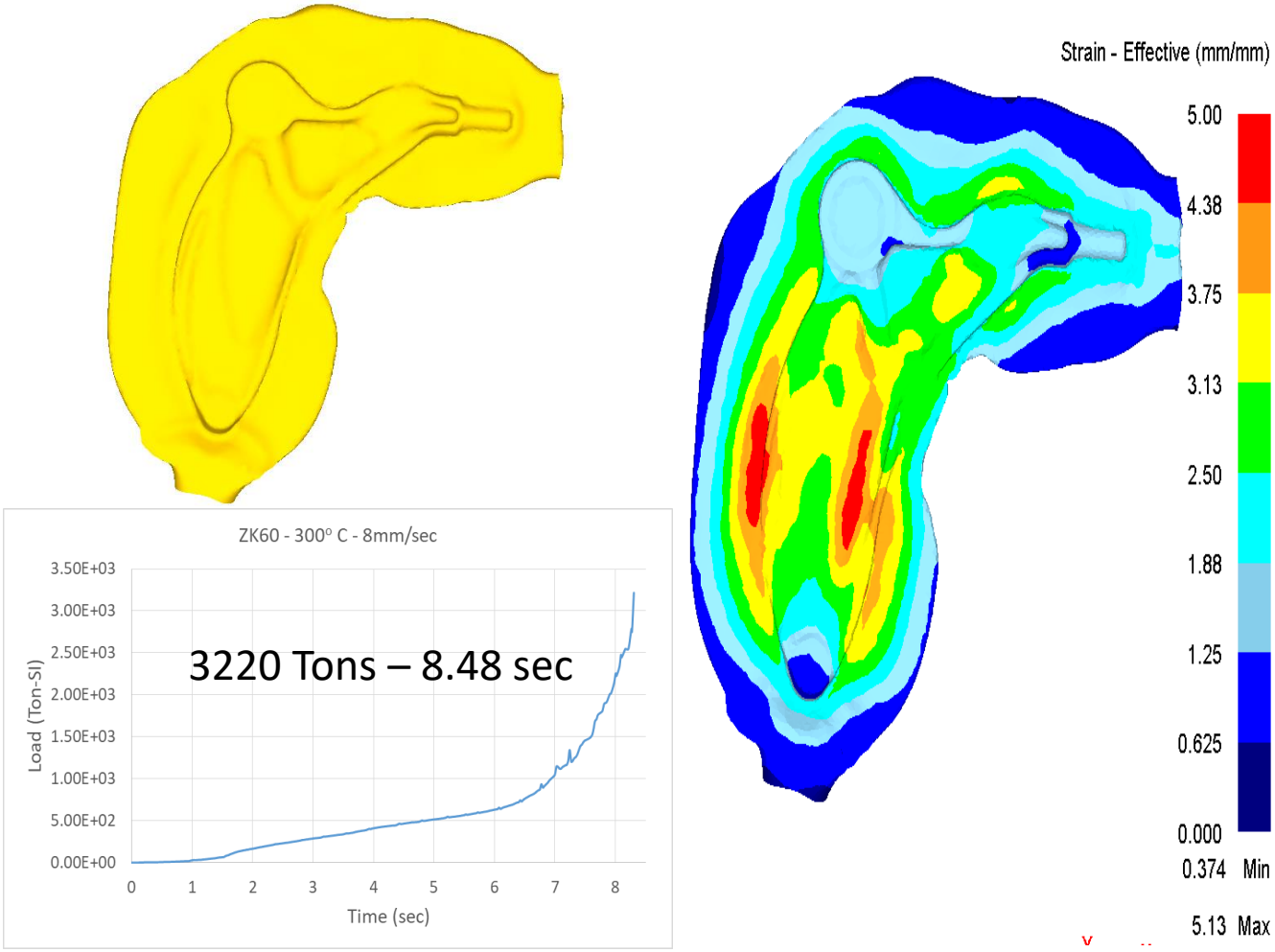

Figure C-2: Simulation results for ZK60 @ 300 °C at 8mm/sec